Jörg Reiff-Stephan
Kou´santa AMOUZOU
Assiongbon ADANLETE

Conference Proceedings

1st German-West African Conference on Sustainable, Renewable Energy Systems SusRES

1st July 2020 – Kara, Togo

Technische Hochschule Wildau
Technical University of Applied Sciences
WILDAU

sponsored by:
DAAD
Deutscher Akademischer Austauschdienst
German Academic Exchange Service

UNIVERSITE DE KARA

Publisher
Jörg REIFF-STEPHAN, Kou´santa AMOUZOU, Assiongbon ADANLETE

Proceedings SusRES‘2020:
1st German-West African Conference on Sustainable,
Renewable Energy Systems SusRES‘2020

ISBN 978-3-9819225-5-4 (E-Book)

Published by TH Wildau, Wildau

Produced in Germany

Table of content

SIII-1 Air Pollution

SIII-2 Thermal Energy

SIV-1 Production

KI

Presentation of the University of Kara

Palakyém Mouzou [1]

1 KARA, A UNIVERSITY TOWN

Kara University, the first decentralised university in Togo, opened on January 23, 2004, with 1 537 students shared by three (03) faculties : the Faculty of Letters and Human Sciences, the Faculty of Law and Political Sciences, and the Faculty of Economic and Management Sciences. Since then, the ambition has been to make of Kara a real famous and international university town, relying on the assets of its geographical location between northern Ghana and northern Benin on one hand, and on the main road of the corridor linking Burkina Faso, Mali and Niger on the other hand. To achieve this, the strategies adopted include, among others, innovative training offers submitted to accreditation to ensure their national and international attractiveness, public-private partnership to facilitate the professional insertion of graduates, high internationalisation to ensure the quality and visibility of the University through a network of established famous partners.

To date, Kara University has 21 000 students shared among five (05) faculties and one (01) high institute. These are:

- ✓ Faculty of Letters and Human Sciences;
- ✓ Faculty of Law and Political Sciences;
- ✓ Faculty of Economic and Management Sciences;
- ✓ Faculty of Sciences and Techniques;
- ✓ Faculty of Health Sciences ;
- ✓ High Institute of Agricultural Trade.

2 A UNIVERSITY UP TO STANDARDS AND AT THE SERVICE OF THE COMMUNITY

In accordance with its Ten-year Strategic Plan, Kara University is committed to becoming and remaining a central actor of the economic, technological and socio-cultural development of Togo, by integrating in its functioning the orientations by the Quality Referentials of the African and Malagasy Council for High Education. Engaged in this dynamics, Kara University displays itself as a « **university at the service of the community** ». Therefore, it works continuously

[1] Dr. Palakyém Mouzou is a Senior Assistant Professor of Linguistics and the Head of the Communication Office at the University of Kara.

towards meeting the various needs of the people and institutions of Togo, Africa and the whole world, while planning for the future.

3 A UNIVERSITY FACING EXCELLENCE IN RESEARCH

The Kara University recruits its university teachers, through a call for application, for the various disciplines. The teachers come from various universities of Africa, Europe, Asia, and America, where they got high academic and research experiences. They do research in various laboratories, many of which are young laboratories, contributing thus to the achievement of the development goals.

- The Kara University owns:
- 01 Multidisciplinary Doctoral School,
- 12 research laboratories,
- 01 technological market-hall for processing agricultural food stuffs, such as aromatic plants for essential oils, and
- 01 centre for computer science under construction.

4 TRAINING MATCHING THE JOB MARKET

In addition to classical training, revised to match the needs of the job market, Kara University innovates by creating professional channels to directly meet the demand from public and private enterprises. Theoretical and, especially, practical courses, coupled with training attachment in businesses, make this professional training special.

In the Faculty of Sciences and Techniques hosting the present colloquium, students are trained in various domains with emphasis on their ability to be immediately employable at the end of their training.

As concerns the Bachelor Degree, the following training channels are offered to students:

- Bachelor Degree in Mathematics and Pedagogical Sciences
- Bachelor Degree in Mathematics, Statistics, and Socio-economic Applications
- Bachelor Degree in Applied Mathematics and Computer Science

- Bachelor Degree in Applied Physics-Energy and Habitation
- Bachelor Degree in Physics and Pedagogical Sciences
- Bachelor Degree in Applied Physics-Electronics and Computer Science
- Bachelor Degree in Chemistry Applied to Environment
- Bachelor Degree in Chemistry of Agrofood and Pharmacological Applications
- Professional Degree in Industrial Maintenance and Services
- Professional Degree in Computer Science Security and Cyber Security
- Professional Degree in Multimedia and internet Trade
- Professional Degree in Food Quality Control and Health Security

Regarding the Master degree, students are trained for:

- Master in Environmental Chemistry
- Master in Water and Sanitation
- Master in Nutrition and Food Security

5 A UNIVERSITY FOR RENEWABLE ENERGIES

Kara University has the ambition to set up a project titled "The solar and biomass: Which sober and durable technologies for a production of renewable energies in rural environment and peri-urban? ". The main innovation in this pilot project is the use of local recovery materials to generate electrical energy at low cost starting from the Stirling engine and/or of a process of transformation of the no fermentable organic into bio carburant. It is thus precisely of the local products and recovery such as the antenna parabola, the aluminum foil, the alternator of older vehicles and the development of chemical reactions transforming the refractory organic matter with the biological breakdown into fermentable compounds.

In addition of this project, Kara University is very determined to create a Master of Physics in renewable energies and habitat. This Master has as an ambition to transmit to the students pointed competences around the most important sets of themes related to renewable energies. The graduates of Master can present themselves on the labor market to contribute to the definition and the implementation of strategies and energy policies within great industry groups, of innovating small structures or organizations public, with the international level.

This Master has also the role to prepare the students with the trades of search and teaching.

KII
Word of welcome and presentation of University of Applied Sciences Wildau

Jörg Reiff-Stephan[1]

1 Overview

The Technical University of Applied Sciences Wildau is an innovative, future-oriented and practice-oriented university in the south of Berlin. The personal atmosphere, the individual support by the teaching staff, the high-quality equipment of the technical-technological and information technology laboratories, the computer, internet and library workstations offer good conditions for a successful course of studies and a goal-oriented preparation for a subsequent career start. In order to ensure the first-class level of study and teaching conditions in the long term, Wildau Technical University was the first university in Germany to have its quality standards in this area externally assessed and certified in accordance with ISO 9.001 in 2009.

2 A modern campus university on Berlin's doorstep

The university opened its doors in 1991 with just 17 students on the mechanical engineering degree programme. Today there are around 3,600 students (as of winter semester 2018/2019), ensuring that the Technical University of Applied Sciences Wildau ("TH Wildau" for short) keeps its familiar atmosphere.
On a modern and compact campus with a direct rail connection to Berlin, aspiring academics enjoy an ideal environment for their studies in a range of disciplines covering the natural sciences, engineering, economics, law, business administration and management.

Figure 1 Library building of the TH-Wildau

[1] Prof. Dr.-Ing. Jörg Reiff-Stephan, Technische Hochschule Wildau

3 Practical and application-oriented

Degree programmes at a university of applied sciences are very practically oriented. The practical orientation of our degree programmes and teaching is one of our distinctive characteristics. Students can carry out practical exercises and experiments with top-quality laboratory and computer technology. An optimal study environment allows creativity and enthusiasm for research to flourish.

4 Close interaction between the university and the economy

Its potential for scientific innovation and development as well as its practically oriented academic offerings are what make TH Wildau a desirable partner for innovative small and medium-sized businesses, as well as large international firms.
Collaborations include input into designing the curricula for our degree programmes, to project work for students within the companies and joint research activities. This allows students to gain valuable practical experience in various fields even before they have completed their studies, thus making them an attractive choice for businesses when starting their careers.

5 Excellent international networking

An international and intercultural outlook shapes each working day at the university. Young people from over 60 countries from around the world study at the TH Wildau. One in five students come from abroad (as of winter semester 2018/19).
TH Wildau actively promotes international exchanges for students and researchers. It is for this reasons that the university cooperates with more than 70 partner universities around the world. We have contacts through our traditional partnerships Eastern and Southern Europe as well as links to Asia, Latin America, the Arab world and Africa. Students have a wide range of attractive options for spending a semester studying or working abroad, for learning foreign languages and interacting with other cultures.

Figure 2 International Week TH Wildau

6 A strong research university

Since 2001, TH Wildau has been among the strongest research universities in Germany. Academics are working in over 40 research groups dealing with the latest topics in applied and fundamental research. This has given the university its reputation as a centre of excellence in key scientific disciplines. The university specialises in the research fields of applied biosciences, information technology/telematics, optical technologies/photonics, production and materials, transport and logistics as well as management and law.

7 International quality standards

In accordance with the university's mission, quality, quality development and quality assurance in teaching, research and administration are measures of our interactions on all levels. They provide the necessary transparency and form the basis for comparisons within our university and with others. The quality management system used by TH Wildau has been certified according to education standard DIN ISO 29990 since 2012. This gives students objective confirmation that the teaching in Wildau conforms to recognised international standards.

8 Healthy university

In cooperation with health insurer "Techniker Krankenkasse", TH Wildau is pursuing its vision of a health-conscious university in a sustainable way. Under our "healthy university" motto we intend to develop a holistic culture of healthy living at all levels, increase health literacy, and give our students and graduates the awareness to spread a message of healthy living to their future work places in business, science and administration.

9 Welcome SusRES'2020

Renewable Energy Systems are, in times of climate change, a fundamental technology to reduce the usage of climate-damaging fossil energy sources with limited availability and replaces them width sustainable energy sources. Furthermore, regenerative energy sources can bring solutions to power hamlets as "off-the-grid electricity solution" in regions without power supply. Together with the increasing role of digitization and the development of smart applications, new technologies arise, which will play an ever-increasing role in future energy issues. This paradigm shift places new demands on research and education and stretches well beyond national borders. The Conference forms a platform for addressing these topics and for exchanging scientific expertise and pedagogical approaches within university teaching.

To all participants we wish a successful conference. You are welcomed to join our network and Center of "Sustainable, renewable Energy Systems". Please take care of you and have a lot of flourishing discussions with your partners of the region and worldwide. We still are in one global world as one nation in mind.

SI-1a
Design, construction and experimental investigation of a linear Fresnel concentrator for sustainable energy services in Sub-Saharan Africa

Kokouvi Edem N'Tsoukpoe [1], Gaëlle Kafira Ko[2], Quentin Falcoz[3], Yézouma Coulibaly[4]

Abstract

Concentrating solar power (CSP) is considered as one of the promising ways for future sustainable electricity generation, especially in the Sahel region, which is characterized by high direct solar irradiation, but also severe and acute energy poverty. In this paper, we focus on the linear Fresnel system, which it is probably the simplest CSP technology and presents the lowest investment costs. However, it is the less investigated CSP technology and several authors expect significant cost reduction of this technology. Therefore, deeper knowledge on the technology is required. We aim at investigating the coupling of a linear Fresnel system with various energy processes in order to bring out its interests for the Sahel region and, hence, provide sustainable energy services such as electricity generation for rural areas, cooling and refrigeration via sorption cold production, hot water or steam supply for semi-industrial or industrial processes. We have built a linear Fresnel collector of 7.5 m². The receiver has been designed as a trapezoidal receiver with multi-tubular absorber; it has been experimentally investigated in order to determine its thermal performance, especially the heat loss coefficients. *Jatropha curcas* oil, a locally produced non-edible vegetable oil is used as heat transfer fluid. The concentrator has been characterised in order to find its optical, thermal and global efficiencies. Paths for the prototype performance improvement have been identified and examined.

1 Introduction

The average electrification access rate in West African Sahel countries is relatively low compared to the average access rate in West Africa, which is however the Sub-Saharan region with the highest electrification access rate [1]. The situation is worse in rural areas (rural electrification rate: 12% in average, with high variation from one country to another, where about 60% of the population actually lives [2]. Concentrating solar power (CSP) is considered as one of the promising ways for future sustainable electricity generation. Apart from electricity generation, the high temperature heat generation may also be imagined for industrial applications that require heat at a temperature level that is not achieved by common solar thermal collectors. Many African countries, especially in the Sahel region, show high potential for CSP plants because of high direct solar irradiation. The initial capital costs, combined with the complexity of the technology, is considered to be the main obstacle to the development of CSP in devel-

[1] Dr.-Ing. habil. Kokouvi Edem N'Tsoukpoe, Laboratoire Énergies Renouvelables et Efficacité Énergétique (LabEREE), Institut International d'Ingénierie de l'Eau et de l'Environnement (2iE), Ouagadougou, Burkina Faso, corresponding author : edem.ntsoukpoe@2ie-edu.org / n_christedem@2ie-edu.org

[2] Dr.-Ing. Gaëlle Kafira Ko, LabEREE, 2iE, Burkina Faso / PROMES CNRS, France

[3] Dr.-Ing. Quentin Falcoz, PROMES-CNRS, 7 rue du Four Solaire 66120 Odeillo-Font-Romeu, France

[4] Prof. Yézouma Coulibaly, LabEREE, 2iE, Burkina Faso

oping countries [3,4]. In addition, to date, CSP technologies have been shown to be economically viable only for high power plants, thus requiring high investment costs. As a result, many of these countries cannot easily invest in this type of facility. Furthermore, the large number of "isolated" rural communities (electrically speaking, for example, there are about 8000 villages in Burkina Faso representing more than ⅔ of the country's population), distant from each other but requiring small powers (a few tens to a few hundred kW_e). Finally, the skills required for the implementation for such power plants are not well currently widely spread in Africa. All this leads to opting for small power plants, given the fact that the construction of electricity networks to connect several dispersed localities is very expensive.

The term "concentrating solar power", which actually includes both concentrating solar thermal (CST) and concentrating photovoltaic (CPV) energy conversion, is often used synonymously with "concentrating solar thermal power" [5]. We adopt this restricted definition in this paper. The basic concept of CSP technology is to generate electricity from the driving of a turbine by steam or vapour, in the same way as in conventional gas, coal or nuclear power plants with a major difference: the steam or the vapour is generated using solar thermal energy. Indeed, CSP use mirrors to concentrate direct solar radiation on a point, the receiver, where the temperature increases (typically above 250 °C); then, the obtained thermal energy is collected by a heat transfer fluid and delivered to a power block, which is in most cases a Rankine cycle for electricity generation. Currently, a part from concentrating photovoltaic, which is not usually listed, four most common CSP technologies are available: parabolic trough, central receiver system or power tower system, linear Fresnel and parabolic dish.

A literature review on small scale concentrating solar power in the world, which we carried out [6], allowed us to count 35 built or planned plants whose electrical power is between 1 kW_e and 500 kW_e. Only a very small number of these small scale CSP are actually operating in the field because of a lack of maturity in terms of an optimized system adapted to electrification, especially for rural areas. The operability of these demonstration units in real situations is necessary to assess their relevance. Apart from South Africa, we could not identify small scale CSP in Sub-Saharan Africa. Hence, the development of micro-concentrating solar power (μ-CSP) (electrical power ≤ 100 kW_e) for the production of electricity for mini-grid and other sustainable energy services has received particular attention in our Institute. The main advantage of CSP technology over photovoltaic is the possibility of storage to produce electricity at times when the resource is unavailable or insufficient. Thermal storage is indeed much cheaper than direct storage of electricity in batteries and the management of the outputs of such a storage is simpler than that of an electrochemical storage (electrical batteries), not to mention the fire safety issues. Another point of attraction for CSP is the fact that a large part of the components of such plants can be mobilized or manufactured locally with local labour, a fact that offer a room to play on the final costs of production.

Of the four CSP technologies, parabolic dish and parabolic troughs require rounded mirrors (non-planar or curvilinear) while power tower and linear Fresnel systems use flat mirrors. Since flat mirrors are readily available in local markets, power tower and linear Fresnel have been considered as the best choice for local μ-CSP development. The fact that the receiver is fixed receiver avoids the need of rotary joints for the heat transfer fluid [5], since skills for high temperature piping are not well spread in the region whereas the local feasibility is a matter of priority in our research approach. These two technologies are the subject of our current studies: the linear Fresnel for relatively low temperature applications and the power tower plant for relatively high temperature applications. The concept of the proposed power tower has been

developed in the framework of the CSP4Africa project [7]. In this paper, we focus on the linear Fresnel technology, which has the advantage of being simple with a low wind load, and would require lower investment costs compared to other CSP technologies.
In the similar way as CSP4Africa, which is devoted to power tower technology, we have initiated activities around a linear Fresnel concentrator with high local content. We aim at developing a pilot of a cost-effective µ-CSP plant for sustainable energy services and by designing and experimenting their components using local low cost materials. The purpose is the study of the coupling of a linear Fresnel concentrator with various energy processes to highlight the interest in the Sahel part of West Africa. “Low-tech” is assumed from the start; the idea being to give up the “high performance Concorde” but to which the users cannot resort because of the prohibitive costs. The approach is specifically designed to address energy access challenges in rural areas in the sub-Saharan region:

- Learning by doing approach with use of local skilled mankind
- Local manufacturing of the components of the system by using as much as possible locally available materials

Our ultimate target is the investigating the coupling of a linear Fresnel system with various energy processes in order to bring out its interests for the Sahel region and, hence, provide sustainable energy services such as electricity generation for rural areas, cooling and refrigeration via sorption cold production, hot water or steam supply for semi-industrial or industrial processes.
In this paper, we present the project and report the current achievements. The faced challenges and the options made from the beginning of the project up to now are briefly presented.

2 The approach to the design of a linear Fresnel collector in Burkina Faso

The first prerequisite is the evaluation of the relevance of the application on the targeted location, as unlike flat plate photovoltaic (PV), CSP are not relevant everywhere: they are best suited to areas with high direct normal irradiation (DNI: typically more than 2000 $kWh \cdot m^{-2} \cdot year^{-1}$), high percentage of clear sky days, in locations that do not have high humidity, smog or dust [5]. 17% of the land area of ECOWAS (Economic Community of West African States) countries received yearly DNI of more than 2000 $kWh \cdot m^{-2}$ while 38% enjoys an average yearly DNI of about 1600 $kWh \cdot m^{-2}$ [8]. Therefore, the West African region, especially the Sahel part, shows a high potential for solar concentrating applications.
A linear Fresnel system consists of two main parts: a concentrator, which constitutes the solar field, and a receiver on which direct solar radiation is concentrated by the reflectors of the concentrators. The heat collected at the receiver is transferred to the target process in order to be converted into the form in which it is used.
We have planned to implement on our campus a pilot of linear Fresnel collector with a capacity of 100 kW_{th}. Within the research work, we target a maximum operating temperature of 210 °C. This temperature is relatively low but the target here is to master the process at relatively low temperature level before increasing the temperature level later. As a first step, we have designed and built a prototype of linear Fresnel collector with a capacity of few kW_{th}. This is prototype is used to acquire a better knowledge of the operation of a linear Fresnel collector. The experimental results from the prototype are collected to supply a model of the pilot that has been developed [9]. This will be used to optimised the design of the final pilot, so the pro-

totype of linear Fresnel collector is to be seen a tool for the design and optimisation of the projected pilot, which has a modular structure.

The built prototype is shown in Fig.1 and its characteristics are summarised in Table 1. The used mirrors are the ones readily available on the local market. We have measured their reflectance and found a solar weighted reflectance of 0.72–0.92, depending on the sample [9]. The mirrors have been assembled in five blocks, each of which consists of five rows of mirrors (Fig.2a). The large number of rows is the result of the necessity to reduce blocking and shading losses. In addition, the size of the mirrors has been selected so that they can be easily purchased on the local market and easily handled manually. Initially, each block was thought to be associated to a specific tracking unit but finally, only one tracking unit is use for the whole concentrator.

Figure 1. Prototype of linear Fresnel concentrator at 2iE-Kamboinsé.

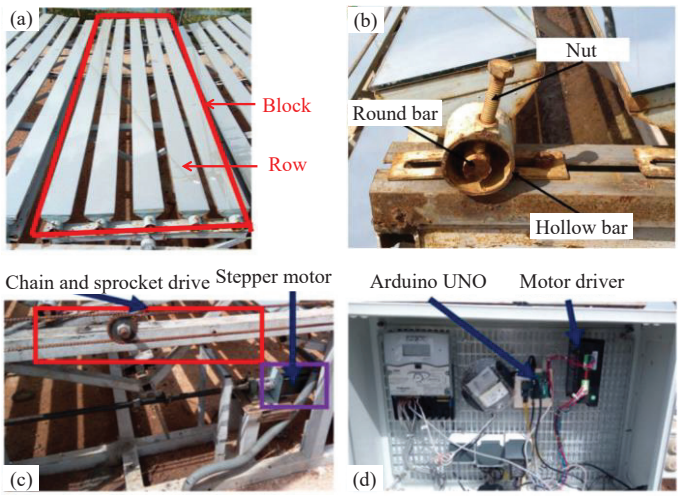

Figure 2. Components of the tracking system of the prototype (a) a block, (b) mirror row tilting mechanism, (c) tracking mechanism and (d) control board.

Concentrator frame	Dimension (l × w × h)	4 m × 3.1 m × 0.7 m
	Area	12.4 m²
	Material of the frame	Steel
Reflecting surface	Shape of mirrors	Flat
	Dimension of each mirror element (l × w × h)	0.75 m × 0.10 m × 0.003 m
	Number of mirrors elements	100
	Total (reflecting) area of the mirrors	7.5 m²
	Number of block of mirrors	5
	Total (reflecting) area of a block of mirrors	1.5 m²
	Reflectance of mirrors	0.72–0.92
Receiver (overall)	Shape	Trapezoidal
	Size of the receiver (l × w × t)	3.2 m × 0.28 m × 0.2 m
	Size of the glass (l × w × t)	3.2 m × 0.28 m × 0.003 m
	Glass transmittance (solar weighted)	0.75
	Insulation material	Glass wool
	Material of the frame	Steel
Absorber	Number of tubes	7
	Diameter of a tube	16 mm
	Length of the absorber	3.0 m
	Surface of the absorber	0.336 m²
	Geometric concentration ratio	22
	Material of the tubes	Copper
	Painting	Solkote HI/SORB-II
	Absorptance of the absorber (solar weighted)	0.87
	Emissivity of the absorber	0.23

Table 1. Summary of the characteristics of the prototype of linear Fresnel collector.

For the receiver, a horizontally downward receiver design has been adopted. It is a multi-tubes trapezoidal cavity receiver (Fig.3). This kind of receiver, which is preferred in low and medium temperatures up to 300 °C [10], has lower cost compared to evacuated tube receivers and is simple to be built. There is no absorber plate in front of the tubes so that they directly absorb the solar irradiation from the reflectors. Hence, the absorber consists of seven copper pipes with external diameter of 16 mm. To increase the absorptance of the absorber, a selective solar absorbing paint (Solkote HI/SORB-II [11]) has been applied on the copper tubes. A mirror is installed on each side of the absorber to operate as a secondary reflector (Fig.3).

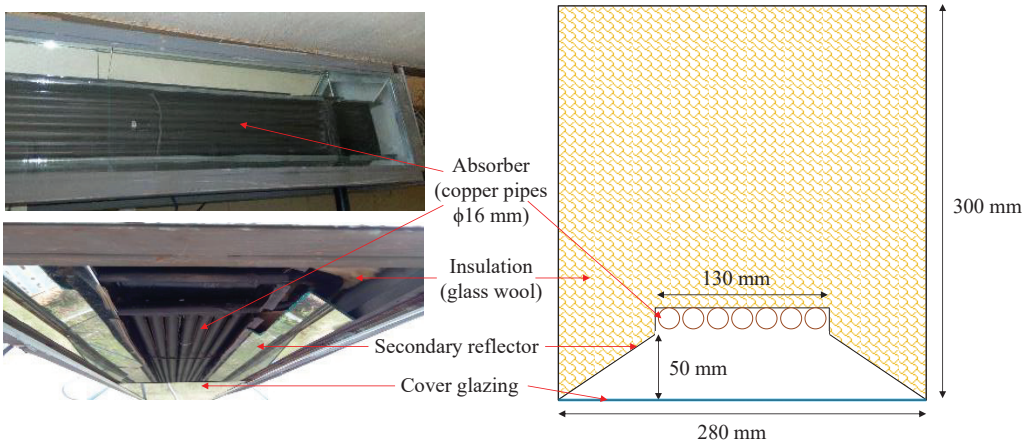

Figure 3. Detail view of the receiver.

A single axis north–south oriented tracking system was designed to drive the system using a single stepper motor for the whole concentrator. The stepper motor is controlled with an Arduino UNO via a microcontroller board (Fig.2d). The tracking system is an open loop operating with the solar position algorithm (SPA) [12], which has replaced the Michalsky's algorithm that was originally used but led to some accuracy challenges. During the solar tracking, all the blocks rotate at the same velocity thanks to the chain and sprocket drive (Fig.2c). The stepper motor is coupled with a threaded rod that is connected to the central block with nuts (Fig.2b,c).

For the heat transfer fluid and the thermal storage material, we consider now the promotion of a vegetable oil that is locally produced: *Jatropha curcas* crude oil (JaCCO). The main advantage of a possible use of JaCCO as thermal storage or heat transfer fluid is that the oil is locally produced and available at low cost [13]. Since JaCCO has never been used as heat transfer or thermal storage medium, we have performed some preliminary studies to check its potential to be used as a heat transfer fluid or thermal storage material in CSP plants. First results show that *Jatropha curcas* oil is a promising heat transfer fluid and storage material for CSP plants [13,14]. The main drawback of using oils is the fact that they are flammable.

In the case of use of the linear Fresnel collector for electricity generation, a power block is needed. It has been decided to acquire a commercially available ORC as a local development of such a unit is not foreseen at this stage. Given the Sahel context, a dry cooler has been selected with the ORC in order to avoid water cooling tower that would result in significant water consumption.

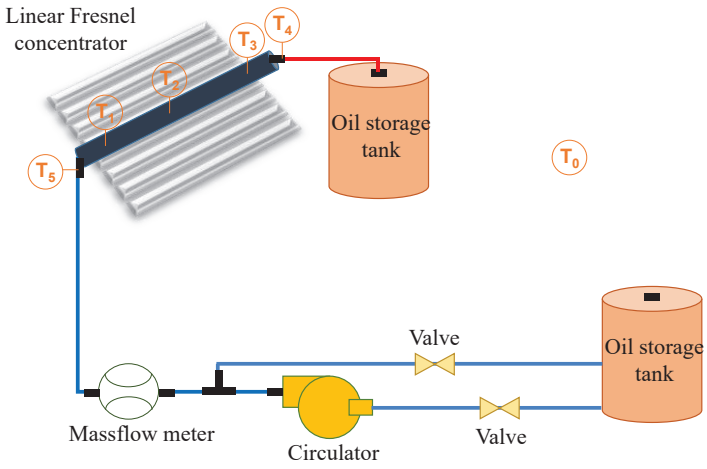

Figure 4. Experimental set-up

3 Experimental results

3.1 Experimental set-up

The prototype of linear Fresnel collector as described above is operated under various conditions in order to quantify its thermal losses. The prototype allows the adjustment of the position of the receiver at various heights above the concentrator. For the tests, the height of the receiver above the concentrator has been set to 3 m. The prototype has been instrumented, to be able to measure temperatures (accuracy: 0.1 °C) at the inlet and outlet of the receiver (Fig.4). The mass flow rate of oil circulating in the receiver was measured using a mass flow

meter (F050S239CQFZFZZZZ, EMERSON, uncertainty: ±1%) and the values are recorded every 5 min. Beam solar irradiance was measured by pyrheliometer (CHP1 KIPP and ZONEN) and with data record every minute.

3.2 Experimental procedure

The experimental procedure to determine the overall heat loss coefficient of the receiver is similar to the one described by Singh et al. [15]. Jatropha oil was heated in an oil storage tank using a gas burner and circulated at a controlled flow rate through the absorber tubes. The concentrator is covered by a tarpaulin to avoid reflection of any solar irradiance, from the concentrator, on the receiver. The oil flow rate was kept constant during the whole experiment. In order to estimate the heat losses at different temperatures, the tests have been performed at pre-defined receiver inlet temperatures. Hence, for any test, the oil is heated until the selected temperature while a manual stirrer is used to promote temperature homogeneity in the oil storage tank. The useful data are the one recorded during a steady state i.e. when the temperature at the inlet of the absorber and the absorber wall temperature remain practically constant (changes < 1 °C) for a duration equals to 4 times the residence time of the fluid in the absorber. Note that there was no control of the air flow rate along the bottom of the absorber during the test so that it was subject to the speed of wind. The decrease in temperature observed through the passage of oil through the receiver gives the magnitude of the heat loss Q_l, which may be estimated as follows (1):

$$Q_l = mC_p(T_i - T_o) \quad (1)$$

where m is the mass flow rate heat transfer fluid and C_p is the specific heat capacity of the heat transfer fluid; T_i and T_o are the heat transfer fluid temperature at the receiver s' inlet and outlet, respectively.

The overall heat loss coefficient U_l was then derived as follows (2) [15]:

$$U_l = Q_l/[A_{abs}(T_m - T_{amb})] \quad (2)$$

where $T_m = (T_i + T_o)/2$.

The receiver is tested over a temperature range of 50 °C to 100 °C because the used pump was not suitable for temperature higher than 100 °C.

3.3 Results and discussion

Figure 5 shows the evolution of temperature for a test during which the receiver inlet temperature was 87±0.5 °C. The resident time during test was 4 min. From 11:34 to 11:42, i.e. during 8 min, the inlet and outlet temperatures are relatively constant so that an average thermal loss may be evaluated to 223 W (Fig. 5).

After several tests, the obtained overall heat losses for individual differences of the oil mean temperature and ambient temperature are depicted in Fig. 6.

Obviously, heat losses increase with the temperature difference between the oil and the ambient temperature. However, the values obtained show a cloud that may question the repeatability of the results, especially around a temperature difference of 40 °C. This is probably due, among other things, to the fluctuation of wind velocity as the tests was conducted under outdoor conditions. Therefore, future tests should take care for a better control of the ambient conditions.

3.4 Estimation of the capacity of the concentrator

The capacity of the single concentrator may be estimated based on measured data using equation (3):

$$Q_u = \eta_{opt} \cdot I \cdot A_c - U_r \cdot A_{abs} \cdot (T_m - T_{amb}) \quad (3)$$

where I is the solar direct normal irradiance, A_c is the surface area of the reflecting area, A_{abs} is the surface area of the absorber, U_r is the heat loss coefficient of the absorber, T_m and T_{amb} are the absorber and ambient temperatures, respectively. η_{opt} is the optical efficiency and is given by Equation (4):

$$\eta_{opt} = \rho \cdot \tau \cdot \gamma \cdot \alpha \cdot K \quad (4)$$

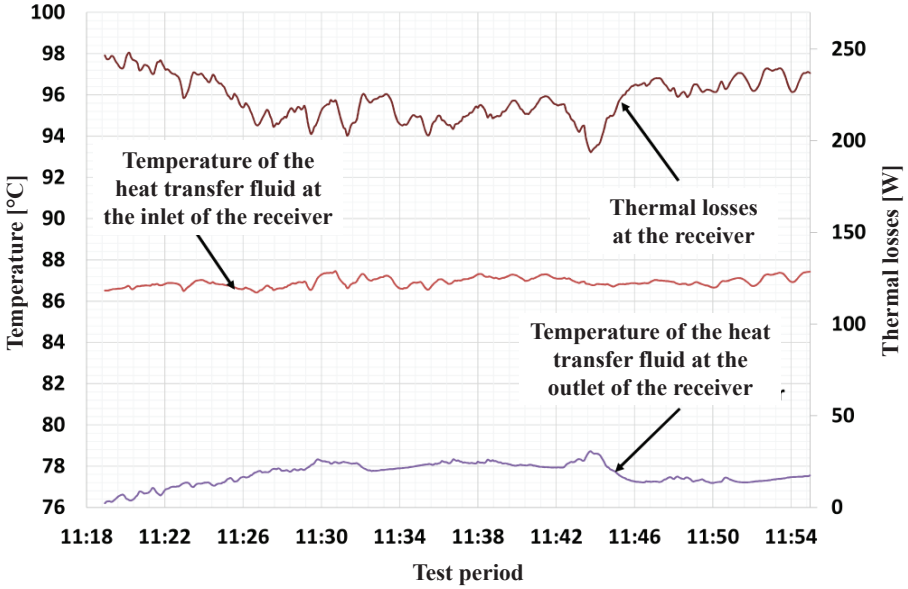

Figure 5. Temperatures and heat losses during a test.

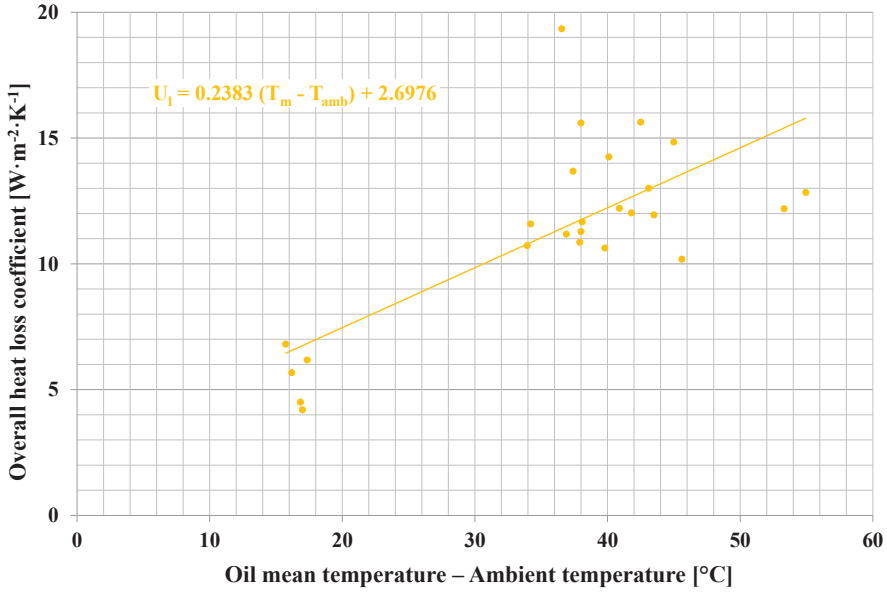

Figure 6. Overall heat loss coefficient as a function of the difference of the oil mean temperature and ambient temperature.

where ρ is the mirror reflectance, τ is the transmittance of the receiver glass, α is the absorbance of the absorber, K is the incidence angle modifier, γ is the intercept factor, which accounts various optical losses such as tracking error, shading and blocking.
ρ, τ and α have been already measured [9]. The heat loss coefficient may be estimated based on data in Fig. 6. For this first estimate, we assume an intercept factor of 1. The incidence angle modifier *K* and the solar beam *I* depend on the assumed design conditions. The majority of the studies use the conditions at the vernal equinox or the summer solstice [16]. In the present case, we consider, at solar noon, both of these conditions and also the day of the solar zenith passage (i.e. when the declination equals the latitude of the collector = 12°27' N, 1°33' W). This is April 23th, when we consider its occurrence in spring or summer. *K* is the product of the longitudinal incidence angle modifier and the transversal incidence angle modifier, are derived from ray-tracing for our prototype [9]. The values of DNI are the average of three years (2011–2013) measured data at the site of 2iE Kamboinsé. To estimate the heat losses, we consider a temperature change of 100 °C in the receiver, that is an inlet temperature of 110 °C and an outlet temperature of 210 °C. The results are presented in Table 2.

Design point	Vernal equinox	Sun at the zenith	Summer solstice
DNI [W·m-2]	460	530	490
Ambient temperature [°C]	41.6	41.8	34.3
ρατγ	0.535	0.535	0.535
KL	0.83	1	0.84
KT	1	1	1
Incidence angle modifier K	0.83	1	0.84
Estimated Ul [W·m-1·K-2]	31	31	33
Heat losses Ql [W]	1262	1226	1379
Useful heat Qu [W]	270	901	273

Table 2. Estimation of the capacity of the linear Fresnel collector under various design point conditions.

The analysis shows that the capacity of the prototype is about 0.3 kW, based on the performance at vernal equinox and summer solstice. It appears that the heat losses are relatively large compared to the useful heat (Table 2). This is either due to the design of the collector or to the correlation used to estimate the heat losses. Indeed, the correlation has been derived from the results of the thermal losses of the receiver, which show however, some repeatability issues, as discussed in the previous section. Furthermore, the correlation has been extrapolated to a temperature level that has not been explored during the tests due the fact that the used pump could not perform above 100 °C. It is therefore necessary to implement the tests at higher temperature while ensuring their repeatability and accuracy.

4 Conclusion

The designed prototype of a linear Fresnel concentrator has been presented and discussed. It has been constructed and has been experimentally investigated in order to quantify its thermal losses. This prototype represents a research and development tool that offers an opportunity to demonstrate the feasibility of a micro-CSP plant in West African Sahel by analysing the system through various aspects such as capacity building, technical and economic issues. Its replication potential, if used, would generate local income and jobs, contributes to energy-water-

food security and poverty alleviation. The capacity of the prototype at the moment could not be accurately estimated due to some experimental limitations. Further experiments are required to overcome these limitations.

5 References

[1] International Energy Agency (IEA). World Energy Outlook (WEO) 2018 Electricity Database: Electricity access in 2017. International Energy Agency (IEA); 2018]. Available from: www.iea.org/media/sdg/WEO2018-Electricity-Database.xlsx.

[2] Worldometers. Population of Western Africa (2019) - Worldometers 2019 [cited August 30, 2019]. Available from: www.worldometers.info/world-population/western-africa-population/.

[3] Amer M, Daim TU. Selection of renewable energy technologies for a developing county: A case of Pakistan. Energy Sustain Dev 2011;15:420–35.

[4] Ziuku S, Seyitini L, Mapurisa B, Chikodzi D, van Kuijk K. Potential of concentrated solar power (CSP) in Zimbabwe. Energy Sustain Dev 2014;23:220–7.

[5] Lovegrove K, Csiro WS. 1 - Introduction to concentrating solar power (CSP) technology. In: Lovegrove K, Stein W, editors. Conc. Sol. Power Technol., Woodhead Publishing; 2012, p. 3–15 [cited February 25, 2015]. Available from: www.sciencedirect.com/science/article/pii/B9781845697693500017.

[6] Seshie YM, N'Tsoukpoe KE, Neveu P, Coulibaly Y, Azoumah YK. Small scale concentrating solar plants for rural electrification. Renew Sustain Energy Rev 2018;90:195–209.

[7] N'Tsoukpoe KE, Azoumah KY, Ramde E, Fiagbe AKY, Neveu P, Py X, et al. Integrated design and construction of a micro-central tower power plant. Energy Sustain Dev 2016;31:1–13.

[8] Ramde EW, Azoumah Y, Brew-Hammond A, Rungundu A, Tapsoba G. Site ranking and potential assessment for concentrating solar power in West Africa. Nat Resour 2013;4:146–53.

[9] Ko KG. Study and dynamic modelling of linear Fresnel concentrator [Étude et modélisation dynamique d'un concentrateur à miroir linéaire de Fresnel]. PhD. Institut International d'Ingénierie de l'Eau et de l'Environnement, 2019.

[10] Bellos E. Progress in the design and the applications of linear Fresnel reflectors – A critical review. Therm Sci Eng Prog 2019;10:112–37.

[11] SOLEC-Solar Energy Corporation. Solkote selective solar absorbing paint technical specifications. 2019 [cited August 31, 2019]. Available from: www.solec.org/solkote/solkote-technical-specifications/.

[12] Reda I, Andreas A. Solar Position Algorithm for solar radiation applications. Colorado: National Renewable Energy Laboratory; 2008]. Available from: www.nrel.gov/docs/fy08osti/34302.pdf.

[13] Kenda ES, N'Tsoukpoe KE, Ouédraogo IWK, Coulibaly Y, Py X, Ouédraogo FMAW. *Jatropha curcas* crude oil as heat transfer fluid or thermal energy storage material for concentrating solar power plants. Energy Sustain Dev 2017;40:59–67.

[14] Gomna A, N'Tsoukpoe KE, Le Pierrès N, Coulibaly Y. Thermal stability of a vegetable oil-based thermal fluid at high temperature. Afr J Sci Technol Innov Dev 2020;0:1–10.

[15] Singh PL, Sarviya RM, Bhagoria JL. Thermal performance of linear Fresnel reflecting solar concentrator with trapezoidal cavity absorbers. Appl Energy 2010;87:541–50.

[16] Wirz M, Roesle M, Steinfeld A. Design point for predicting year-round performance of solar parabolic trough concentrator systems. J Sol Energy Eng 2013.

SI-1b
The contribution of solar energy to environmental protection and poverty reduction.

N ' detigma Kata[1], Hodo-Abalo SAMAH [2] and Gabriel Jean-Philippe TEVI[3]

1 Abstract

The neighborhood population pressure one Djamdè reserve is investigated in this paper. After noting and observing changes in the microclimate of Djamdè, a survey was conducted. At the end of this survey, market gardening was proposed not only to remove the increased pressure on the reserve, but also to provide an income generating activity for this very vulnerable population.

The collection of data on existing wells in the vicinity of the site shows that the availability of water for market gardening can be ensured by drilling. A comparative study between a pumping system with a petrol-powered pump and a photovoltaic system in the town of Kara has been carried out.

The solar pumping system is by far the most interesting for Djamdè site. Considering the very high initial investment cost of the components of the solar pumping system, its size can be reduced by organizing and planning the watering of the crops.

Keyword: Renewable energies, environmental protection, solar pumping.

2 Introduction

The majority of the population of Kara (North of Togo) are farmers [1]. But the development effort in this farming sector is reduced by many problems [1] [2]. Indeed, most of the work is done manually. The production capacity using this method is drastically limited. Their capacity to process agricultural products is embryonic with a reduced water control [3]. This results in a significant loss of production, expedited crop sales, flooding in the wet season and drying out of surface water in the dry season. The few irrigation systems for market gardening are also forced to shut down because of this drying up of easily exploitable surface water.
All these difficulties mark a part of the year in northern Togo called the "lean season" characterized by the absence of agricultural activities, food and financial difficulties in several families. During this period protected areas such as Djamdè's neighborhood break the law and cut firewood and make charcoal for sale in surrounding towns [3] [4]. This reserve, which contributed to the regulation of the microclimate in the area [4], is gradually losing this role and over the years signs of global warming have been felt.
The purpose of this study is to formulate a mature and economically viable technique that will enable the residents of the Djamdè Reserve to resolve their difficulties during the lean season

[1] University of Kara, Laboratoire Electronique, Informatique, Télécommunication et Energies Renouvelables Université Gaston Berger, Saint-Louis, Senegal

[2] University of Kara, Laboratoire sur l'Energie solaire LES/GPTE, Université de Lomé, Lomé -TOGO

[3] Laboratoire Electronique, Informatique, Télécommunication et Energies Renouvelables Université Gaston Berger, Saint-Louis, Senegal

while relieving pressure on the reserve. The proposed solution for solar-powered irrigation is the result of a comparison study of different irrigation systems in the town of Kara.
Solar-powered irrigation as a development tool will enable the population to diversify their source of income and increase the autonomy of women, who are the main actors in the cutting of fire-wood.

3 Methodology

The diagram below (figure 1) summarizes the process followed in this work. This study involves two sites: The first one is located in the Djamdè area. The climatic conditions, which are very specific to the area due to the presence of the nature reserve, have changed in recent years. A survey was then carried out among the population followed by a visit to a certain part of the reserve to witness the pressure exerted by the local residents on the reserve [3] [4]. The data collected on the increased pressure from the population led to the proposal of a market garden-ing system. Thus, in order to provide this very vulnerable population with an economically viable and ecologically acceptable solution, a second site was defined in the town of Kara. It is an area of 0.75 hectares on the banks of the Kara's River where market gardening was already practiced using water from the river through a small generator (figure 2) for water pumping.
Therefore, the study ascertained the availability of water in the vicinity of the surveyed sites by recording a sample of wells and boreholes, their depths and, for wells, the time of year they dry out. Rainfall data were provided by the ASECNA metrological station of Niamtougou, supple-mented by sunshine data obtained from the RETScreen International database.

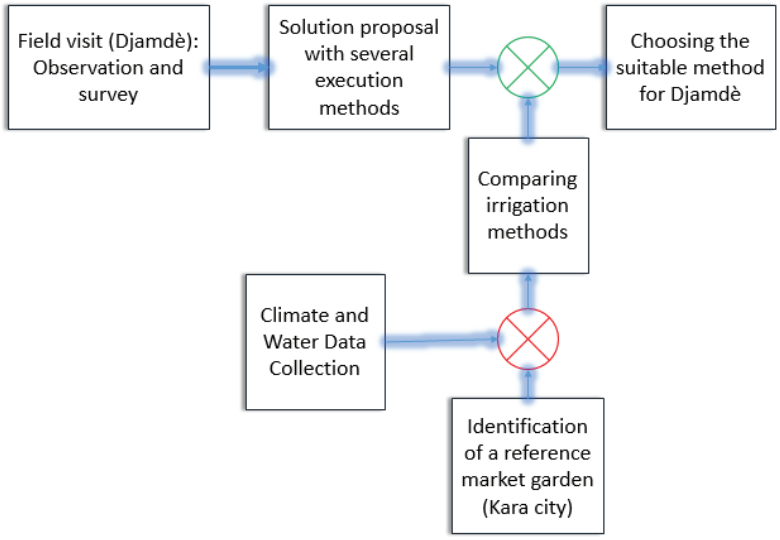

Figure 1: diagram of the process followed in this work

Figure 2: moto pump generator set

The amount of water needed for irrigation is determined based on different crops water require-ments [7]. The water requirement (in mm or liters/m²) is then calculated by the equation (1):

$$\text{Daily water requirement of a crop} = ETP \times K_C \times Surface \quad (1)$$

Where K_C is culture coefficient and ETP is potential evapotranspiration
From this flow rate and the manometric height (HMT), the daily energy required (E_{elec}) to extract this amount of water is easily determined by the formula (2):

$$E_{elec} = \frac{Hydraulic\ constant \times daily\ flow\ rate \times HMT}{Motopump\ unit\ efficiency} \qquad (2)$$

The manufacturer's datasheet allow to determine the generating set from the previous calculations. The photovoltaic field power required for a pumping system is given by the equation (3):

$$P_{modul} = \frac{E_{elec}}{irradiation \times (1 - losses)} \qquad (3)$$

To estimate the costs of the irrigation system, an economic analysis is necessary. In this case, this analysis takes into account the information collected on the study site. Two types of information can be extracted from the economic analysis: the updated cost, significant from the investor's point of view and the annual cost, for the system user's evaluation. The updated cost incorporates the cost of capital financing, operating, maintenance and replacement costs over the expected life of the pumping system. Thus, to investigate and propose an economically acceptable pumping system for Djamdè, the determination of the updated cost provides a good indicator of choice. Indeed, some systems such as solar-power systems may require a large initial investment and relatively low operating and maintenance costs, while others have the opposite situation. Investments for the installation and operation of an irrigation system include one-off and annual investments [8].

The update of one-off costs is calculated from the equation (4):

$$D_{acs} = D_{ini}(1 + \sigma)^{-\alpha} \qquad (4)$$

With D_{acs} the simple present value of the expenditure, D_{ini} the initial value of the expenditure, σ the update rate and α the lifetime of the expenditure component. The update rate is a difference between the investment rate and the inflation rate.

The annual update costs is obtained from the equation (5) where D_{acu} is the uniform present value of the annuity, D_{ann} the value of the annuity and n the lifetime of the system.

$$D_{acu} = \frac{D_{ann}(1 - (1 + \sigma)^{-n})}{\sigma} \qquad (5)$$

The value of the annuity is the product of the value of the annual expenditure by a coefficient called the annuity coefficient calculated by:

$$Coeff.ann = \frac{(1 + i)^n \times i}{(1 + i)^n - 1} \qquad (6)$$

With i the investment rate.

4 Results and discussions

At the date of publication of this article, the study is still ongoing. So the results we present here should be considered as preliminary results.

The Djamdè field visit made it possible to observe the onset of desertification due to woodcutting. Figure 3 shows the cutting of wood on the reserve and its purpose for sale. The survey also revealed that some streams/rivers that not dry out are drying out more rapidly as they are gradually being blocked by the erosion phenomenon. This wood cutting activity is mostly carried out by women who are the most exposed to financial insecurity.

Figure 3: Woodcutting in the reserve of Djamdè

Figure 4: Sale of cut firewood

The proposed market gardening solution will not only release the pressure on the reserve but will also guarantee the local resident alternative and income-generating activities with a low impact on the environment.
The figure 5 shows the different depths of wells and drilling in the vicinity of the study areas as well as the periods during which they were dewatered.
Wells usually dug by hand are shallow due to the rocky structure of the subsoil. The permanence of water is not linearly related to the depth of the well. This can be explained by the morphology of the aquifer, which does not have the same depth at all levels. Thus with an adequate method for digging wells such as drilling, water availability will not be a major problem.

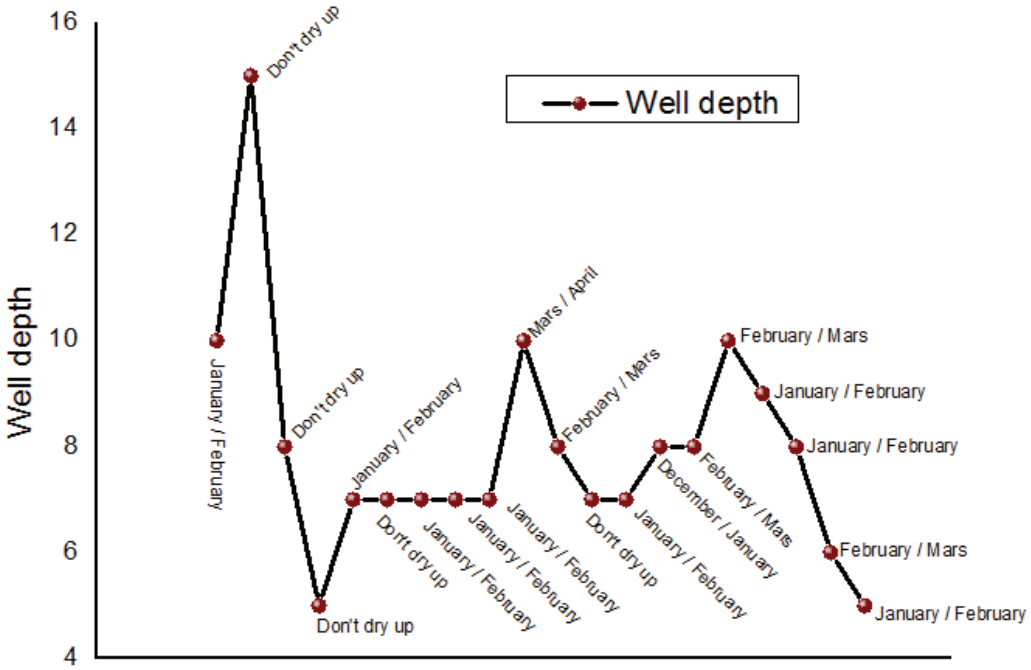

Figure 5: different depths of wells and drying up period.

The season in Northern Togo is divided into two: the rainy season covering the months from mid-May to the end of October and the dry season which extends from November to mid-May. During this dry season, the need for vegetables is provided by the market gardening products of Kara and other towns. At the study site in Kara, the most dominant vegetables are tomatoes, cabbage and lettuce. Based on these, we have determined their water requirement (figure 6).

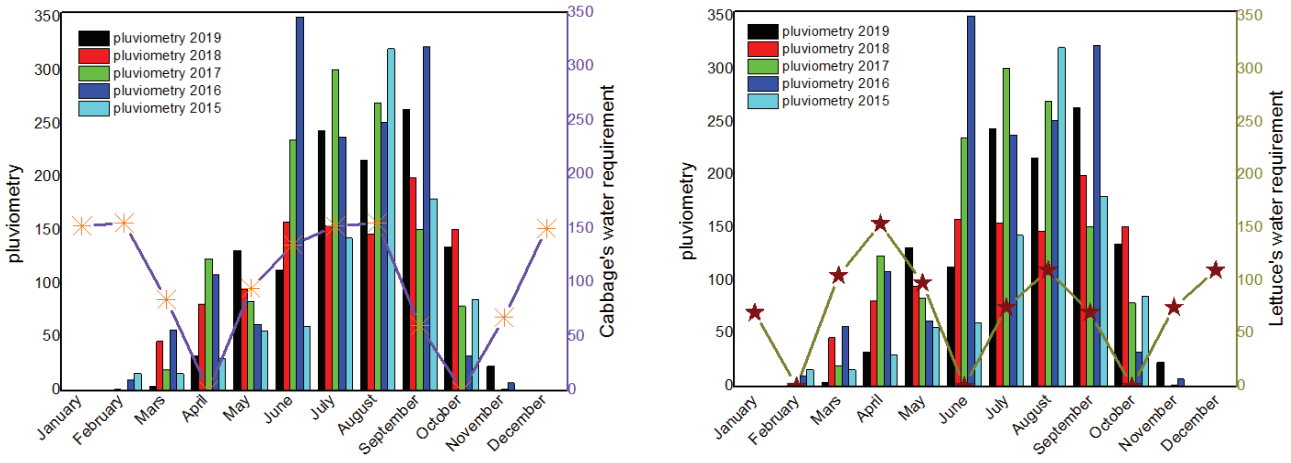

Figure 6: Water requirement for some vegetables

By comparing the water needs of the different crops and the rainfall in Kara, we can notice that the period from June to September is favorable for market gardening without irrigation. But this period cannot solve the problem of pressure on the Djamdè reserve.
Indeed, from the beginning of May to October, the residents of the study area, mainly agricultural, devote themselves to their work in the fields. The pressure on the reserve is at its peak in the other half of the year, matching with the absence of this agricultural work. Thus, for the market gardening solution to be effective, it should cover the months from October to May. As seen in the figure 6, to meet the water needs of different crops in this dry period, an irrigation system is needed. Several techniques can be used to irrigate market gardening [8]: buckets or watering cans (at the edge of a river or dam), manual pumps, motor pump units, pumps powered by solar or wind energy or the network. The first two not only require a great human effort but are also less suitable for large areas such as those under study. In fact, they are by far the most used in the city of Kara. This choice is specifically of a financial nature. For this reason, in order to cover the needs for fresh vegetables and fruit in the dry season, it is necessary to resort to the neighboring towns of Kara, including that of Benin and Ghana. On the other hand, the study site in Kara, thanks to the use of the generator, allows us to compare the performance of this system with that equipped with a solar-powered irrigation system.
Table 1 presents the components that made it possible to analyze the costs for this market garden operation on the Kara site.

	Solar pump unit			Gasoline Pump unit		
	Duration	**Valeur**	**Update Value**	**Duration**	**Valeur**	**Update Value**
Solar pump + tank		*993,09*				
Generating set					*114,59*	
Annuity	*15*	*130,57*	*1355,22*	*15*	*15,07*	*156,38*
Maintenance	*15*	*0,00*	*0*	*15*	*30,56*	*317,20*
Gasoline + motor oil				*15*	*479,74*	*4979,54*
Replacing the group				*7*	*114,59*	*663,06*
Control system replacement	*7*	*152,78*	*884,04*			

Updated Cost	**2239,27**		**6116,18**

Table 1: Different components used for the comparison

One can note the absence of many components necessary for irrigation, such as water pipes as an example. Since these components are the same on site regardless of the type of system, they are not included in the cost analysis. Referring to the crop water requirements for the 0.75 hectare area shown in the figures, the pumping systems proposed here seem insufficient to cover these needs. The reduction in the size of the pumping systems benefited from a perfect organization in the field.
In fact, the production of fresh vegetables at the Kara site is programmed to be able to satisfy customer demand at times when demand explodes such as December 25th (Christmas), January 1st (New Year's Day), April (Easter) and May 1st for Workers' Day. Thus, taking into account the irrigation dose of these soils, the amount of water demanded by this area can be spread over several days.
One outcome we had on the table is that for the exploitation of this plot, solar energy without surprise requires a very high initial investment fund. But the high cost of operation and maintenance of the irrigation system with the generator make it less profitable over the 15-year pay-off period. Over this period, the petrol-driven pump system is 2.7 times more expensive than the solar-powered pumping system.

5 Conclusion

The study presented here is a case of daily based problem of vulnerable populations in the northern of Togo. The pressure of neighborhood population living in that area on Djamdè's nature reserve has been studied and discussed.

With a view to reducing population pressure on the reserve, market gardening activities operating with solar pumping systems is proposed as solution to overcome the issues encountered by the population. Considering the very high initial investment cost of the components of the solar pumping system, its size can be reduced by organizing and planning the watering of the crops.

6 References

[1] FAO, «Aperçu général de l'agriculture Togolaise à travers un pré-recensement Volume1,» 2013.

[2] FAO, NEPAD «TOGO: Appui à la mise en œuvre du NEPAD–PDDAA,» 2005.

[3] PNUD, RAPPORT SUR LE DEVELOPPEMENT, 2011.

[4] Tchamie, K. Thiou Tanzidani, «Les problèmes sociaux dans les réserves de faune et de flore du Togo,» *Les cahier d'Outre Mer,* vol. 46, n° %1181, pp. 61-73, 1993.

[5] D., Agbato, «Impact des actions humaines dans la zone adjascente au Parc national de la Kéran (Togo),» 1982.

[6] UICN/PACO, « Evaluation de l'efficacité de la gestion des aires protégées : aires,» 2008.

[7] PACO, UICN, «Evaluation de l'efficacité de la gestion d'Oti-Kéran et Oti-Mandouri (Togo),» 2013.

[8] «RETScreen international,» [En ligne]. Available: http://www.retscreen.net. [Accès le 12 May 2020].

[9] Luc ARNAUD, Bernard Gay, «De l'eau pour le maraichage,» Gret, 1994.

[10] Jimmy Royer, Thomas Djiako, Eric schiller, Bocar Sada Sy, Pompage photovoltaïque: Manuel de cours à l'intention des ingénieurs et des techniciens, Multimondes, 1998.

SI-2a
Review of Condition Based Maintenance approaches for vapor compression refrigeration systems

from Ron van de Sand[1], Sandra Corasaniti[2], Jörg Reiff-Stephan[3]

1 Abstract

Vapor compression refrigeration systems are subject to performance degradation over time due to the presence of faults. However, latest work in the field of condition-based maintenance shows promising results in the automatic early detection of anomalous behaviour as well as in accurate machine diagnostics and can, therefore, increase the overall system reliability by simultaneously preventing machine downtimes. In this paper, the latest research works carried out within the last decade are reviewed and the approaches are classified regarding their working principles. Furthermore, the work at hand depicts the current research trend in this field and outlines current obstacles.

2 Introduction

Vapor compression refrigeration systems (VCRS) are used in many industrial and commercial applications and are considered as large energy consumers. Particularly in the food industry, but also in other branches, such as the chemical or pharmaceutical industries, these systems are subject to high reliability standards and can account for 20% - 40% of a facility's energy consumption [2] depending on the application scenario. Consequently, this sector offers particularly high potential for optimisation in terms of energy savings and reliability considerations. As the overall system performance is often decreased due to the presence of faults, energy efficient systems should be equipped with a condition monitoring system in order to enable the online system assessment of the respective appliance. Based on this measure, system faults may automatically be detected and diagnosed, thus, preventing energy waste and high maintenance costs [3]. Therefore, Condition-Based Maintenance (CBM) techniques have attracted attention for decades, and many approaches are well described across the literature. Due to CBM, maintenance actions can be scheduled based on the actual system condition [4] rather than on predetermined time intervals leading to lower operating costs [5]. Moreover, as VCRS can lose about 30% efficiency due to degradation processes by simultaneously seeming fully functional [6], CBM enables to detect and diagnose faults at an early stage of development and can, therefore, avoid energy waste. The main objective of a CBM systems is the automated detection and classification of faults with the lowest possible degree of severity, so that maintenance measures can be initiated in time. Besides the many subsystems of a CBM model, such as *data-filtering* or *feature extraction*, most researchers focussed on the development of automatic VCRS degradation assessment strategies. Especially fault detection and diagnosis (FDD) has been treated recently, which is indeed the most critical part in the CBM model development. Therefore, the work at hand reviews research contributions to the field with a special view to fault detection and

[1] Ron van de Sand, M. Eng., Technische Hochschule Wildau

[2] Sandra Corasaniti, Ph. D., University of Rome "Tor Vergata"

[3] Prof. Dr.-Ing. Jörg Reiff-Stephan, Technische Hochschule Wildau

diagnosis for VCRS published within the last decade and points out promising results. Furthermore, this paper provides an overview of the most common mythologies applied and describes the current state of the art.
After this introduction, the paper is organized as follows; Section 3 outlines the field of CBM and describes the implementation of FDD as a prerequisite for machine prognostics and summarizes the model approaches in regards to their operating principle. In section 4, the research work of the last decade in this field is reviewed and subsequently summarized in section 5.

3 Conditon Based Maintanance

3.1 Terms and Definitions

The term *Conditon Based Maintanance* is defined within the ISO 13372 [7] and replaces the older term *Predictive Maintenance* (PM), which is still commonly used across the literature. In many cases, authors use both terms equivalently and no difference is made between machine diagnostics and prognostics. However, as accurate machine diagnostic is a prerequisite for the implementation of a prognostic model, that may be applied for estimating the Remaining-Useful-Life (RUL) of a machine or component, the work at hand follows the classification suggested in [1]. As illustrated in Figure 1, PM can be divided into CBM and *Prognostic Health Management* (PHM), whereas PHM primarily concerns life cycle management and the prediction of future events [8], such as the fault evolution. CBM, on the other hand, aims to assess the current condition of a machine by use of run-time data and to determine its current fault/failure state [1]. It is generally understood that such a model can correctly diagnose occurring faults as well as estimating their severity level [9].

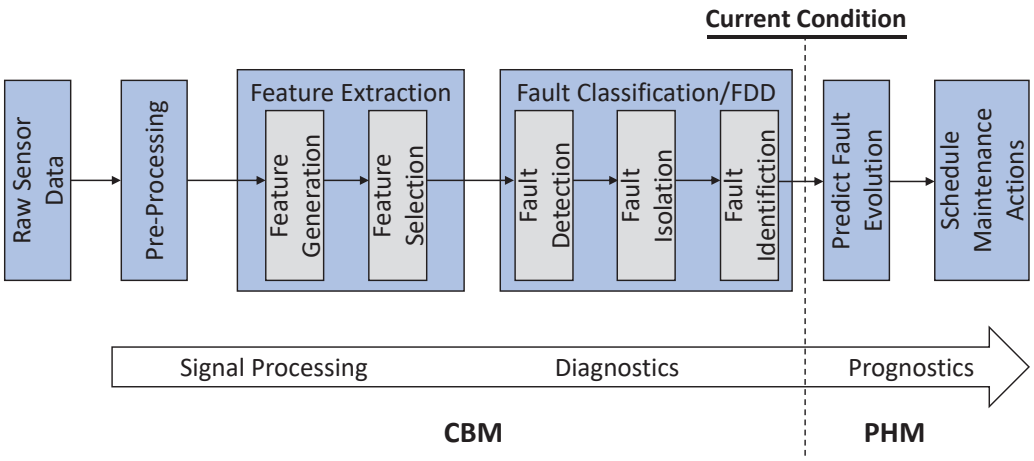

Figure 1 CBM – PHM cycle [1]

A CBM model constitutes three consecutive steps, namely; *data pre-processing*, *feature extraction* and *fault classification*. The former step is primarily applied for increasing the signal-to-noise ratio [8] of the collected data in order to improve the prediction accuracy of the respective fault model. It is worth noticing that this step could also include the detection of the stationary system state, which is especially important for VCRS. Such steady-state detectors are often employed in order to exclude data stemming from transient system states (for example during start-up or

shutdown phases) as such may not represent the actual system state and consequently lead to inadequate machinery health assessment. The objective of the second step is to extract characteristic features (CF) [9], which indicate the presence of a fault and enable to distinguish multiple fault patterns from one another. During the *feature generation* phase, such features can either directly be obtained from sensor readings or can be computed through arithmetic operations as well as thermodynamic dependencies [9], such as the coefficient of performance or the condenser/evaporator heat flow. In the following step, fault indicative CFs are selected to improve the overall FDD accuracy of the subsequent model by rejecting features with low fault sensitivity as well as redundant features. Generally, *feature selection* is a crucial step within the CBM model development as it significantly impacts its diagnostic capabilities. Thus, several methods have been proposed in recent years, for instance the Relief+AGA approach proposed by Yan et al. [3]. The final phase includes the actual *fault classification*, which we refer to as FDD in the following. In the first instance, *fault detection* is applied though anomaly recognition methods in order to identify abnormal behaviour. Subsequently, *fault isolation* is applied in order to identify the failing component or subsystem and is followed by *fault identification* which is used to determine the fault origin [1] as well as its severity. Although all steps are indeed important in order to develop a highly reliable CBM model, most researchers focussed specifically on the development of FDD strategies, as this constitutes the most challenging part. Therefore, the work at hand reviews research contributions to this field of research published within the last decade and points out promising results.

3.2 Approaches

FDD methods can generally be classified into two categories: model-based and data-driven [9–13]. The major difference between both methods is that the former relies on a dynamical reference model of the observed system, whereas data-driven ones make use of historical data [1] for machinery health assessment. It goes without saying that both categories come with their respective pros and cons. Most of all, model-based FDD systems may even detect unanticipated faults as they consider the residuals between a model $F(\cdot)$ and the actual system parameters. The presence of a fault is consequently indicated by rising residuals between both outputs. On the other hand, the definition of a mathematical formulation of a physical system may be difficult or even infeasible for systems with high complexity, which seems to be a drawback of such white-box models. This still constitutes a major challenge for VCRS as modelling multi-phase flows inside the refrigerant cycle, especially for complex geometries, can be challenging. Black-box models [10, 14–17] in turn, do not depend on the underlying physical structure of a system, but rather are based on learning the relationships between input and output variables of $F(\cdot)$ using statistical and machine learning methods. As shown in Figure 2, another widely applied approach is to apply data-driven models enabling learning of fault patterns on the basis of historical machine data.

According to Dai and Gao [13], such models can be further subdivided into *qualitative* and *quantitative* methods, whereas the former applies symbolic intelligence, which can be expressed through domain knowledge in form of, for example, fault pattern libraries, fuzzy expert systems [1] or fault trees [13]. In contrast, *quantitative* models aim to learn underlying fault patterns from historical data in order to enable FDD in an automatic fashion. This is further classified into supervised (learning with target labels) [9, 11, 12, 18–28], unsupervised (learning without target labels) and semi-supervised (learning from partly labelled data) [3]. Reinforced-learning models have also recently attracted attention as they enable to learn from trial-and-error by repetitively

receiving awards. However, in the considered field of application, no successful reinforced-learning approaches are known, so that their practicability for FDD purposes remains questionable. A major drawback of data-driven approaches may lie in the low availability of datasets containing fault samples, as faults are commonly rare events [29]. Furthermore, the fault isolation capabilities of these models are often limited to anticipated faults [1] and therefore adding new faults to the FDD model requires associated data to retrain it.

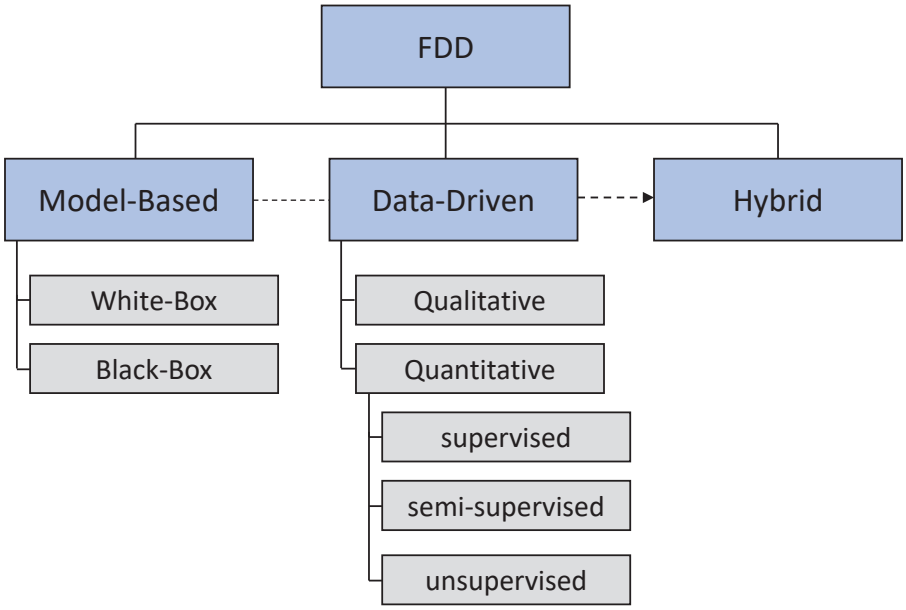

Figure 2 Overview FDD Approaches

Besides, authors have also tried to implement *hybrid* models [3, 30] by combining both model-based and data-driven methods. Following this classification, it can be concluded that the designation of whether an FDD approach is model-based, data-driven, or hybrid is reasonable for the fault detection phase as faults isolation is always conducted in a data-driven fashion. For example, in most of the reviewed model-based systems, faults are detected if the residuals between the reference model and the monitored process exceed predefined limits and the fault is then classified using decision tables. As a consequence, this can clearly be determined as being qualitative data-driven. Other fault isolation methods may also apply quantitative fault classification algorithms, such as support vector machines (SVM) or artificial neural networks. Therefore, the rest of the paper refers only to the classification of the working principle regarding the fault detection phase.

4 Review

4.1 Model-Based

Although most works carried out during the last decade utilized black-box models for their model-based FDD approach, some researchers developed white-box models as well. Zhao et al. [31], proposed a simplified physical-model based on the basic principle of a VCRS for the computation of performance indicators, of which the normalized heat transfer coefficient of the condenser

is used for fault detection. The residual threshold triggering the alarm is subsequently determined empirically based on the false alarm rate in the fault-free case.

Nonetheless, most of the latest research is based on black-box models, which do not require detailed modelling of the target domain. In [15], the model is developed by applying the reference model based on multiple linear regression (MLR) as proposed by Comstock et al. [32] and an adaptive estimator is used for setting the residual alarm threshold. In [17], the reference model has been replaced by support vector regression and exponentially-weighted moving average (EWMA) control charts are applied to further reduce the false-negative rate. This idea has later been adopted by Tran et al. [14], who showed that a radial basis function (RBF) neural network as a reference model can yield higher fault detection accuracy. Furthermore, the authors compared three different reference models [33] combined with EWMA control charts and showed that the RBF neural network based one achieved the highest accuracy. In the same year, the authors proposed a new reference model [34] based on the least square support vector regression. In conjunction with an evolutionary optimization algorithm for hyperparameter optimisation, the model outperformed the former black-box models regarding their fault detection accuracy. Zhao et al. [16] investigated three reference models for fault detection, namely MLR, simple linear regression, and the decoupling based FDD approach [35], of which the later was shown to be the most effective one. Their research particularly investigated the FDD strategies in the presence of multiple simultaneous faults. Another contribution to the topic is given by Beghi et al. [10], where different multiple-input-single-output models (ARMAX, ARX, etc.) were empirically identified for each selected CF respectively.

Even though the fault detection part varies greatly among the model-based methods, the fault diagnosis approach always appears similar as all contributions utilize decision tables for fault classification purposes. However, some papers applied different fault diagnosis strategies as shown in [27], where faults are detected by the use of residuals generated from the MLR model and diagnosed using Bayesian Belief Network.

4.2 Data-Driven

Generally, qualitative data-driven FDD methods are well suitable for diagnosing faults but are mostly limited in terms of detecting abnormal behaviour. Thus, most data-driven fault detection approaches mostly utilize quantitative methods relying on historical data only. In [12], a SVM classifier was utilized to detect and isolate multiple simultaneous faults. Han et al. [21] proposed a SVM based diagnostic tools that combines FDD in one algorithm. They also applied a genetic algorithm to identify CFs and demonstrated how this improved the diagnostic performance. The feature reduction problem has been particularly addressed in great detail across the literature and many researchers have shown significant improvement in the FDD performance when used in conjunction with data-driven classifiers. One widely applied dimensionality reduction method is known to be principal component analysis (PCA), which aims to identify a lower dimensional space of uncorrelated features by decomposing any observation into the modelled principal component subspace and an un-modelled residual subspace [28]. Similar to the proposed SVM diagnostic tool described in [21], Han et al. [19] earlier proposed to apply PCA on the given dataset and to train the SVM on the most significant principal components. A similar idea was also expressed by Zhao et al. [28] who applied a support vector data description (SVDD) clas-

sifier on the principal components for anomaly detection using only normal (fault-free) data samples in the training phase. In the following year, Beghi et al. [29] applied the same approach, but used the ϑ-OCSVM one class classification algorithm proposed by Schölkopf et al. [36] for fault detection and applied a heuristic approach for choosing the gaussian width parameter of the RBF kernel. It is worth noticing that the SVDD and the ϑ-OCSVM classifier reach equal results when implemented using the RBF kernel [36]. PCA has also been adopted by Li et al. [26], who modelled a SVDD classifier using the residual subspace instead of the principal component subspace. It was furthermore demonstrated that their proposed PCA-R-SVDD algorithm outperformed its principal component counterpart. Another fault detection model is described in [37], where a SVDD classifier is trained for the normal operating class as well as for each investigated fault respectively. Han et al. [20] described the use of a Least Squares Support Vector Machine (LS-SVM) for chiller FDD and compared the approach with a standard SVM and a RBF neural network. Their work demonstrated that by selecting the most significant features, the correct rate of the LS-SVM is slightly higher. Besides the application of the SVM and its derivatives for machine diagnostic purposes, some contributions also described the use of other algorithms. For instance, Wang et al. [23] used a bayesian network in different variations and Li et al. [25] proposed to apply linear discriminant analysis for both fault detection and isolation.

Recently, researchers have particularly addressed the lack of available datasets, as this is still a major problem in the development of quantitative FDD methods. One example is given by Beghi et al. [9], who first applied PCA in conjunction with a statistical model. In their work, faults are further diagnosed through a decision table. In [24], a generative adversarial neural network has been proposed to generate augmented data samples in the presence of only a few real fault samples. The authors demonstrated the effectiveness of their approach by applying a SVM for the automatic classification of faults. Another problem is also the transferability of FDD models across different domains, as data stemming from different refrigeration systems are subject to different distributions. This issue was i.a. treated by Fan et al. [11], who proposed a transferable model from a known source domain (labels are known) to a partly known target domain (only a few fault labels are known). The model transfer could be realised by oversampling the known samples from the target domain using the combined principal component subspace. The authors then applied a SVM to classify the unknown labels of the target domain. Their work was later enhanced in [18].

4.3 Hybrid

Although the great variety of model-based and data-driven methods have been shown to reach decent results, few researchers have also tried to combine both. In [3], Yan et al. proposed to apply an extended kalman filter in combination with an ARX model from which 18 parameters could be extracted and fitted recursively into a ϑ-OCSVM classifier in a semi-supervised manner. The authors also suggested a twostep feature selection approach by first reducing the feature space using the ReliefF algorithm and then to reject redundant features by applying the adaptive genetic algorithm. Similarly, in [30] they proposed to use the ARX parameters for the application of a multi class SVM and demonstrated its effectiveness.

5 Summery

Based on the number of reviewed contributions, a clear trend in the development of CBM models for VCRS can be derived. Many authors addressed the development of model-based fault detection strategies and demonstrated promising results. As illustrated in Figure 3, 30% of the 27 reviewed contributions followed this idea, of which 88% rely on black-box models using variations of regression or moving average reference models. However, the majority of contributions describe data-driven approaches for FDD. In fact, around 63% of all contributions in the last ten years are based on such quantitative models, which demonstrates the importance of the topic in this research field. In contrast, only 7% proposed hybrid systems combining both philosophies.

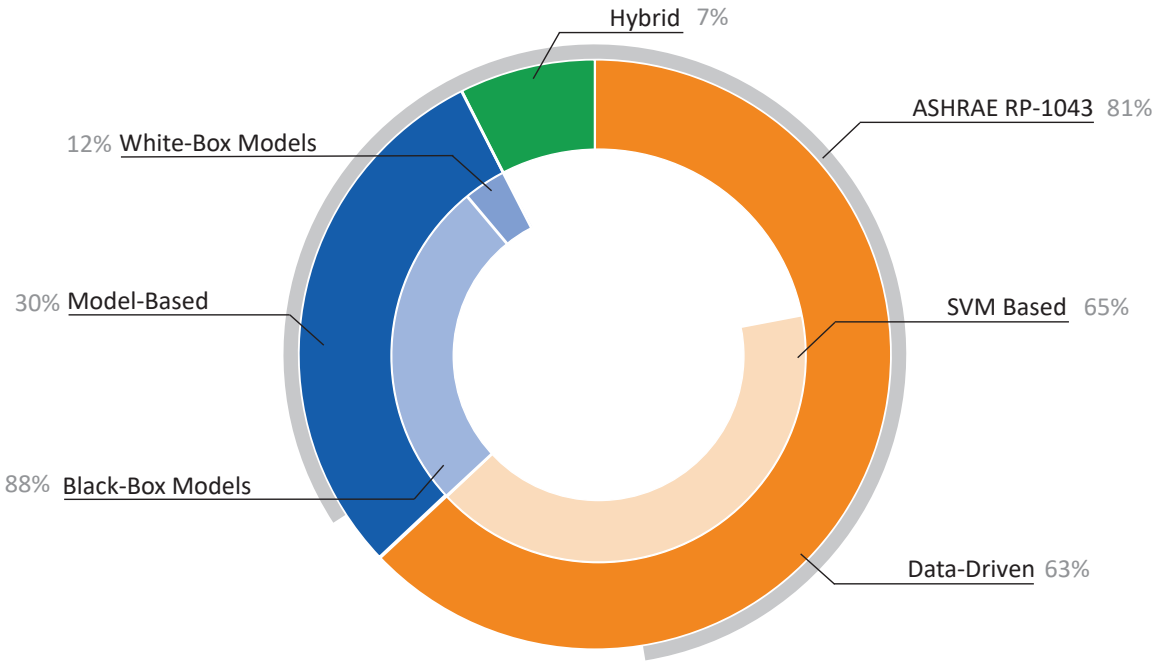

Figure 3 Summery - FDD approaches for VCRS

It is worth noticing, that 65% of the data-driven models consider the application of the SVM or its derivatives (multi-class SVM, SVDD, ϑ-OCSVM, etc.). Moreover, this algorithm has also been applied in the development of hybrid models as well as for model-based FDD. The later primarily used support vector regression to build a reference model as it can capture non-linear relationships by applying the kernel-trick [38], such as RBF or polynomial kernels. In general, it can be stated that 56% of all reviewed publications in this field use a modification of the SVM for the respective purposes. The reason for this might be that this algorithm shows goods generalization performance and is quite effective even with a small amount of data available. Furthermore, training is usually conducted by solving a quadratic optimisation problem and is therefore considered to be computationally effective.

In addition, the review at hand shows that a large proportion of the contributions are based on the same dataset. About 81% of the papers validate their approach solely on the basis of the ASHRAE research project RP-1043 conducted by Comstock et al. [32], where common VCRS faults were investigated using a 360kW centrifugal chiller. As mentioned earlier, the lack of available datasets containing a wide range of different fault samples still constitutes a major problem,

especially for data-driven models. As a result, this may degrade the FDD prediction accuracy as data is commonly subject to different distributions across various domains and, thus, inhibit their broad application. So far, only two contributions concern the transferability of data-driven methods across domains, which enable to transfer knowledge from a source domain using small amount of fault instances stemming from the target domain. However, it must be concluded that no approach is described which enables the transfer of knowledge across domains with unknown target domain labels. Due to the great variety of VCRS, this must be further addressed in future research projects in order to allow the broad application of CBM models and to benefit from their advantages.

6 Conclusion

The work at hand reviewed papers published within the last decade concerning CBM approaches for VCRS. Besides the clarification of the classification of all partial aspects of the topic and the classification of these, the current research trend in this field was pointed out. It was shown the majority of the proposed utilize data-driven methods and primarily apply the support vector machine classifier in its numerous variations for both fault detection and fault diagnosis. Moreover, it can be stated that almost all contributions use machine learning methods in different ways. This shows the importance of this topic for this field of research and can, therefore, be seen as an important key enabler. Yet, the low availability of appropriate datasets remains a challenge in the development of CBM models and should therefore also be addressed in the future.

7 References

[1] G. J. Vachtsevanos, *Intelligent fault diagnosis and prognosis for engineering systems*: Wiley Hoboken, 2006.

[2] X. Zhao, “Lab test of three fault detection and diagnostic methods’ capability of diagnosing multiple simultaneous faults in chillers,” *Energy and Buildings*, vol. 94, pp. 43–51, 2015.

[3] K. Yan, Z. Ji, and W. Shen, “Online fault detection methods for chillers combining extended kalman filter and recursive one-class SVM,” *Neurocomputing*, vol. 228, pp. 205–212, 2017.

[4] *Begriffe der Instandhaltung*, 13306.

[5] L. Wen, X. Li, L. Gao, and Y. Zhang, “A new convolutional neural network-based data-driven fault diagnosis method,” *IEEE Transactions on Industrial Electronics*, vol. 65, no. 7, pp. 5990–5998, 2017.

[6] S. Wang, Q. Zhou, and F. Xiao, “A system-level fault detection and diagnosis strategy for HVAC systems involving sensor faults,” *Energy and Buildings*, vol. 42, no. 4, pp. 477–490, 2010.

[7] ISO, *Condition monitoring and diagnostics of machines-Vocabulary*, *ISO 13372*.

[8] C. Anger, “Hidden semi-Markov models for predictive maintenance of rotating elements,” Technische Universität, 2018.

[9] A. Beghi, R. Brignoli, L. Cecchinato, G. Menegazzo, M. Rampazzo, and F. Simmini, “Data-driven fault detection and diagnosis for HVAC water chillers,” *Control Engineering Practice*, vol. 53, pp. 79–91, 2016.

[10] A. Beghi, L. Cecchinato, F. Peterle, M. Rampazzo, and F. Simmini, “Model-based fault detection and diagnosis for centrifugal chillers,” in *2016 3rd Conference on Control and Fault-Tolerant Systems (SysTol)*, 2016, pp. 158–163.

[11] Y. Fan, X. Cui, H. Han, and H. Lu, “Chiller fault diagnosis with field sensors using the technology of imbalanced data,” *Applied Thermal Engineering*, vol. 159, p. 113933, 2019.

[12] H. Han, B. Gu, Y. Hong, and J. Kang, “Automated FDD of multiple-simultaneous faults (MSF) and the application to building chillers,” *Energy and Buildings*, vol. 43, no. 9, pp. 2524–2532, 2011.

[13] X. Dai and Z. Gao, “From model, signal to knowledge: A data-driven perspective of fault detection and diagnosis,” *IEEE Transactions on Industrial Informatics*, vol. 9, no. 4, pp. 2226–2238, 2013.

[14] D. A. T. Tran, Y. Chen, M. Q. Chau, and B. Ning, “A robust online fault detection and diagnosis strategy of centrifugal chiller systems for building energy efficiency,” *Energy and Buildings*, vol. 108, pp. 441–453, 2015.

[15] F. Xiao, C. Zheng, and S. Wang, “A fault detection and diagnosis strategy with enhanced sensitivity for centrifugal chillers,” *Applied Thermal Engineering*, vol. 31, 17-18, pp. 3963–3970, 2011.

[16] X. Zhao, “Lab test of three fault detection and diagnostic methods’ capability of diagnosing multiple simultaneous faults in chillers,” *Energy and Buildings*, vol. 94, pp. 43–51, 2015.

[17] Y. Zhao, S. Wang, and F. Xiao, “A statistical fault detection and diagnosis method for centrifugal chillers based on exponentially-weighted moving average control charts and support vector regression,” *Applied Thermal Engineering*, vol. 51, 1-2, pp. 560–572, 2013.

[18] Y. Fan, X. Cui, H. Han, and H. Lu, “Chiller fault detection and diagnosis by knowledge transfer based on adaptive imbalanced processing,” *Science and Technology for the Built Environment*, pp. 1–18, 2020.

[19] H. Han, Z. Cao, B. Gu, and N. Ren, “PCA-SVM-based automated fault detection and diagnosis (AFDD) for vapor-compression refrigeration systems,” *HVAC&R Research*, vol. 16, no. 3, pp. 295–313, 2010.

[20] H. Han, X. Cui, Y. Fan, and H. Qing, “Least squares support vector machine (LS-SVM)-based chiller fault diagnosis using fault indicative features,” *Applied Thermal Engineering*, vol. 154, pp. 540–547, 2019.

[21] H. Han, B. Gu, J. Kang, and Z. R. Li, “Study on a hybrid SVM model for chiller FDD applications,” *Applied Thermal Engineering*, vol. 31, no. 4, pp. 582–592, 2011.

[22] S. He, Z. Wang, Z. Wang, X. Gu, and Z. Yan, “Fault detection and diagnosis of chiller using Bayesian network classifier with probabilistic boundary,” *Applied Thermal Engineering*, vol. 107, pp. 37–47, 2016.

[23] Z. Wang, Z. Wang, S. He, X. Gu, and Z. F. Yan, “Fault detection and diagnosis of chillers using Bayesian network merged distance rejection and multi-source non-sensor information,” *Applied Energy*, vol. 188, pp. 200–214, 2017.

[24] K. Yan, A. Chong, and Y. Mo, “Generative adversarial network for fault detection diagnosis of chillers,” *Building and Environment*, vol. 172, p. 106698, 2020.

[25] D. Li, G. Hu, and C. J. Spanos, “A data-driven strategy for detection and diagnosis of building chiller faults using linear discriminant analysis,” *Energy and Buildings*, vol. 128, pp. 519–529, 2016.

[26] G. Li *et al.,* “An improved fault detection method for incipient centrifugal chiller faults using the PCA-R-SVDD algorithm,” *Energy and Buildings*, vol. 116, pp. 104–113, 2016.

[27] Y. Zhao, F. Xiao, and S. Wang, “An intelligent chiller fault detection and diagnosis methodology using Bayesian belief network,” *Energy and Buildings*, vol. 57, pp. 278–288, 2013.

[28] Y. Zhao, S. Wang, and F. Xiao, “Pattern recognition-based chillers fault detection method using support vector data description (SVDD),” *Applied Energy*, vol. 112, pp. 1041–1048, 2013.

[29] A. Beghi, L. Cecchinato, C. Corazzol, M. Rampazzo, F. Simmini, and G. A. Susto, “A one-class svm based tool for machine learning novelty detection in hvac chiller systems,” *IFAC Proceedings Volumes*, vol. 47, no. 3, pp. 1953–1958, 2014.

[30] K. Yan, W. Shen, T. Mulumba, and A. Afshari, “ARX model based fault detection and diagnosis for chillers using support vector machines,” *Energy and Buildings*, vol. 81, pp. 287–295, 2014.

[31] Y. Zhao, S. Wang, F. Xiao, and Z. Ma, “A simplified physical model-based fault detection and diagnosis strategy and its customized tool for centrifugal chillers,” *HVAC&R Research*, vol. 19, no. 3, pp. 283–294, 2013.

[32] M. C. Comstock and J. E. Braun, “Development of analysis tools for the evaluation of fault detection and diagnostics in chillers, ASHRAE Research Project RP-1043,” *American Society of Heating, Refrigerating and Air-Conditioning Engineers, Inc., Atlanta. Also, Report HL*, 99-20, 1999.

[33] D. A. T. Tran, Y. Chen, and C. Jiang, “Comparative investigations on reference models for fault detection and diagnosis in centrifugal chiller systems,” *Energy and Buildings*, vol. 133, pp. 246–256, 2016.

[34] D. A. T. Tran, Y. Chen, H. L. Ao, and H. N. T. Cam, “An enhanced chiller FDD strategy based on the combination of the LSSVR-DE model and EWMA control charts,” *International Journal of Refrigeration*, vol. 72, pp. 81–96, 2016.

[35] H. Li and J. E. Braun, “A methodology for diagnosing multiple simultaneous faults in vapor-compression air conditioners,” *HVAC&R Research*, vol. 13, no. 2, pp. 369–395, 2007.

[36] B. Schölkopf, R. C. Williamson, A. J. Smola, J. Shawe-Taylor, and J. C. Platt, “Support vector method for novelty detection,” in *Advances in neural information processing systems*, 2000, pp. 582–588.

[37] Y. Zhao, F. Xiao, J. Wen, Y. Lu, and S. Wang, “A robust pattern recognition-based fault detection and diagnosis (FDD) method for chillers,” *HVAC&R Research*, vol. 20, no. 7, pp. 798–809, 2014.

[38] B. Schölkopf, A. J. Smola, and F. Bach, *Learning with kernels: support vector machines, regularization, optimization, and beyond*: the MIT Press, 2018.

SI-2b

A Short Approximation Method

to Pre-estimate the Electric Yield of Wind Farms

Lutz B. Giese[1] & Stefan Fürkus [2]

Abstract

Amongst the Renewable Energy Sources (RES) contributing to the worldwide electricity production, wind energy became very important. Germany and several other countries own significant wind potentials. 2% of a country's area can be used for wind farms, thus Germany could produce easily up to 200 TWh_{el} yearly just onshore. However, often legal and especially financial aspects decide about the speed of development. Careful project preparation guaranteed by professional management is obligatory. Beside factors such as (i) rights to the property and (ii) electric grid connection, (iii) the sufficiency of the wind and peripheral conditions need to be known. A proper wind forecast and yield prognoses are important items. To solve these tasks, professional programs are sold on the markets. To offer a convenient alternative, authors will present software based on Excel named as WindCalc 1.5, which is still under development.

1 Introduction

Within the last decades, a significant growing of the wind energy branch had been observed. Whereas amongst the Renewable Energy Sources (RES) in terms of global electricity still the hydropower rules - contributing around 20% of the worldwide electricity production - starting from the early 90s, the wind energy became the second important RES technology after the hydropower. However, by the end of 2019 Germany operated wind fields with a total capacity of 53.9 GW_{el} onshore and 7.5 GW_{el} offshore [1]. Thus, the yearly electricity production was estimated to have reached 132 TWh_{el} in 2019 [1], which covered nearly 25% of the annual electricity net consumption in Germany. For comparison, according to the former German Ministry for Environment BMU reported in 2013, in 2012 onshore/offshore still only 49.9/0.72 TWh_{el} had been produced from wind energy [2].

Around 2000, Germany reached the point of equivalence at 4 GW_{el} with Denmark, traditionally the wind energy pioneer. Within the following years Spain came up to be one of the first European nations, later than firstly USA and finally China won the leadership in the markets. Whereas the entire installed capacity amounted to 369.6 GW_{el} worldwide in 2014 [3], by the end of 2019 this grew up towards 650.6 GW_{el} (reported by the German Wind Association BWE and Global Wind Energy Council GWEC, [1] - 36% of it in China. However, also smaller countries in transition are already developing the wind power successfully. For instance, since 2010 the Turkey passed the magical 1-GW_{el}-border [4]. At the end of 2011 Turkey operated an in-

[1] Lutz B. Giese, University of Applied Sciences [TH] Wildau, Fac. of Engineering and Natural Sciences, Hochschulring 1, D-15745 Wildau, Germany

[2] Stefan Fürkus, ÖKOtech e.V.
Grünberger Str. 55, D-10245 Berlin, Germany

stalled wind capacity of nearly 1.7 GW_{el} aiming at 5 GW_{el} in 2015 and under optimistic assumptions maybe more than 20 GW_{el} in 2025 [4]. This examples may show, that

1. wind energy is a strong Renewable Energy Source, and
2. countries in transition easily can develop own domestic wind energy application.

For Germany, today serious estimations including (i) expanding the onshore installation, (ii) repowering old onshore wind farms by modern systems, and (iii) further developing the offshore area show that it might be feasible to develop the wind energy in Germany to contribute finally more than 30-40% of the national net electricity demand.

2 Wind Basics and Wind-turbine Yield Simulation

Basics on wind, wind energy and wind technology can be found in [5], [6] or [7]. However, this chapter 2 is foreseen firstly to give basic information on how wind regimes work and especially how electric yields generated from them can be predicted, and secondly, to prepare how to manage computional simulation, comparing (briefly) professional but often expensive software tools with a simple but forceful new Excel based program code named as WindCalc 1.5 in chapter 3.

2.1 Basics on Wind Performance – Input to the Simulation Models

In order to simulate electric yield from wind energy systems, due to the compatibility of the input some transformations are necessary. As well, some background theory is needed [8], [9]: Wind often is measured close to surface, standardized at 10 m above the ground. If measurements had been taken at higher levels, it will be remarked in wind speed maps or data will be reduced down to a reference level. Long-term observations result in statistical averages. This data are fundament of the calculation.

First point of interest is the long-term average (= mean) of the wind speed at reference level, in order to obtain afterwards a statistical distribution in hub elevation. There are three steps to obtain this:

1. Evaluation of data and calculation of long-term ground wind-speed average
    a. Data can be collected or measured
2. Height correction and evaluation of long-term hub wind-speed average which must be expected
    a. The height formula is one opportunity to simulate the wind speed profile, thus minimum the roughness z_0 as function of the landscape typ is required
3. Calculation of the wind-speed distribution by Weibull or Rayleigh theory
    a. In terms of Weibull theory, the so-called shape factor C is needed, a property of the landscape typ and altitude

To complete the technical calculation, machine parameters and mechanical calculations finally are needed. In order to prepare a wind field, also further information due to air temperature, airpressure and humidity functions during the season will be collected and evaluated. To solve the question how to adjust the wind-farm shape, further investigations and evaluation on the direction distribution will be done (wind-rose). However, this can be respected later to estimate the farm factor.

2.2 Estimating the Mean of Wind Speed at Hub Elevation

Formula (1) shows the height formula to calculate wind-speed average in hub elevation according to a logarithmic model, formula (2) is the Hellmann formula [8], [9].

Height formula

$$v_2 = v_1 \frac{\ln\left(\frac{h_2 - d}{z_0}\right)}{\ln\left(\frac{h_1 - d}{z_0}\right)} \quad (1)$$

with
v_2: Wind speed on the upper level h_2 (e.g. hub) (in m/s)
v_1: Wind speed on the lower level h_1 (e.g. measurement) (in m/s)
z_0: Roughness (in m)
d: Shift (in m)

Hellmann formula

$$v_2 = v_1 \left(\frac{h_2}{h_1}\right)^{\alpha} \quad (2)$$

with
v_2: Wind speed on the upper level h_2 (e.g. hub) (in m/s)
v_1: Wind speed on the lower level h_1 (e.g. measurement) (in m/s)
α: Hellmann exponent (---); starting α = 0.10

In table 1 the landscape types, roughness factors z_0 and other properties can be found. Wind speed data estimated from the calculation according to formula (1) and (2) can be compared with results of mast-based long-term anemometer measurements in different levels, respectively.

Table 1: Landscape types, roughness (according to European Wind Atlas) and other properties [8] [9] [10]

Class of Roughness	Roughness z_0 (m)	Energy Index (%)	Typ of Landscape
0	0.0002	100	Ocean
0.5	0.0024	73	Flat land, greenland, coastal land
1	0.03	52	Open agricultral land
1.5	0.055	45	Wide agricultural land
2	0.1	39	Medium agricultural land
2.5	0.2	31	Narrow agricultural land
3	0.4	24	Settlements, forest etc.
3.5	0.8	18	Cities with high buildings
4	1.6	13	Big cities

2.3 Calculating the Wind Speed Distribution Using Statistical Methods

Formula (3) shows the statistics by the Rayleigh distribution, formula (4) shows the mother function, the Weibull distribution. If the shape factor C of Weibull is set = 2, it results in the simplified so-called Rayleigh distribution [8], [9].

Rayleigh distribution

$$f(v_i) = \frac{\pi}{2} \frac{v_i}{v_m^2} e^{-\frac{\pi}{4}\left(\frac{v_i}{v_m}\right)^2} \tag{3}$$

Weibull distribution

$$f(v_i) = \frac{C}{A}\left(\frac{v_i}{A}\right)^{C-1} \quad e^{-\left(\frac{v_i}{A}\right)^C} \tag{4}$$

with
C: Shape factor = form factor (---)
A: Scale factor (m/s)

$$A = \frac{2}{\sqrt{\pi}} * v_m$$

Figure 1 (a) shows as an example of a Rayleigh probability distribution of the wind-speed v at hub elevation of 100 m a.s.l. as f(v) in the nearshore in Germany (Northern Sea), calculated with the program Excel.

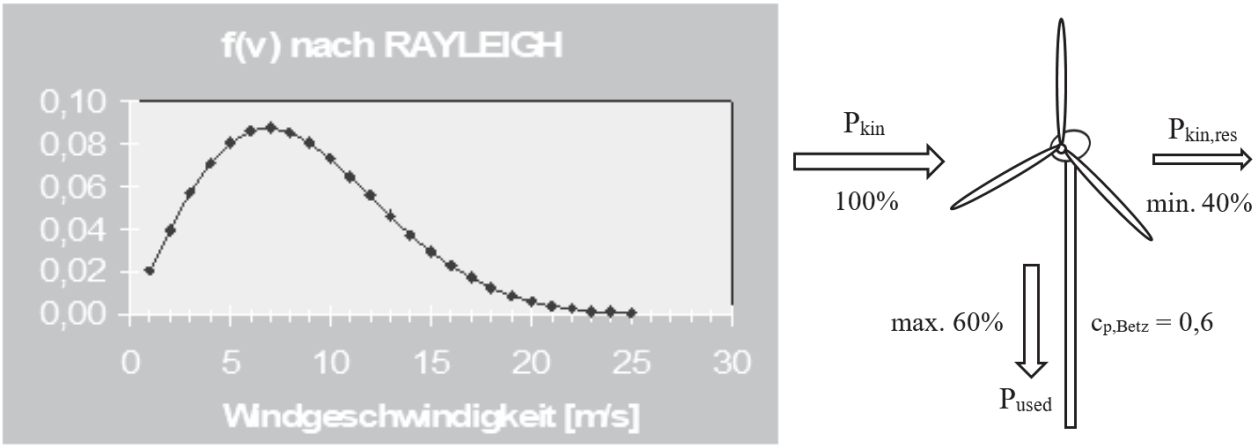

Figure 1: (a) Example of Rayleigh distribution of wind-speed, (b) Scheme of the ideal energy flow at the hub

Figure 1 (b) shows idealized energy flow scheme at the hub of a wind energy turbine. In the early 20th century Albert Betz postulated the so-called Betz-theorem, which defines the maximum efficiency of an aerodynamic updraft system (Albert Betz in 1923) not to exceed 0.5926 [11].

3 Numerical Simulation with WindCalc 1.5 – Forecasting the Yearly Electrical Yield

In order to get input data for the calculation mentioned above, (i) to estimate the local wind potential in form of wind speed distribution or mean data, wind direction etc., the following sources and/or tools usually are used:

1. Weather forecast service authorities (long-term statistics)
2. In Europe: Regional and European wind atlas
3. Wind simulation programs
    a. WindPRO 3.4 (EMD) [12]
    b. WindCalc 1.5 (authors, [13])
    c. Others
4. On-site-measurement surveys
5. Expertise without measurement

3.1 Calculating the Rated Power and Estimating the Yearly Electrical Yield

The formulas (5) and (6) explain the flow of kinetic energy in the wind, the extractable electric power respecting technical efficiences and finally the total yield (refer to figure 1 (b)).

Physics of the wind and the machinery

$$P_{el}(v_i) = 0.5\, c_{p,anl}(v_i)\, A\, \rho\, v_i^{\,3} \tag{5}$$

and

$$W_{el,a} = \sum_{i=1}^{n} \left(P_{el}[v_i]\, t[v_i]\right) = \sum_{i=1}^{n} \left(0.5\, c_{p,anl}[v_i]\, A\, \rho\, v_i^{\,3}\, t[v_i]\right) \tag{6}$$

with
$E_{kin} = 0.5*m*v^2 \mid d/dt$
$dE_{kin}/dt = P_{kin} = 0.5*dm/dt*v^2$
$V = A * x \mid d/dt$
$dV/dt = A * v$
$m = V * \rho \mid d/dt$
$dm/dt = dV/dt * \rho = A * \rho * v$
$P_{kin} = 0.5 * dm/dt * v^2$
$P_{kin} = 0.5 * A * \rho * v^3$
$P_{el} = 0.5\, [c_{p,Betz} * \Pi_j \eta_j] * A * \rho * v^3$
$c_{p,anl} = c_{p,Betz} * \Pi_j \eta_j = c_{p,Betz} * \eta_{rotor} * \eta_{bearing} * \eta_{gearbox} * \eta_{generator}$

As an object of an own former investigation, the wind farm Rüdersdorf near Berlin had been examined. Task was to investigate whether (i) the 20 years old field can be repowered by modern technology, under the limitation (ii) that the nine wind turbines are to be replaced only by one new system, (iii) taking into account the same electric yield.
It could be shown, that the tool was sufficient to solve such technical questions in a quick and financially convenient way. Indeed, it proved one new wind energy system can substitute more than 5 machines from the 90ies. Results of this former simulation of the wind farm Rüdersdorf near Berlin using the Enercon E-101 are presented below (see Figure 2).

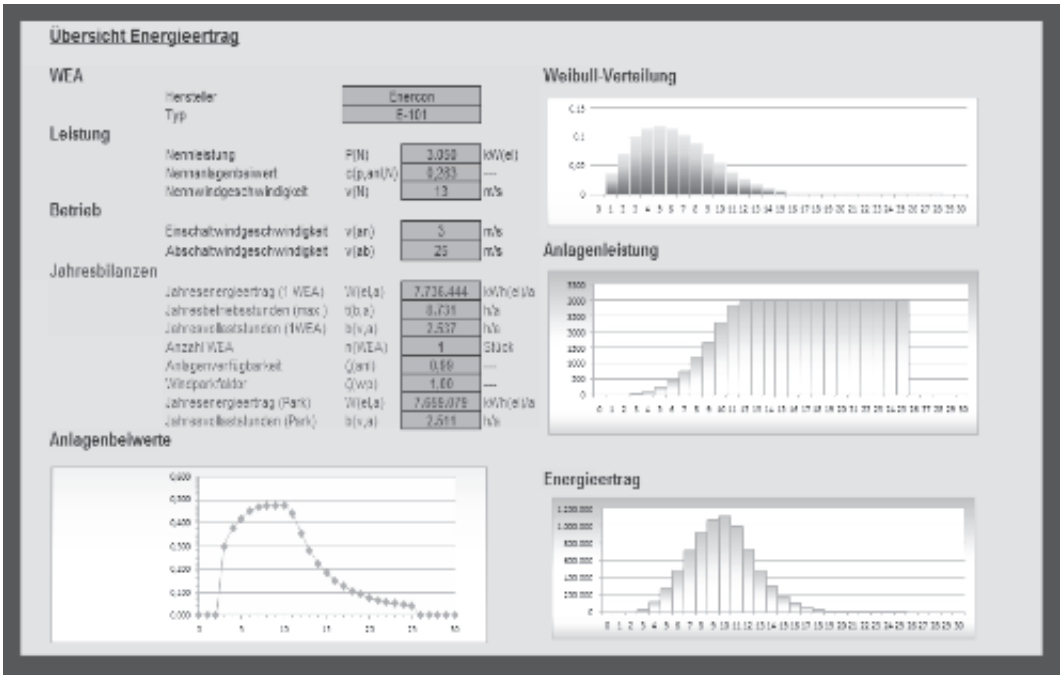

Figure 2: Results for simulation scenario taken from WindCalc 1.5 (repowering of the Rüdersdorf wind farm, nearby Berlin, [13])

3.1.1 Resume

The Excel based program code WindCalc had been established as an alternative calculation tool to professional simulation programs such as WindPRO. Their advantage is to cover several of the needs of professional work in the field of developing wind farm project often on high level, so noise emission and shading analysis, computer flow simulation and so on. On the other hand, in the field of science and education often such tools simply are too expensive to be applied.

4 Conclusions

This paper had been targeted (i) to report about development and state of the art of the wind energy to contribute clean electricity for the future, (ii) to show the importance to support and develop the further application while there are significant potentials in several countries, (iii) to demonstrate that wind energy is an environmentally friendly and clean technology in order (iv) to provide a certain portion of the domestic electricity at a feasible price.

On one hand, in countries such as Germany during the last decades wind energy grew fast and properly to contribute nowadays around 25% of the net electricity consumption. On the other hand, still electricity (hereby mainly the coal power) contributes nearly 40% of the national CO_2 emission in Germany, around 290 Mill. tons per year from power plants in 2018 [14].

Several countries own significant wind potentials. 2% of a country's area can be used for wind farms, thus Germany could produce easily up to 200 TWh_{el} yearly just onshore. However, often legal (or political) and especially financial aspects decide about the speed of development, so the German EEG [15]. Careful project preparation guaranteed by professional management is obligatory. Beside (i) rights to the property and (ii) electric grid connection, (iii) the sufficien-

cy of the wind plus peripheral conditions need be known. A proper wind forecast and yield prognoses are important items.
To solve these tasks, professional programs are sold on the markets, such as the WindPRO issued by the Danish software producer EMD. To offer a convenient alternative for students and researchers as well as project developers, authors presented the software based on Excel named as WindCalc 1.5 which is still under development.

5 References

[1] BWE [Bundesverband Windenergie], https://www.wind-energie.de/themen/zahlen-und-fakten/, 2020.
[2] BMU [German Federal Ministry for Environment, Nature Conservation and Nuclear Safety], „Erneuerbare Energien in Zahlen - nationale und internationale Entwicklung“, [brochure], 112 p., 2013.
[3] GWEC [Global Wind Energy Council], „Global Wind Statistics 2014“, https://gwec.net/publications/global-wind-report-2, 2015.
[4] R. Ata, “The Current Situation of Wind Energy in Turkey”, *Journal of Energy*, vol. 2013, [8 p.], 2013, Art. 794095.
[5] R. Gasch, J. Twele [ed], “Wind Power Plants – Fundamentals, Design, Construction and Operation”, (2nd ed.), Springer, Heidelberg, 2012.
[6] V. Quaschning, “Renewable Energy and Climate Change”, (2nd ed.), Wiley IEEE, London, 2019.
[7] S. Heier, „Nutzung der Windenergie“, (7th Ed. [in German]), Frauenhofer IRB, Stuttgart, 2016.
[8] BWE [Bundesverband Windenergie], „Online Skript Windenergietechnik“, http://www.wind-energie.de/de/technik, 2009.
[9] B. Schmidt, D., Schmidt, „Grundkurs Windenergie“, Solarinitiative Mecklenburg-Vorpommern e.V., 69 p., 2002.
[10] I. Troen, E. Lundtang Petersen, „Europäischer Windatlas“, *Roskilde Risø National Laboratory*, 1990.
[11] A. Betz, „Das Maximum der theoretisch möglichen Ausnützung des Windes durch Windmotoren“, *Zeitschrift für das gesamte Turbinenwesen*, vol. 26, 1920.
[12] EMD [International A/S], WindPRO 3.4, http://www.emd.dk/windpro/, 2020.
[13] L.B. Giese, S. Fürkus, A. Eltez, S. Rolle, “Simulating the Electric Yield of Wind Farms – A Short Introduction into how to Develop Wind Projects Supported by an Excel Based Program Code”, *Proc. 3rd Anatolian Energy Symposium (AES) Muğla/Turkey*, 10 p., 2015.
[14] BMWi [German Federal Ministry for Economics and Technology], “Energiedaten - nationale und internationale Entwicklung”, EXCEL file, (internet update 2020/03/31 download: www.bmwi.de), 44 sheets, (2020).
[15] Deutscher Bundestag, „Gesetz für den Ausbau erneuerbarer Energien (Erneuerbare-Energien-Gesetz – EEG 2017), https://www.bgbl.de/xaver/bgbl/start.xav?startbk=Bundesanzieger_BGBl#__bgbl__%2F%2F*%5B%40attr_id%3D%27bgbl116s2258.pdf%27%5D__1592139475498, 2020.

SII-1a
Estimation of the Global Solar Radiation Received on the Soil in Nalohou and Natitingou (Northern Benin)

Gabin Koto N'Gobi[1], Hagninou E. V. Donnou[1], Médard Agbazo[1], Aristide. B. Akpo[1], Basile. B. Kounouhewa[1]

Email: kotgabin36@yahoo.fr

1 Abstract

The design of solar energy systems requires knowledge of the global solar radiation received by solar panels on the ground. However, for many developing countries such as the Benin Republic, there is a serious lack of radiometric stations everywhere in the country. The unavailability of these data, therefore, limits knowledge regarding the optimal functioning of solar installations. To cope with these difficulties, a method for estimating the global irradiation is developed at Nalohou AMMA CATCH station and Natintingou synoptic station, two sites in North-West Benin. This model depends on meteorological and astronomical parameters. Meteorological data such as sunshine duration, relative humidity, and air temperature have been collected on the synoptic station of Natitingou, and observed data of irradiation are collected from Nalohou. They are used to validate the model. The results show that the estimation of the mean square deviation value is around 10^{-2}. Overall solar radiation is significant in this region and its annual average value varies between 9.80 kWh/m² and 10.50 kWh/m². This model can, therefore, be used by solar system operators to optimize energy production in the region.

2 Introduction

Access to energy is essential for the social and economic well-being of populations worldwide. In most African developing countries, energy accessibility is difficult despite the high potential of renewable sources of energy. Among these sources of renewable energy, solar energy is considered as the most efficient, the best alternative resource [1] adapted for providing heat, electricity, and water in rural and urban areas. However, accurate knowledge of the incoming solar radiation resource at a site is required for the design and the efficiency in the estimation of any solar energy system [2]. Let's remember that solar plants functioning depends mainly on the climatic conditions of the specific location [3]. In Benin Republic (West Africa), few stations consistently measure global daily solar radiation. But, the lack of reliable data on global solar radiation can lead to erroneous evaluation of the solar pants efficiency. Therefore, the availability of certain climatic parameters such as relative humidity, air temperature, and astronomical parameters are necessary for the construction of an empirical model [4,5]. In the literature, several empirical formulations have been developed to predict global solar radiation using several meteorological variables such as sunshine duration, cloud cover, relative humidity, maximum temperature, water vapor pressure, etc. [4-9]. Quansah et *al*. [10] proposed an empirical model for estimating Global Solar Radiation (GSR) as a function of the sunshine relative duration over the Ashanti region in Ghana. The model can predict very well the pattern of the measured monthly daily mean GSR for the entire period of study with the smallest values of errors. Trabea and Shaltout [7] established a model in which input depends on the mean daily

1 Laboratoire de Physique du Rayonnement (LPR), Faculté des Sciences et Techniques (FAST), Université d'Abomey-Calavi (UAC), 01 B.P. 526, Cotonou, Benin.

maximum temperature, the mean daily relative humidity, the mean daily sea level pressure, the mean daily vapor pressure, and hours of sunshine in Egypt. The Results show values of correlation coefficients varying from 89% to 99% and the errors of estimation are between 0.01 and 0.04. The Angstrom-type model also allows estimating the global solar irradiance by simple linear regression. It has been used by several authors [10-12]. Falayi et al [4, 12,13] correlated global solar radiation and meteorological parameters using monthly mean daily global solar radiation, sunshine duration, temperature, and relative humidity data from Nigeria. Several other authors such as Karoro et al [14], Coulibaly and Ouedoraogo [15], Onyango and Ongoma [16], Yisehak [17], Afungchui and Neba [18], Adeola et al [19], Safari and Gasore [2], Hassan et al. [20], Dankassoua [21], Ajayi et al. [22], Olomiyesan et *al*. [23] have established models for determining GSR. These authors have estimated global solar radiation in several areas of Africa. The diversity of methods for estimating global solar radiation to improve the design and optimization of solar energy systems clearly shows the interest given by authors on this topic. However, the reliability of these models depends largely on the strong correlation between estimated and measured variables, and many models (from cited above) have shown their limitations the reproduce GSR at other sites. Very few studies have experimented with the estimation of global solar radiation in Benin. One can cite Amoussa [24] who is the first to provide information on the characteristics of solar radiation in Benin using a linear model from Frère and Rietveld's to determine correlation constants of dimensionless parameters for many stations located in Benin. Unfortunately, the linear model is not reliable everywhere to reproduce global solar radiation measurements in the country. To overcome this lack in the current study, we develop and validate a global solar radiation model, capable of better estimation of solar radiation at the ground Surface in Nalohou, a typical and nearest village of Natitingou synoptic station where observed data are available. The reason behind the choice of the location is that solar radiation's data are available for some period in the location. So that we can easily calibrate the model with data recorded at the Nalohou station and regenerate those of Natintingou. This model was then used to generate global solar radiation at this meteorological site with the same meteorological parameters, geographical and topographical characteristics as Nalohou. The remaining parts of the paper are organized as follows: in section 3, study sites, the dataset, and methods are described. Analysis of results and their interpretations are made in section 4. Finally, we conclude the paper with a summary and outlook for further research in section 5.

3 Materials and Methods

3.1 Materials

3.1.1 Study sites

Benin is located between latitudes 6°30-12°30 N and longitudes 1°-4° E. It is bordered in the North by the Niger River, in the North-West by Burkina Faso, in the West by Togo, in the East by Nigeria and in the South by the Atlantic Ocean. Two (02) study sites (Nalohou and Natitingou) are chosen in this study. Nalohou AMMA CATCH station is located in the Donga watershed in northern Benin, where the global solar radiation model is developed and used to estimate this parameter at Natitingou, the nearest synoptic meteorological station (~70km). The climate in these two locations is Sudanian and characterized by a single dry season from October or November to February or March and a single rainy season from April to October. Figure 1 and Table 1 show the location and the geographical characteristics of these two sites. The rainy seasons transport humid air from the Atlantic Ocean into the continent when the Intertropical Front (ITF) advances toward the North. The dry seasons release a mixture of dusty and dry air

from the Sahara toward the Atlantic Ocean when the ITF is fastly returning to the south. Natitingou is the Rainiest región of the country (1300 mm/year).

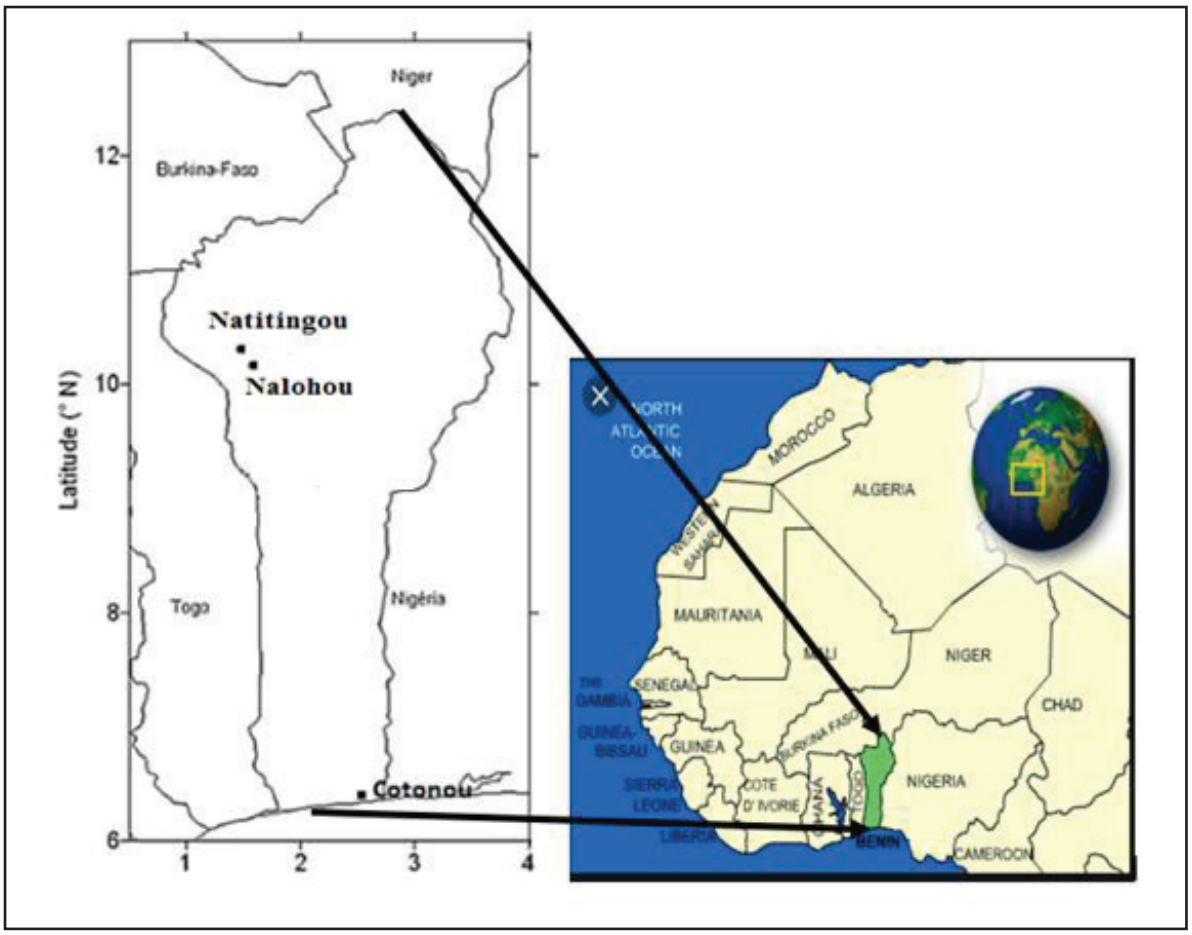

Figure 1: Geographical location of the study sites

Table 1: Geographical characteristics of study sites

Site	Latitude	Longitude	Altitude (m)
Natitingou	10° 19′ N	1°23′E	426
Nalohou	9°744N	1°60E	449

3.1.2. Data used

At the Nalohou site, global solar radiation data and meteorological parameters such as ambient air temperature and air relative humidity are measured during the AMMA CATCH project at 2m above ground level every 15 min in the period from July 10, 2007, to July 10, 2010 [25]. As insolation data was not measured at Nalohou, the data recorded at Natitingou was used during the same period. Data were split into two parts: (i) one part covers the period from July 10, 2007, to July 09, 2009 and used to develop the new model; (ii) the second part covers the period from 10 July 2009 to 10 July 2010 which were used to validate the proposed model. Figure 2 gives us an overview of the Nalohou experiment site showing the installed solar radiation sensor.

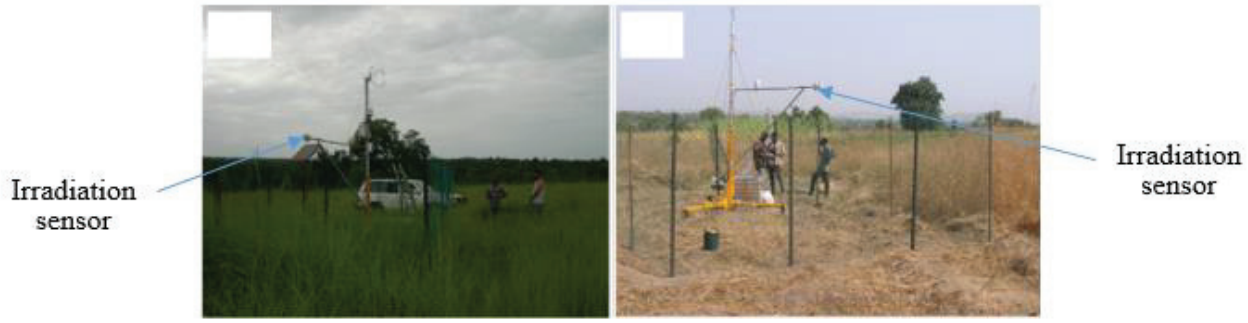

Figure 2 : Nalohou experimental site (Mamadou [25])

Natitingou site is a synoptic meteorological station of the National Meteorological Agency (ANM). Insolation duration, ambient air temperature, air relative humidity was used as input parameters in the developed model to estimate the global solar radiation at this site. These meteorological parameters were measured hourly over the period from 1st January 2016 to 31 December 2016.

3.2 Methods

3.2.1 Formulation of the new model

In the work of Chukwujindu [26] who reviewed more than 760 different models for estimating global solar radiation in Africa, we noted that most of the models are based on the Angstrom formulation which is a function of the solar fraction.

Let us thus consider the relation between the components of the global solar irradiation on a horizontal plane and the fraction of insolation given by Angström in Hinrichsen 1994 [27]:

$$\frac{H}{H_0} = a + b\sigma \quad (1)$$

H (W/m²) is the global solar irradiation on a horizontal plane, a and b are model calibration constants, σ is the fraction of daily sunstroke. It is expressed as:

$$\sigma = \frac{n_j}{N_{oj}} \quad (2)$$

n_j is the insolation duration on the day j, expressed in hours (h) and N_{oj} is the astronomical duration, expressed as follows:

$$N_{oj} = \frac{2}{15}\omega_j \quad (3)$$

ω_j is the daily hourly angle of sunrise on a horizontal plane expressed in radians. It is given by:

$$\omega_j = \text{Arcos}\left(-\tan(\delta_j)\tan(\phi)\right) \quad (4)$$

ϕ is the latitude in degrees and δ_j is the daily solar declination in degrees:

$$\delta_j = 23.45\sin\left(\frac{360}{365}(N_j + 284)\right) \quad (5)$$

with Nj being the number of the day counted from January 1st. The expression of the daily average H_0 (in W/m²) of solar irradiation from a horizontal plane outside the atmosphere is given by Tadili and Bargach [28]:

$$H_0 = \frac{24}{\pi} I_o \left(\cos(\delta_j)\cos(\phi)\sin(\omega_j) + \omega_j \sin(\delta_j)\sin(\phi)\right) \quad (6)$$

I_o(W/m²) is the corrected solar constant which expression is given by equation (7) as follows:

$$I_o = 1367\left[1 + 0.034\cos\left(\frac{360}{365}(N_j - 3)\right)\right] \quad (7)$$

By analyzing the models of global solar radiation developed in Africa and reported in the work of Chukwujindu [26], the hybrid models established by several authors have proved to be more reliable than the other formulations encountered. However, no formulation of these Hybrid models exploited in Africa takes into account simultaneously the solar fraction at order greater than 1. The power form of the solar fraction as well as the ambient air temperature and relative humidity is often 1. In this study, we, therefore, preferred to estimate global solar radiation as a function of these meteorological variables.

In equation (1), we therefore optimally introduce the solar fraction with an unknown exponent α, the ambient temperature (T_a) and air relative humidity (R_r) meteorological factors that directly influence global solar radiation. To further reduce the divergence between observation data and estimated ones, we have also introduced calibration constants for the proposed model. The expression of global solar radiation is given by equation (8) as follows:

$$\frac{H}{H_0} = \left(a + b\left(\frac{n_j}{N_{oj}}\right) + c\left(\frac{n_j}{N_{oj}}\right)^{\alpha} + dT_a + e\,RH\right) \quad (8)$$

α, *c, d*, and *e* are model calibration constants. All the constants α, *a, b, c, d*, and *e* are determined by numerical simulation of the Nelder-Mead simplex algorithm [29]. Indeed, the simplex algorithm, one of the most widely adopted methods for unconstrained nonlinear multidimensional optimization, was used in this study to better calibrate the proposed model. In the Matlab software, the function ***"fminsearch***" was used to simulate this algorithm. "Fminsearch" finds the minimum of a scalar function of several variables, starting with an initial estimation. This is generally called unconstrained nonlinear optimization. The method consists of wrapping the minimum in a simplex. A simplex is a set of (N+1) points surrounding the minimum (a line in one dimension, a triangle in 2 dimensions, and a pyramid in 3dimension). Each simplex is characterized for N+1 vectors at the vertices of the simplex. A new point is taken inside or next to the simplex at each calculation step. The value of the function at this point is compared with the values of the functions evaluated at the vertices. One of the vertices is then replaced by the new point generating a new simplex (by reflection, expansion, or contraction). The procedure is repeated as long as the diameter of the simplex is not smaller than a specified tolerance.

3.2.2 Statistical Testing

To evaluate the discrepancies between global solar radiation measurements and model estimates, the square root mean square error (RMSE) and absolute mean error (MAE) estimators were determined:

$$RMSE = \sqrt{\frac{1}{n}\sum_{i=1}^{n}(p_i - f_i)^2}$$

$$MAE = \frac{1}{n}\sum_{i=1}^{n}|(p_i - f_i)|$$

Where p_i represents measurements, f_i the predictions and n the number of observations. When these estimators are low and close to zero the estimates are in agreement with the measurements.

4 Resultats and discussion

4.1 Daily variation of solar declination δ_j, the irradiation out of the atmosphere I_o, the angle of sunrise ω_j and the astronomical length of the days N_{oj}

Figure 3 presents the variations of the astronomical parameters of the sun in the Nalohou AMMA CATCH measurement site.

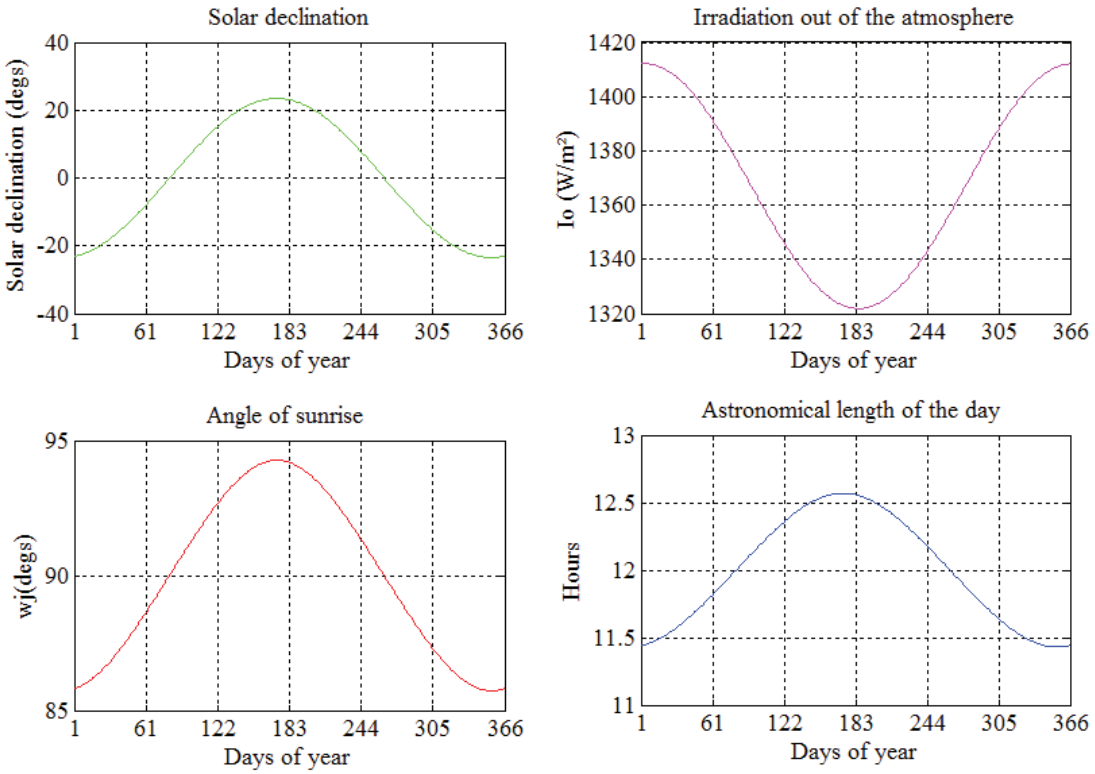

Figure 3: Daily mean variation of δ_j, I_o, ω_j, N_{oj} during the year in Nalohou (2007-2009)

Sun's declination angle during the period from July 2007 to July 2009 varies on average from -19° to 21°. The peak of this angle is observed in early July. The irradiation outside the atmosphere varies between 1320W/m² and 1410W/m² with the minimum recorded at the beginning of July. The angle of the sunrise is between 86° and 94° during the year and the astronomical length of the day varies from 11.4 h to 12.6 h with a peak always observed around the beginning of July. The lowest values of out of atmosphere irradiation are therefore reached when the sun's declination angle, the sunrise angle, and the astronomical length of the day are at their maximum values.

4.2 Simulation and validation of the proposed model at Nalohou site

Figures 4 and 5 present the results of the simulation from the proposed model using global solar radiation data measured at the Nalohou site. The calibration's constants of the model are also evaluated throughout the year. From figure 4, one can notice a seasonal variation of the solar irradiation. So, figure 5 is drawn to compare the seasonally observed data to those generated by the model.

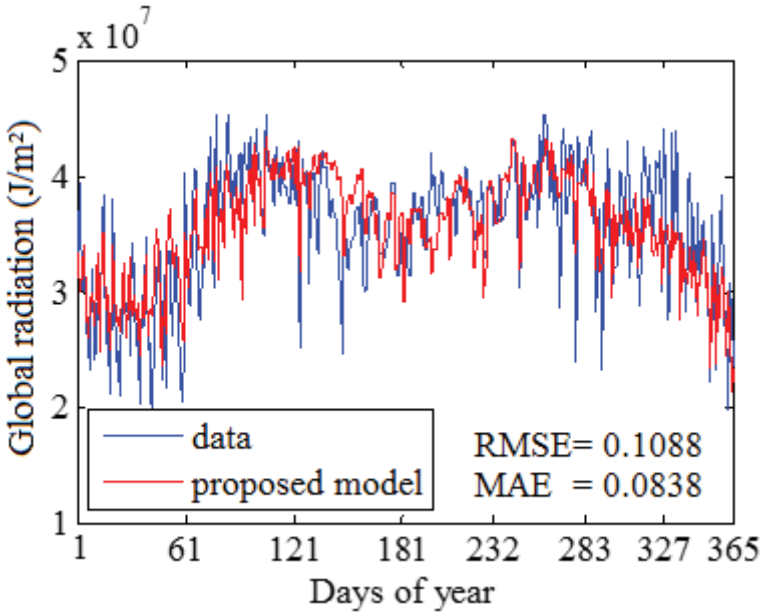

Figure 4: Correlation between the proposed model and the global solar radiation observed data for 2016

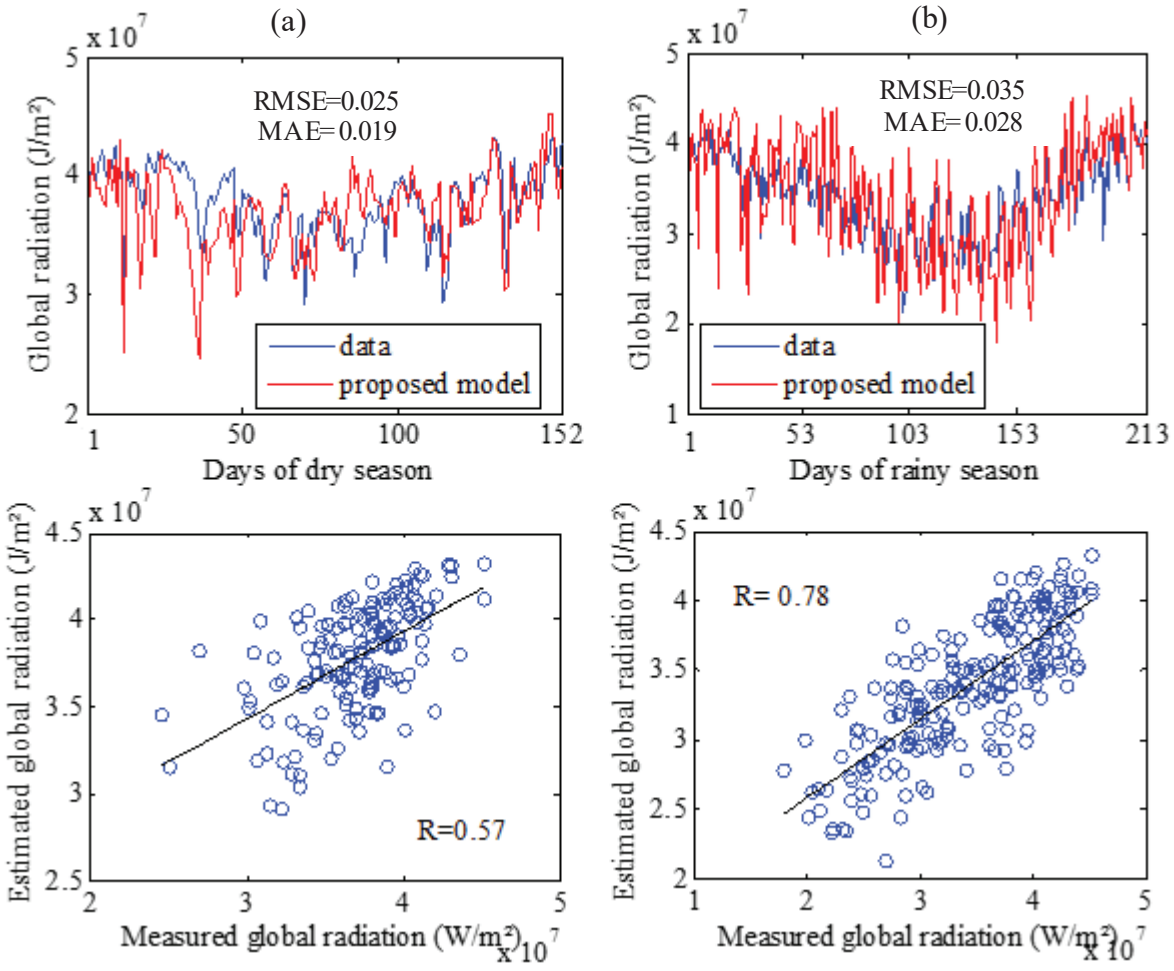

Figure 5: Correlation between proposed model estimates and global solar radiation data in 2016: (a) dry season and (b) rainy season

The model proposed in this study and the measurements of global solar radiation generally show good agreement throughout the year. The error estimators of the square root mean square error (RMSE) and the absolute value of the mean error (MAE) values are 0.1088 and 0.0838, respectively. Similarly, a seasonal analysis of the correlation between estimated values of GSR and observed data shows that during the dry season from November to March, the errors of estimates (RMSE, MAE) values are 0.025 and 0.019 respectively, showing the model's seasonal efficiency. During the rainy season from April to October, these values are 0.035 and 0.028, respectively. One can notice that the seasonal error estimators are lower than those of the entire year 2016 form figure 4. Therefore in the study site, the seasons have a greater influence on global solar radiation. From November to December, there is a divergence between the regenerated GSR values and the measurements. This observation is confirmed by the low value of the correlation coefficient obtained during the dry season (0.57). This gap could be due to the influence of "Harmattan" flux (dry air blowing from Sahara toward the Atlantic Ocean) in the study area at this period of the year. This dry and dusty wind brings suspended particulates maters in the atmosphere which could attenuate the global solar radiation received on the ground. A model integrating the aerosol rate in the atmosphere could therefore better reproduce this radiation sequence at our site during the period. On the other hand, during the rainy season, the measurements and the estimates values of GSR show the same direction of variation, justified by a fairly good value of the correlation coefficient (0.78). However, we note that the model slightly overestimates the measurements throughout the rainy season. This observation could be justified by the presence of frequent clouds events in the sky during the rainy season. The integration of cloud cover parameters in the model could correct this overestimation.

The error obtained in this study were compared to those observed by other authors who used the Angström formulation to estimate GSR in Africa. Adeyemi *et al.* [30] developed global solar radiation estimation models for the nine South African provinces using several meteorological parameters such as insolation, ambient temperature, relative humidity, and wind speed. The accuracy of the models was verified by comparing the estimated values with the measured values, using the following statistical error tests: mean bias error, mean absolute bias error, mean absolute percentage error, root mean square error. His results indicate that these error estimators range from 5.40% to 11.19% at the study sites. Adeniji *et al.* [31] estimated global solar radiation from the distribution of sunshine hours and the brightness index in Enugu (Nigeria). The authors then evaluated the margins of error between models and measurements and the values obtained did not exceed 2.5%. Okundamiya and Nzeako [3] proposed a model based on the monthly mean global solar radiation temperature on horizontal surfaces for selected cities, representing the six geopolitical zones of Nigeria. The results of three statistical indicators: mean bias error (MBA), root mean square error (RMSE) and *t-statistic* test (TS) evaluated indicate that the RMSE and MBA ranged from 0.0023 at the Benin City site, 0.2685 for Katsina site. Quansah *et al* [10] after estimating global solar radiation by empirical models in the Ashanti region of Ghana obtained error estimators mean percentage error (MPE), mean bias error (MAE) and root mean square error (RMSE)) ranging from 0.0102 to 1.7075.

Coulibaly and Ouedraogo [15] correlated the global solar radiation of eight synoptic stations in Burkina Faso based on linear and multiple linear regression methods. The results show that the relative errors obtained range from 3.16% to 3.65% in Dedougou. In the study of Ajayi *et al.* [22], the authors proposed five models for estimating

global solar radiation over 12 sites spread over the six geopolitical zones in Nigeria based on the solar fraction, maximum temperature, relative humidity, the latitude of the site. The estimation errors of these models vary between 3.9 10^{-5} and 0.36. In the study of Asilevi *et al*. [5], the global solar radiation in Ghana was quantified using the Angström-Prescott sunshine model and sunshine duration data from 22 synoptic stations distributed over the ecological zones of the country. The absolute mean percentage error obtained by the authors range from 3% to 29%**.** Onyango and Ongoma [16] estimated the global solar radiation potential over the city of Nairobi. Hassan *et al.* [20] have presented new ambient temperature-based models for estimating global solar radiation at several sites in Egypt as alternatives to the widely used sun-based models due to the unavailability of solar radiation's data. Seventeen new temperature-based models are established, validated, and compared to the three other models proposed in the literature to estimate monthly mean daily global solar radiation on a horizontal surface. The estimation errors of these models range from 0.006 to 0.70. Solar irradiation data recorded in three localities (Lomé, Atakpame, and Mangue) representing the climate and geographical areas of Togo were analyzed by Banna and M. Gninin ri [32]. The monthly daily global radiation on a horizontal surface for the three cities is deduced from the relative sunshine data using the method developed by Angstrom. Appropriate regional parameters are determined and used to predict the solar irradiation in the three localities with an error of less than 8%.

Because of these various studies, one can see that the performance of solar radiation estimation models vary from one site to another. Some values of the error estimators found in the literature are higher than those observed in the current study, especially at some sites in Egypt, Nairobi, Ghana, Nigeria, and South Africa. Others, on the other hand, are lower than the estimators obtained in Nalohou, particularly in Dedougou sites in Burkina Faso, Enugu in Nigeria, and at other sites in Ghana, Nigeria, and Egypt. However, models with margins of error of 10 to at most 20% have been approved and validated by the various authors. Given these observations, the errors in the estimation of global solar radiation presented at the Nalohou site are tolerable and thus allow us to confirm the performance of the proposed model. The margins of error of the model estimation is tolerable as they are of the order of 10^{-1} to 10^{-2}. However, this model could be improved by integrating meteorological parameters such as aerosol content in the atmosphere and cloud cover data.

In Table 2, the values of the calibration constants of the proposed model are presented

Table 2: Model fitting constant

Proposed model (Nalohou)						
Constant	a	b	c	α	d	e
Along year	0.0571	0.1589	0.3739	0.7216	0.0173	0.0021

Figure 6 presents the validation of the proposed model.

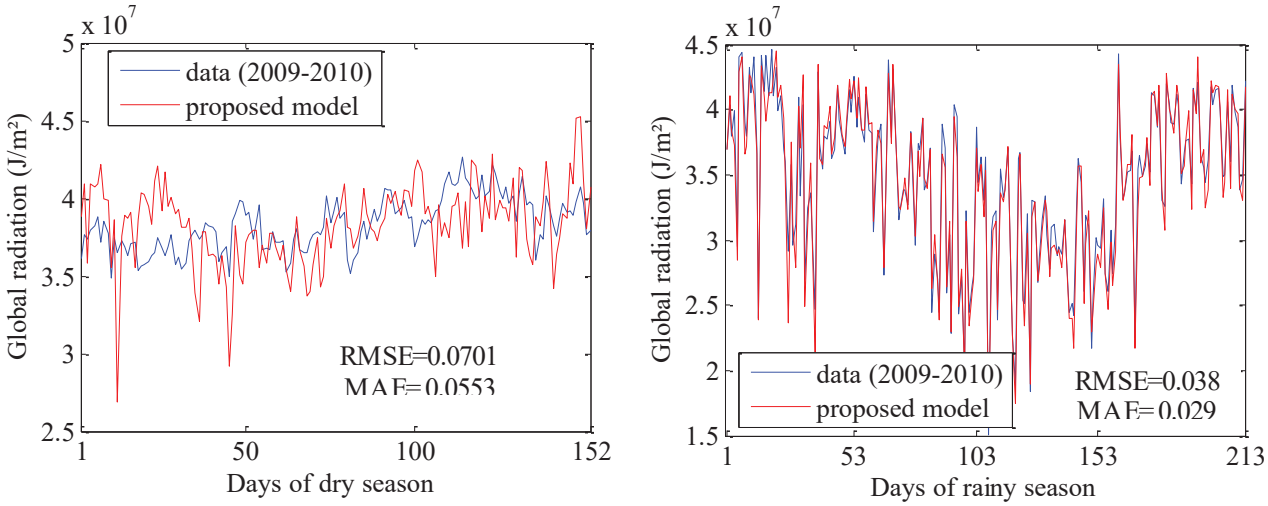

Figure 6: Validation of the proposed model (2009-2010)

The estimation errors (RMSE; MAE) of global solar radiation obtained from the proposed model and the data measured over the period from 10 July 2009 to 10 July 2010 are 0.0701 and 0.0553 for the dry season; they are 0.038 and 0.029 for the rainy season. These small margins of error allow us to validate the proposed model, which can now be used in this region of north-west Benin as a model for estimating global solar radiation.

4.3 Estimation of global solar radiation

Based on the proposed model, the estimated global solar radiation at Natitingou synoptic station is presented in Figure 7 for an entire year (2016).

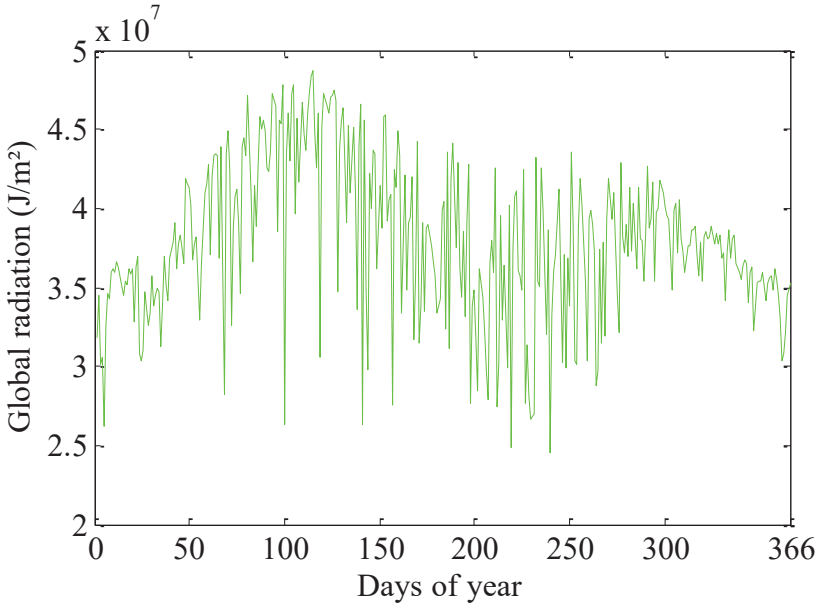

Figure 7: Daily variation in global solar radiation at Natitingou (2016)

In Figure 7, the estimated global solar radiation at the Natitingou meteorological station is of the same order of magnitude as that measured at Nalohou but varies between 2.45 X 10^7J/m² and 4.86 X 10^7J/m² (i.e. 6.80 kWh/m² to 13.5 kWh/m² or 283.56 W/m² to 562.50 W/m²) as opposed to the Nalohou site where measurements are between 1.79 X 10^7J/m² and 4.53 X 10^7 J/m². The annual average global solar radiation is estimated at 3.78 X 10^7J/m² (10.50 kwh/m²) at Natitingou and 3.53 X 10^7 J/m² (9.80 kWh/m²) at Nalohou. There is therefore a slight increase in GSR at Natitingou. The range of global solar radiation observed in this region of north-western Benin is therefore very useful for designers and installers of solar systems, which now have a reliable database of solar radiation that can be used for all purposes.

5 Conclusion

At the Nalohou site in northern Benin, a model for estimating global solar radiation was developed and validated using solar radiation data recorded at this site. Based on the proposed model, global solar radiation was estimated at the Natitingou site, which has climatic similarities to the Nalohou site. The main results of this study indicate that the annual average global solar radiation observed in the north-western region of Benin varies between 3.53 X 10^7 J/m² and 3.78 X 10^7J/m² (9.80 kWh/m² to 10.5 kWh/m²). The proposed global solar radiation estimation model can be used with a small margin of error of 8 to 10% throughout the year. During the dry and rainy season, the model can reproduce the measurements with an error of 2% to 3% respectively. However, the model could always be improved by combining aerosol content and cloud cover data, which are two parameters that influence the radiative fluxes received on the ground in our study area.

As a result of this study, a reliable database of global solar radiation is now available to solar system designers and installers to better size their installations.

6 References

[1] C. Schillings, R. Meyer, F. Trieb, Solar and wind energy resource assessment (swera), High-Resolution Solar Radiation Assessment for Kenya. *Final country report prepared by DLR*–submitted to UNEP/GEF, 2004.

[2] B. Safari and J. Gasore, "Estimation of Global Solar Radiation in Rwanda Using Empirical Models", *Asian Journal of Scientific Research*, vol 2, pp68-75, 2009.

[3] S. Okundamiya and A. N. Nzeako, "Empirical model for estimating global solar radiation on horizontal surfaces for selected cities in the six Geopolitical zones in Nigeria" *Journal of Control Science and Engineering*, Vol 2011, Article ID 356405, pp1-7 2011.

[4] E. O. Falayi and A. B. Rabiu, "Estimation of global solar radiation using cloud cover and surface temperature in some selected cities in Nigeria" *Archives of Physics Research*, vol.2, no.3, pp.99-109, 2011.

[5] P. J. Asilevi, E. Quansah, L. K. Amekudzi, T. Annor, N. A. B. Klutse, “Modeling the spatial distribution of Global Solar Radiation (GSR) over Ghana using the Angström-Prescott sunshine duration model“ *Scientific African* vol.4, 2019, e0 0 094.
[6] A. M. Muzathik, W. B. W. Nik, M. Z. Ibrahim, K. B. Samo, K. Sopian, and M. A. Alghoul, "Daily global solar radiation estimate based on sunshine hours", *International Journal of Mechanical and Materials Engineering*, vol.6, no.1, pp.75-80, 2011.
[7] A. A. Trabea and M. A. M. Shaltout, "Correlation of global solar radiation with meteorological parameters over Egypt", *Renewable Energy*, vol 21, no.2, pp. 297-308, 2000.
[8] E. B. Pereira, F. R. Martins, S. L. Abreu, H. G. Beyer, S. Colle, R. Perez, D. Heinemann, "Cross-validation of satellite radiation models during SWERA project in Brazil", in Proceedings of the ISES Solar World Congress, pp.14–19, Göteborg, Sweden, June 2003.
[9] M. J. Ahmad and G. N. Tiwari, "Solar radiation models a review” *International Journal of Energy Research,* vol.35, no.4, pp.271-290, 2011.
[10] E. Quansah, L. K. Amekudzi, K. Preko, J. Aryee, O. R. Boakye, D. Boli, and M. R. Salifu, "Empirical models for estimating global solar radiation over the Ashanti region of Ghana", *Journal of Solar Energy*, vol 2014, Article ID 897970, pp1-6, 2014.
[11] L. E. Akpabio, S. O. Udo, and S. E. Etuk, "Empirical correlations of global solar radiation with meteorological data for Onne, Nigeria", *Turkish Journal of Physics*, vol.28, no.3, pp. 301-307, 2004
[12] E. O. Falayi and A. B. Rabiu, "Modeling global solar radiation using sunshine duration data", *Nigeria Journal of Physics*, vol 17, pp. 181-186, 2005.
[13] E. O. Falayi, J. O. Adepitan, and A. B. Rabiu, "Empirical models for the correlation of global solar radiation with meteorological data for Iseyin, Nigeria, " *International Journal of Physical Sciences*, vol. 3, no. 9, pp. 210-216, 2008.
[14] A. Karoro, T. Ssenyonga, J. Mubiru, "Predicting global solar radiation using an artificial neural network single-parameter model", *Adv Artif Neutral Syst*, pp 1-7, September 2011.
[15] O. Coulibaly and A. Ouedoraogo, "Correlation of global solar radiation of eight synoptic stations in Burkina Faso based on linear and multiple linear regression methods", *J Sol Energy*, pp1-12. January 2016.
[16] A. O. Onyango and V. Ongoma, "Estimation of mean monthly global solar radiation using sunshine hours for Nairobi City, Kenya", *J Renew Sustain Energy*, vol 7, n°5, pp 1-11. 2015.
[17] A. Yisehak, "Comparison of different empirical models in the estimation of mean global solar radiation using sunshine duration measure at Dire Dawa, Ethiopia". Published MSc. Project 2014, pp 1-63.
[18] D. Afungchui and R. N. Neba, "Global solar radiation of some regions of Cameroon using the linear Angstrom and non-linear polynomial relations (Part 1) models development", *Int J Renew Energy Res*. Vol 3, n° 4, pp 984-92, 2013.
[19] A. A. Adeola, Z. Huan, C. C. Enweremadu, "Evaluation of global solar radiation using multiple weather parameters as predictors for South Africa Provinces", *Therm Sci*, vol 19, pp 495-509, 2015.
[20] G. E. Hassan, M. E. Youssef, E. Mohamed, M. A. Ali and A. A. Hanafy, ‘‘New Temperature-based Models for Predicting Global Solar Radiation’’, *Applied Energy* vol 179, pp 437-450. 2016.
[21] M. Dankassoua, ‘‘Etude du rayonnement solaire global à Niamey de la période de pré-mousson et de la mousson de l’année 2013 (mai à octobre) ’’, *Revue des Energies Renouvelables*, vol 20, n°1, pp 131 -146, 2017.
[22] O. O. Ajayi, O. D. Ohijeagbon, C. E. Nwadialo, O. Olasope, ‘‘New model to estimate daily global solar radiation over Nigeria’’. *Sustainable Energy Technol*, vol 5, pp 28-36, 2014.

[23] B. M. Olomiyesan, D. Onyedi, O. D. Oyedum ‘‘Comparative study of ground measured, satellite-derived, and estimated global solar radiation data in Nigeria’’. *J Sol Energy*, 2016. Pp 1-7, 2016.
[24] S. Amoussa, ‘‘Estimation of global radiation in Benin’’. *Renewable Energy*, Vol 2, N°3, pp311-317, 1992.
[25] O. Mamadou (2014) Etude des Flux d’ Evapotranspiration en Climat Soudanien: comportement comparé de deux couverts végétaux au Bénin. Thèse de doctorat, Université de Grenoble, France.
[26] N. S. Chukwujindu, ‘‘A comprehensive review of empirical models for estimating global solar radiation in Africa’’, *Renewable and Sustainable Energy Reviews*, vol 78, pp 955-995, 2017.
[27] K. Hinrichsen, ‘‘The Ångström formula with coefficients having a physical meaning, Solar Energy Vol 52, Issue 6, pp 491-495, 1994.
[28] R. Tadili and M. N. Bargach, ‘‘Une méthode d’estimation du rayonnement solaire global reçu par une surface inclinée Application aux sites marocains’’, *La Météorologie - n° 50*, pp 46-50, 2005.
[29] J. C. Lagarias., J. A. Reeds, M. H. Wright, and P. E. Wright, ‘‘Convergence Properties of the Nelder-Mead Simplex Method in Low Dimensions’’, *SIAM Journal of Optimization*, vol. 9, n°1, pp. 112-147, 1998.
[30] Adeyemi, Adeola*, Z.* H*uan* and C. C. Enweremadu, "Evaluation of global solar radiation using multiple weather parameters as predictors for south Africa provinces", *Thermal Science*, Vol. 19, Suppl. 2, pp. S495-S509, 2015.
[31] N. O. Adeniji, J. A. Akinpelu, S. O. Adeola, J. O. Adeniji, "Estimation of Global Solar Radiation, Sunshine Hour Distribution and Clearness Index in Enugu, Nigeria", *J. Appl. Sci. Environ. Manage*, Vol. 23 (2), pp. 345-349, 2019.
[32] M. Banna and M. Gninin ri, ‘‘Estimation of monthly average hourly and daily global irradiance in Togo’’, RERIC International Energy Journal, vol 20, n°1, pp 21-37,1998.

SII-1b

Solar power in product development

An application for Western Africa

Jörg Reiff-Stephan [1]

The availability of electrical energy is one of the essential basic elements for economic growth and humanitarian living conditions. In one of the poorest regions of Western Africa - in the savannah region of northern Togo - the central expansion of electricity grids has not taken place. Decentralized solutions based on renewable energy systems can help here and promote the region's development. In the presented paper, the various renewable energy carrier systems were examined with regard to their use in the savannah region of Western Africa. The solar energy carrier system could be used as a power supplier in the secondary conversion process to mechanical power. Subsequently, a prototype for a clay brick production machine was designed and a digital mock -up was developed. Together with the partners in Togo, the prototype is built and tested in the field. Experiences are being gathered in cooperation with Bonita-Haus and will be incorporated into the educational content in Togo as well as at the Technical University of Wildau. This will make a significant contribution to the utilization of the technology at the site and to improving the living conditions in Western Africa.

1 Introduction

A large part of the African continent is still affected by poverty [1]. This state of affairs is particularly characteristic of the Western African republic of Togo. The nation is one of the poorest countries in the world. Especially in the northern savannah region the population has only limited financial means. The average income is between 30 and 120 Euros per year. The causes of poverty are complex and partly still rooted in the colonial past. The country's infrastructure is equally poor. The north-south bypass is a simple road connection. The accessibility of the adjacent areas is strongly dependent on the soil conditions and the degree of erosion due to the climatic conditions. This situation is accompanied by the fact that a central energy supply and distribution is only guaranteed up to the centre of the country. Remote settlements have no electricity and no running water supply and disposal. At the same time, however, these areas are heavily dependent on the use of electrical energy sources, for example to operate pump systems or similar mechanical auxiliary elements and lighting systems [3]. The lack of these basic facilities hampers the country's development, and this is particularly true of the region's education system. Without electrical energy, teaching can only take place in daylight. In the evening hours, students can only do their homework to a limited extent, as oil lamps and candles are usually the only sources of light. The same applies to the preparation of lessons by the teachers. Furthermore, under the given circumstances no school meals can be guaranteed. However, the lack of energy not only makes the operation of the school system difficult, but also

[1] Prof. Hon.-Prof. Dr.-Ing. Jörg Reiff-Stephan, TH Wildau, Wildau - Germany

its expansion. For the region of Northern Togo, an acute undersupply of school places can be observed (Figure 1).

Figure 1: School class in Kourdjoak

Funds for the creation of new capacities are scarce. Nevertheless, the cost-intensive use of diesel generators (Figure 2) is the only way to generate electricity on corresponding construction sites.

Figure 2: Energy system diesel generator as the only power source to supply the construction site

It will be essential for further regional development that new, sustainable energy sources are identified. In addition to the opportunities arising from this economic exploitation, the creation of

training and the fundamental further development of existing knowledge structures should also be created. To this end, it will be indispensable that technological knowledge is transported in a form that focuses on cooperation rather than on teaching [2, 4]. Teaching and training institutions in Western Africa will be embedded in the development processes through the concepts of Distant Learning, especially Distant Product Development (DτD) (Figure 3) [7]. In this way, the "help for self-help" approach is considered and further development is supported in a sustainable manner.

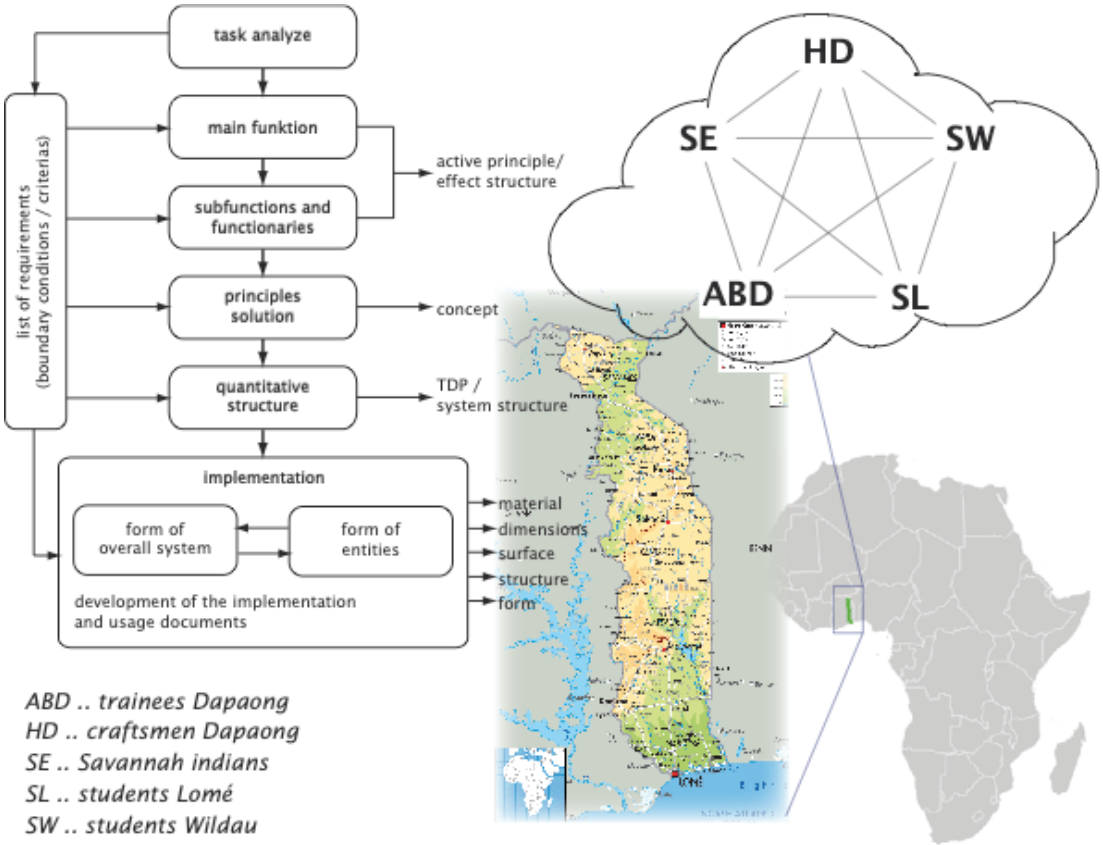

Figure 3: Concept "Distant Product Development (DτD)" in teaching

The analysis and synthesis phases of the projects are carried out both with the local people (users of the developments) and in the developmental context with the trainees and students of the region as well as with students from the author's direct development environment. The main goal of the partnership support is to show the population of Northern Togo ways to use the high potential of renewable energy and to illustrate its concrete application with examples. In dealing with the users of the technology, the focus is primarily on personal contact. With an increasing level of education, the use of the Internet and the advantages of distributed working are generally known. Communication and data exchange can be supported by appropriate cloud systems.

In addition to the Technical University of Applied Sciences Wildau, the Berlin School of Arts, the German Association for "German-African Cooperation e.V." (DAZ) as well as the University of Lomé, the IT Village (Dapaong) and the training centre Bonita-Haus (Dapaong) are cooperation partners in the DτD network.

2 Requirements

The Republic of Togo is one of the states of Western Africa and is surrounded by the countries Ghana, Benin and Burkina Faso. The Gulf of Guinea of the Atlantic Ocean forms the narrow southern border of Togo. The country is located between the 6th and 12th latitudes of the northern hemisphere. For the estimation and evaluation of a possible renewable energy source it is essential to derive and define climatic conditions and usage requirements.

2.1 Climatic conditions

Due to its geographical proximity to the equator, the country enjoys an annual average of about 6.5 hours of sunshine per day. Figure 4 shows a graphical representation of the hours of sunshine over the year for the Togolese capital Lomé. For a better illustration of the order of magnitude, the curve for the location Berlin is also shown.

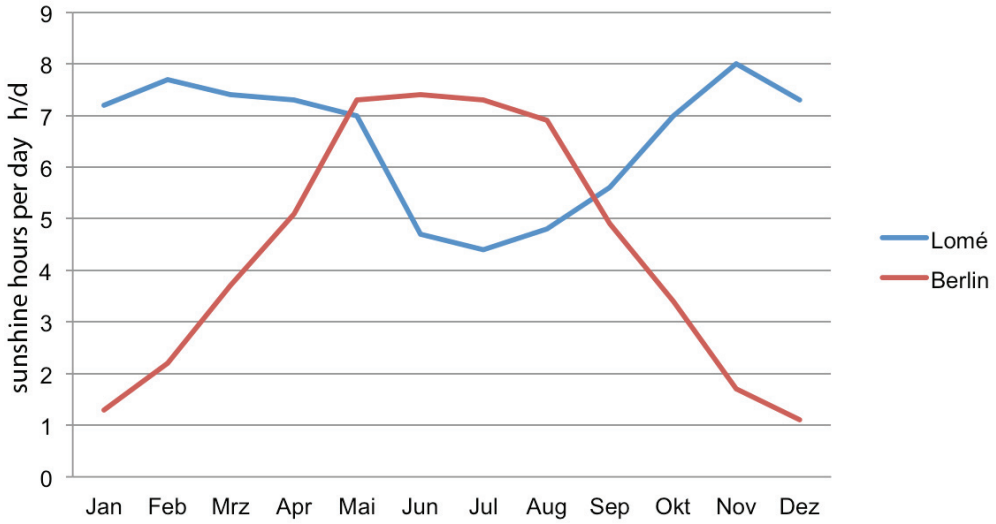

Figure 4: Comparison of the sunshine hours

The climate of Togo can be described as tropical-humid all year round. It should be noted, however, that there are significant climatic differences between the southern and northern parts of the country. The climate of the southern regions is influenced by the Atlantic Ocean, which leads to a year-round high humidity of about 80%. In the south the average temperature is 27°C and there are two rainy seasons per year. These are to be expected in the period between April and June and September and November. In contrast to the south, the north of the country has a dry, savannah-like climate. The average temperature is 30°C and the rainy season occurs only once a year between May and October.

2.2 Usage requirements for an overall system

The development of a transportable plant for decentralized energy conversion must be carried out with special requirements in mind. Of central importance here are simple operability as well as low maintenance of the plant. Due to the aforementioned deficits in the educational system there is a lack of qualified personnel. Consequently, the system must also be operable by persons who have only received brief instruction in this respect. However, such measures are made more difficult by the diversity of languages. Togo is a multi-ethnic state and unites 42 different

ethnic groups and 39 languages. However, the official language French is not spoken by all parts of the population, especially in the rural areas. For these reasons, the probability of operating errors increases with increasing operating requirements. When selecting the energy system, it is important to ensure that operating errors are avoided as far as possible and that no serious consequences result for the operator or the system. In the event of damage to the system, it is advantageous to have a low maintenance requirement. On the one hand, this is due to the above mentioned lack of qualified personnel. Furthermore, the weak infrastructure in northern Togo makes it difficult to obtain spare parts. Therefore, a low susceptibility to failure should be aimed for during the development. In particular, the extreme climatic conditions play a decisive role here. When implementing an appropriate solution, one should therefore not go to the limits of what is technically feasible. In the sense of "*help for self-help*", the population should be motivated to copy such systems in order to use them in many different ways. For this purpose, a low production effort and low production costs are a prerequisite. Usually the use of diesel generators is the preferred way of self-sufficient power generation. Although they have relatively low acquisition costs, they are expensive during operation. The main reasons for this are the high maintenance effort and fuel costs. A practicable alternative to the diesel generator must therefore convince through low operating costs, high energy availability and the lowest possible level of environmental impact.

3 Analysis of potential energy sources

The term energy generally defines the ability to perform physical work. If an energy source is inexhaustibly available after human time horizon, one speaks of renewable energy sources [6].

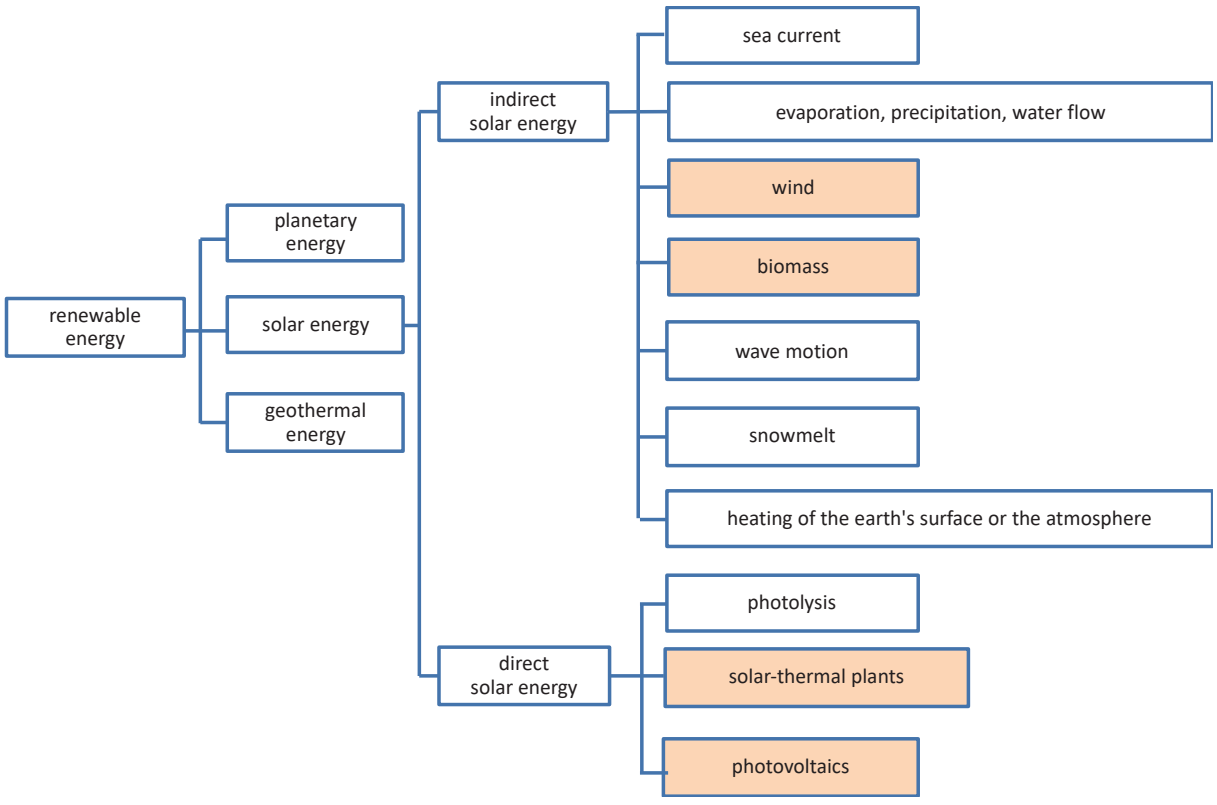

Figure 5: Classification of energy sources

The north of Togo does not have a significant power grid. For the rural regions of the country the decentralized and self-sufficient energy supply is therefore of particular importance. From the spectrum of renewable energy sources and conversion processes, the following technologies have the potential for such an application in Northern Togo. These include wind power plants, photovoltaic technology, solar thermal power plants and the use of biomass energy sources (given in Figure 5).

The highlighted areas were analysed and discussed in detail by the DπD partners with regard to their applicability. One example of this is the Photovoltaic technology. Compared to the countries of Central Europe, Togo has good conditions for the use of photovoltaic technology. Figure 6 shows a comparison of the radiation sum for the locations Berlin and Dapaong. The curves refer to a surface oriented horizontally to the ground.

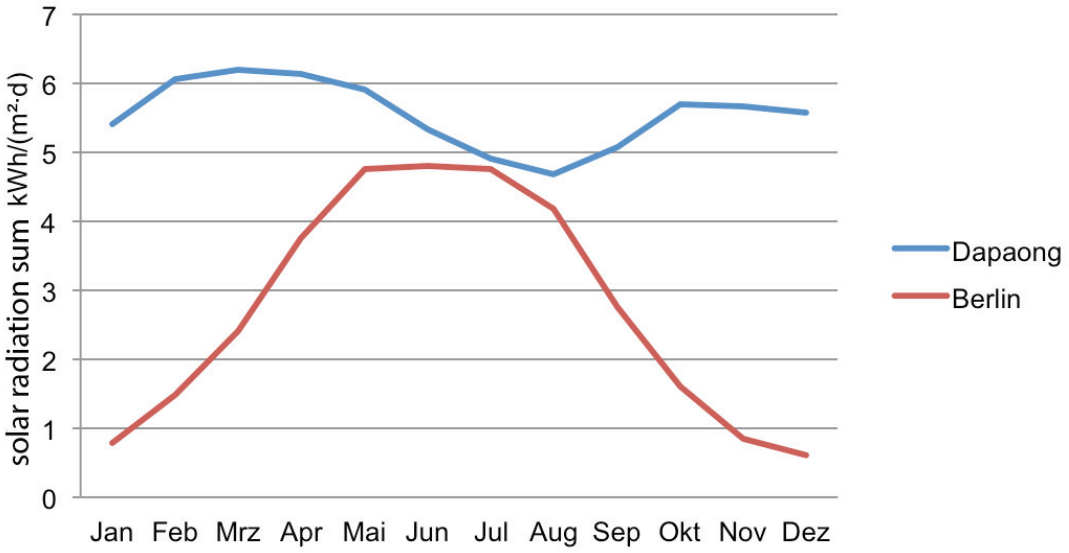

Figure 6: Solar radiation sum (average of three decades since 1983)

It can be seen that Togo has a high supply of solar radiant energy all year round. This results in a large number of possible applications for photovoltaic technology in the form of off-grid standalone solutions. When designing such systems, however, it must be borne in mind that the extreme climatic conditions place great demands on the PV modules and the electrochemical storage elements.

The selection of a suitable energy source for the northern Togolese savannah region is based on a utility value analysis (UVA) according to VDI 2225. Figure 7 shows a comparison of the degree of fulfilment and the electricity production costs for the respective technologies. Technology-related and economic parameters were added as essential criteria of the UVA. Strong distinctions can be seen when considering the availability of the primary energy source at the "Northern Togo" location as well as the social and environmental compatibility of the technology. It can be observed that biomass systems, in particular, act fundamentally contrary to the humanitarian possibilities. Neither the cultivation of biomass nor the consumption of waste products in agriculture can be sensibly used for electricity generation. With regard to the expected investment costs, it must be mentioned that initial installations are largely covered by foreign aid

organisations. Nevertheless, the correlation of a promotion or development potential of the plant should consider the multiplication of the technology. Finally, it is essential that the technology to be selected has the lowest possible operating and maintenance costs and is robust in its use. A daily influence by trained personnel should not be necessary.

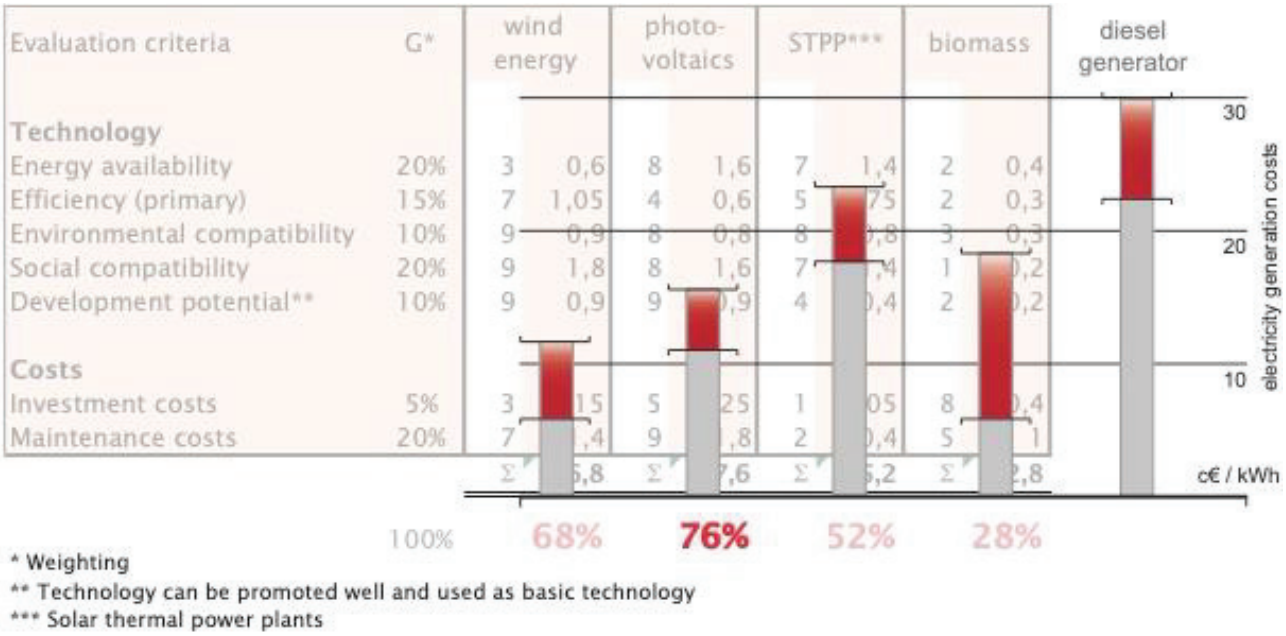

Figure 7: Utility value analysis of the energy carrier systems and electricity production costs in comparison to diesel generators

It can be seen that photovoltaic technology comes closest to the ideal solution with a degree of fulfilment of 76 %. Although it has a poorer efficiency compared to wind generators, a high yield is not to be expected due to the low wind speeds at the site. Furthermore, the consideration of the electricity production costs shows that the energy conversion with PV systems, compared to the diesel generator, is much cheaper. Therefore, under the given circumstances, photovoltaic technology can be considered the most suitable energy source for the north of Togo.

4 Clay brick press case study

The alternative drive of a manual clay brick press offers a possibility of using renewable energy. This is used, as mentioned at the beginning, for the extension and new construction of school buildings in northern Togo. With the clay brick press of the type Terstaram (Figure 8) from the Belgian manufacturer ApproTechno, an average of 60 clay bricks per hour can be produced. With a ten-hour working day, the daily production is 600 clay bricks.

For the production of the mentioned amount of mudstones, about 660 Wh of physical labour are required at the moment. This statement is based on the following rough calculation. It is assumed that during the pressing process two workers operate the levers of the press with a force F of 400 N each. The levers have a length l of 0.7 m and a resulting torque M = 560 Nm.

Figure 8: Manual clay brick machine *Terstaram*

The rotary movement takes place at an angle of 270° and a speed of n = 10 rpm. If these parameters are transferred to equation (1), the resulting power is P = 587 W.

$$P = M \cdot \omega = M \cdot 2 \cdot \pi \cdot n = 560\,Nm \cdot 2 \cdot \pi \cdot 0{,}167\ {}^{1}/_{S} = 587\,W \tag{1}$$

With 600 pressing processes per day with a duration of t = 4.5 s each and the previously determined power, the energy required is related according to equation (2):

$$E = P \cdot t = 587W \cdot 4{,}5s \cdot 600 = 0{,}587kW \cdot 0{,}00125h \cdot 600 = 0{,}44kWh \tag{2}$$

For the pressing processes, an energy of E_P = 0.44 kWh is therefore required. Assuming that only half of the force is required to release the press, the energy requirement for the pressing process is E_L = 0.22 kWh. In total, a total energy of E_G = 0.66 kWh is required for the production of 600 clay bricks. If the torque produced by the workers is now to be generated mechanically, the efficiency of the motor and gearbox must also be considered. For the press drive system an electrical input power of $P_{el,p}$ = 814 W or $P_{el,l}$ = 407 W is required. For the mechanical drive of the press an energy of E_{el}=0.916 kWh is required.

The provision of this amount of energy is to be guaranteed by an island system based on photovoltaic technology. The central system components here are the PV generator and accumulator. An initial rough calculation of the required output of the PV generator is made according to equation (3) with parameters from Table 1 [5].

$$P_{\mathrm{PV}} = \frac{W}{N_{\mathrm{Sonne}} \cdot K_{\mathrm{Schräg}} \cdot K_{\mathrm{Temp}} \cdot V_{\mathrm{Leitung}} \cdot V_{\mathrm{Umwandlung}} \cdot V_{\mathrm{Anpassung}}} = 475\,Wp \tag{3}$$

Parameters		Value
energy demand	W	916 Wh
sunshine hours	N_A	4.55 h
correction factor	$K_{Schräg}$	1
correction factor	K_{Temp}	0.625
line loss factor	$V_{Leitung}$	0.94
conversion loss factor	$V_{Umwandlung}$	0.8
adjustment loss factor	$V_{Anpassung}$	0.9

Table 1: Technical system parameters I/II

A total module output of P_{PV}= 475 W_p must therefore be provided for the PV generator. Equation (4) is used to roughly determine the battery capacity C_N. The corresponding parameters are shown in Table 2 [5].

$$C_{\mathrm{N}} = \frac{W \cdot N_{\mathrm{A}}}{K_{Entl} \cdot U_{\mathrm{N}}} = 153\ \mathrm{Ah} \tag{4}$$

Parameters		Value
energy demand	W	916 Wh
autonomy Days	N_A	2
discharge threshold correction factor	K_{Entl}	0.5
system voltage	U_N	24 V

Table 2: Technical system parameters II/II

The previously calculated values for P_{PV} and C_N serve as a basis for orientation in order to make a pre-selection of usable PV modules and accumulators. The exact dimensioning of the system is carried out with the PV*SOL Expert design program. The parameters of the most common PV modules and accumulators are stored in its database. The software can be used to simulate and compare corresponding scenarios for the selected component combination. Depending on the cell technology and the calculation parameters, an area of 3.5 - 5 m² can be expected for the PV generator to be implemented later.

Since the location of the energy supply unit changes according to the respective construction site, the mobility of the system must be guaranteed. For this purpose, the PV generator is mounted on a trailer. The road conditions in the northern Togolese regions can be described as poor. To keep the torsion in the PV generator as low as possible, a single-axle trailer is provided for the carrier system. In addition, several small and therefore stiffer modules are used instead of a few large modules. In addition, these must be mounted with sufficient distance to the trailer and to each other to allow good rear ventilation of the modules. Since water is a precious commodity in the region, gutters are provided below the PV generator. In this way, the water used for module cleaning can be collected and used as service water. Figure 9 shows the prototype of the clay brick machine.

Figure 9: Prototype of automated clay brick machine

The conversion and transmission of the energy to the clay brick press takes place via a hydraulic driving system. The integration of these components into the existing system of the clay brick press is carried out under the condition that the option for manual operation is retained.

5 Conclusion

Together in the DπD network, various renewable energy carrier systems were examined for their use in the savannah region of Western Africa. In addition to the theoretical approaches for deriving the usable output for the primary conversion process into electric current, climatic conditions were analysed and a utility value analysis was carried out with regard to technological and economic operating conditions. In this context, it could be concluded that photovoltaics is the energy source with the highest degree of performance in comparison. This method is also favoured for use in the region in terms of correlation with electricity production costs.

The energy carrier system was used as a power supplier in the secondary conversion process to mechanical power. As an example, a conversion for a clay brick production machine could be presented. The constructive design was carried out and the prototype was presented in mock-up. After the theoretical implementation, the concept will be implemented in the DπD network with the cooperation partners on site and tested in the field. Experience in the use of the technology and in development will be gained in cooperation with the University of Lomé and the Bonita-Haus training centre in Dapaong and will be incorporated into the training content in Togo and at the Technical University of Applied Sciences in Wildau. This makes a significant contribution to the utilization of technology at the site and to improving living conditions in Western Africa.

6 References

[1] E. Yonazi, et al. “The Transformational Use of Information and Communication Technologies in Africa”. *World Bank, African Development Bank*, 2012

[2] P. Link, „Risikomanagement in Innovationskooperationen“. *Technische Wissenschaften ETH Zürich*, DISS. ETH Nr. 14240, 2001

[3] J. O. Löfken, „Afrika entdeckt die Sonne“, *Technology Review* 6, pp. 26-32, 2011

[4] F. Malik, „Strategie des Managements komplexer Systeme“. 10. Auflage, Hauptverlag, 2008

[5] K. Mertens, „Photovoltaik – Lehrbuch zu Grundlagen, Technologie und Praxis“. München: Carl Hanser Verlag, 2011

[6] V. Quaschning, „Erneuerbare Energie und Klimaschutz“. München: Carl Hanser Verlag, 2010

[7] J. Reiff-Stephan, „Der Design-Prozess in der technischen Produktentwicklung: Last oder Chance?“, *ZWF* 104 / 11, pp. 938-943, 2009

[8] J. Reiff-Stephan, „Nachhaltige Produktentwicklung mit dem „Design-Factor“. *SciConomy Frühjahr*, pp. 32-33, 2011

[9] J. Reiff-Stephan, „Innovationskooperation im Spannungsfeld von „Design & Technik“. *Entwerfen-Entwickeln-Erleben: Technisches Design in Forschung, Lehre und Praxis*. TUDPress, Dresden, pp. 105-118, 2012

SII-2a
Optical simulation of a parabolic solar concentrator

Serge Dzo Mawuefa AFENYIVEH [1], Assiongbon ADANLETE ADJANOH[1], Dam-Be Lardja DOUTI[1]

1 Abstract

This work presents a 3D ray tracing approach for the optical simulation of a parabolic solar concentrator for a thermo-magnetic (Curie motor) experiment. An approach based on Snell's law of reflection (geometrical optics) in vector form is used in this study. We consider the solid angle of the sun through a rotation of the concentrator around an axis. This paper aims to set up a digital technical tool as flexible as possible for applications in the field of renewable energy. Mathematical modelling as well as numerical simulation in Python environment are presented. The aim of the proposed algorithm is to be used for the concentration of light rays on any optical system, symmetrical or not. Better yet, offers a solar tracking model.

Keywords: solar parabolic concentrator, optical modelling, ray tracing simulation

2 Introduction

The issue of energy availability is of great interest to the scientific community. As an alternative to this concern, the development of renewable energies has become necessary [1]. This is how sources of renewable energy are included in the list of solutions to the critical situation of the energetic crisis that the world is facing. Indeed, the exploitation of these sources not only reduces the dependence on traditional resources but also preserve the environment. Thermodynamic solar transforms solar energy into heat at high temperature, then converts this heat into electrical energy. Several thermodynamic conversion technologies are presented in the literature (parabolic trough systems, solar tower systems, solar dish systems and linear Fresnel system) [2]. However, the performance of the system depends on several parameters. The parabolic solar concentrator system offers the possibility of producing heat from solar energy, temperatures can easily exceed 800℃ and the conversion efficiency is generally high [3]. By the way, since the sun's disc has a finite angular size of 0.53°, light rays reaching the earth surface are not really parallel. Therefore, instead of the incident rays being reflected on the focal point, the reflected rays form an image centered at the optical focus [4, 5, 6]. The image formed on the focus can be analyzed using a ray tracer [7]. Indeed, the ray tracing is a technique that tracks rays from the source to the final point [8]. It consists of tracing the individual trajectories of the solar rays passing through the optical system and their spatial distribution. This technique has the ability to handle any kind of geometry with a great precision. The ray tracing model is then important for the design of a suitable geometry of ray concentrator. This study aims to develop a homemade calculation code as general as possible for our laboratory, for the concentration of solar radiation and which can follow the solar axis. The work is presented in 3D system and the vector formulation of Snell's law of reflection [9] is used to represent the reflected rays.

[1] Laboratoire Matériaux, Energie Renouvelable et Environnement (LaMERE), Université de Kara

3 Theoretical description

We describe here the analytical concepts and present the mathematical approach which will be subsequently solved under Python.

3.1 Geometrical aspects

Let's first of all determine the 3D parabolic surface according to the axe and angle of rotation. The general equation of paraboloids in (O,X,Y,Z) coordinate system is given by:

$$\left(E^0_{surf}\right): Z = \alpha X^2 + \beta Y^2 \qquad (1)$$

The rotation of a vector $\vec{V}$ by an angle ψ around a unit vector $\vec{u}$ can be described by a transfer matrix R^{ψ}_{u} ; so that the coordinate of the new vector $\overrightarrow{V'}$ is define by the relation:

$$\overrightarrow{V'} = R^{\psi}_{u} . \overrightarrow{V} \qquad (2)$$

with

$$R^{\psi}_{u} = \begin{bmatrix} u_x^2(1-\cos\psi)+\cos\psi & u_x u_y(1-\cos\psi)-u_z\sin\psi & u_x u_z(1-\cos\psi)+u_y\sin\psi \\ u_x u_y(1-cos\psi)+u_x sin\psi & u_y^2(1-\cos\psi)+\cos\psi & u_y u_z(1-cos\psi)-u_x\sin\psi \\ u_x u_z(1-cos\psi)-u_y sin\psi & u_y u_z(1-cos\psi)+u_x sin\psi & u_z^2(1-sin\psi)+cos\psi \end{bmatrix}$$

For a rotation around the (OX) axis, $\vec{u} = (1,0,0)$, the transfer matrix R^{ψ}_{u} can be expressed as:

$$R^{\psi}_{OX} = \begin{bmatrix} 1 & 0 & 0 \\ 0 & cos\psi & -sin\psi \\ 0 & sin\psi & cos\psi \end{bmatrix} \qquad (3)$$

The general equation of the paraboloid is then given by:

$$E^{\psi}_{surf} = R^{\psi}_{u} * \ E^0_{surf} \qquad (4)$$

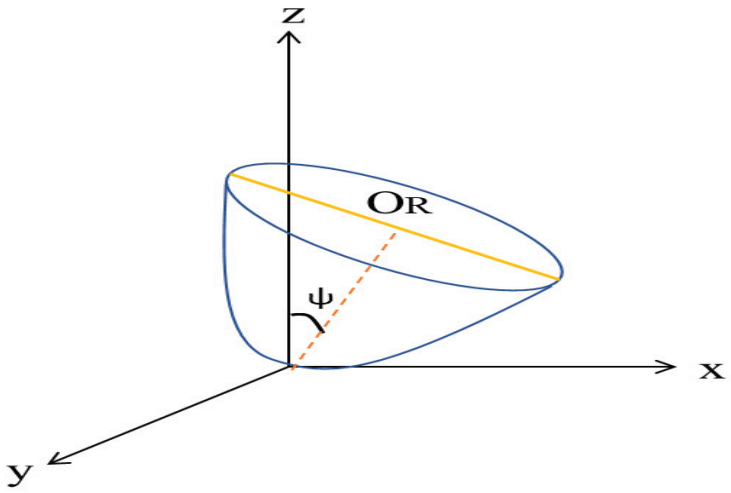

Figure 1: Parabolic surface inclined at angle ψ

The solar collector is characterized by its minor and major axes lengths, which will define the solid angle of the solar collection. For the optical calculations, we have to define the maximum angle of the solar rays that will be collected. The sun position is denoted by $S(x_s, y_s, z_s)$ and the solar rays localised using spherical coordinate angles (θ, φ) so that an incident ray from the sun will be characterised by its unit vector $\vec{u}_i$, defined by:

$$\begin{cases} x_i = sin\theta cos\varphi \\ y_i = sin\theta \sin\varphi \\ z_i = cos\theta \end{cases} \quad (5)$$

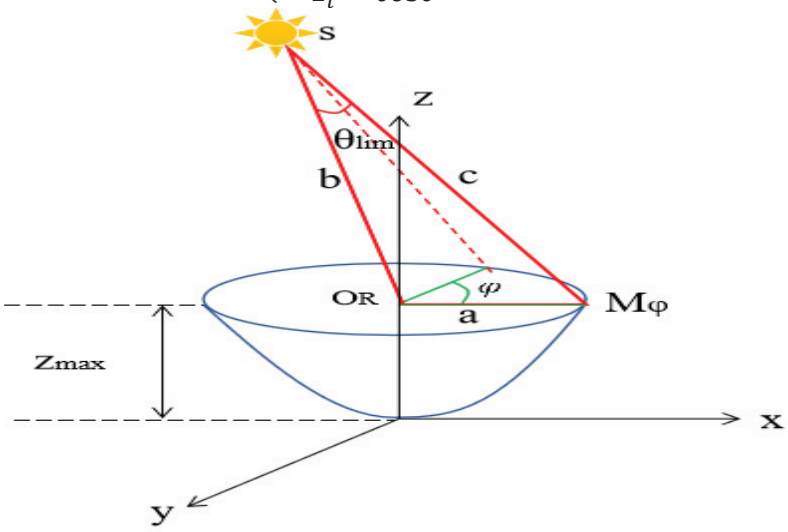

Figure 1: Geometric representation of the system

Without rotation, the aperture of the parabola is defined by an ellipse which parametric equation can be written as:

$$\begin{cases} x_e^0 = \dfrac{diam_x}{2} cos\varphi \\ y_e^0 = \dfrac{diam_y}{2} sin\varphi \\ z_e^0 = Zmax \end{cases} \quad (6)$$

After rotation, the aperture equation will now be defined as:

$$R_{OX}^{\psi} * \begin{pmatrix} x_e^0 \\ y_e^0 \\ z_e^0 \end{pmatrix} = \begin{pmatrix} x_e \\ y_e \\ z_e \end{pmatrix} = \vec{u}_{conic} \quad (7)$$

Let's call the centre of the aperture ellipse O_R, and $M\varphi$ any point on the ellipse , We have then:

$$O_R = R_{OX}^{\psi} \begin{pmatrix} 0 \\ 0 \\ zmax \end{pmatrix} \quad \text{and} \quad \overrightarrow{O_R M_\varphi} = \vec{u}_{conic} \quad (8)$$

The limit angle, θ_{lim} of the incidence can then be deduced by Al-kashi theorem applied on the triangle $(SO_R M_\varphi)$:

$$cos(\theta_{\lim}) = \frac{b^2 + c^2 - a^2}{2bc} \quad (9)$$

With

$$\begin{cases} a = \left\| \overrightarrow{O_R M_\varphi} \right\| \\ b = \left\| \overrightarrow{O_R S} \right\| \\ c = \left\| \overrightarrow{S M_\varphi} \right\| \end{cases}$$

3.2 Optical aspect

The interest of this section is to find the reflected ray for each incident on the solar parabolic surface on the basis of the vector formulation of Snell's reflection law.

Let M$\begin{vmatrix} x \\ y \\ z \end{vmatrix}$ be a point in 3D space. The incident ray equation (E_i), is define by its origin S (sun position) and unit vector $\overrightarrow{u_i}$ as given by the relation:

$\overrightarrow{SM} = \lambda\overrightarrow{u_i}$, which implies that $\begin{cases} x = x_s + \lambda x_i \\ y = y_s + \lambda y_i \\ z = z_s + \lambda z_i \end{cases}$ (10)

Let's now deduce the intersection point of the incident rays with the parabolic surface, by equalizing the incident ray equation (E_i) with the parabola surface $\left(E_{surf}^{\psi}\right)$. One would have a second order equation to be solved:

$$(E_{inters}) : \mu_1 z^2 + \mu_2 z + \mu_3 = 0 \quad (11)$$

The appropriate value of Z_{inters} is expressed by:

$$z_{inter} = Roots\{[E_{inters}]\} \cap \left[0, z_{\vec{u}_{conic}}\right] \quad (12)$$

The normal vector is defined by equation 13 and is computed according to $(\theta,\ \varphi)$

$$\vec{n} = \frac{\vec{\nabla} E_{surf}^{\psi}}{\left\| \vec{\nabla}\, E_{surf}^{\psi} \right\|} \quad (13)$$

Now, we have all the necessary elements to compute the reflected ray. Let's then consider equation 14, which is the vector formulation of Snell's law of reflection.

$$\vec{u}_r = \vec{u}_i - 2[(\vec{u}_i . \vec{n}) . \vec{n}] \quad (14)$$

Knowing the coordinates of the intersection point $M_{inters}(x_{inters}, y_{inters}, z_{inters})$ and the reflected rays vector orientation $\vec{u}_r(x_r, y_r, z_r)$, the parametric equation is given by:

$$\begin{cases} x = x_{inters} + \lambda x_r \\ y = y_{inters} + \lambda y_r \\ z = z_{inters} + \lambda z_r \end{cases} \quad (15)$$

4 Simulation results

The results of numerical simulation under Python programming language is presented here. Rays are represented considering the astronomical unit and the solid angle of the solar collector. The proposed calculation code is quite flexible. Thus, values such as the coefficients α and β of the general equation of the parabolic surface as well as the Z_{max} of the concentrator and the number of rays to be represented can be varied depending on the application.

$\boldsymbol{\alpha}$	$\boldsymbol{\beta}$	$\boldsymbol{Z_{max}}$	**Number of rays**
0.1	0.1	1	1e4

Table 1: Input parameters of simulation

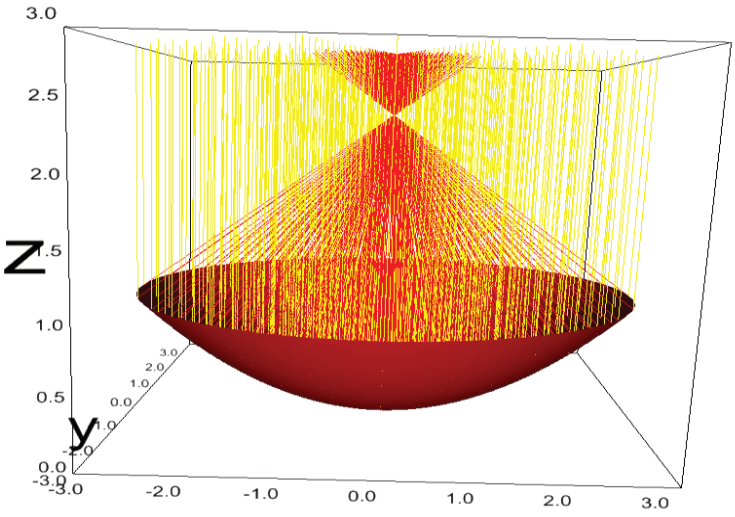

Figure 3: Representation of incident (yellow) and reflected (red) rays

Note that in reality, incident rays are not parallel as shown in the figure. Indeed, this impression comes from the fact that the source is very far from the parabolic surface.
Now we can simulate the ray distribution at the focal point.

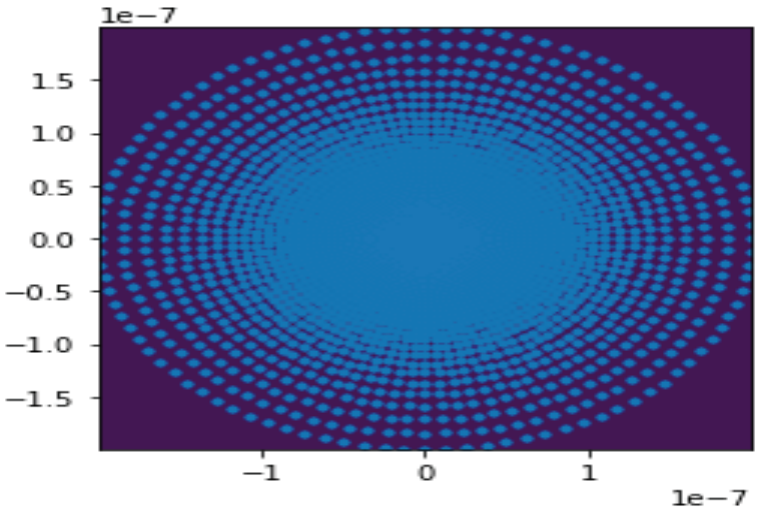

Figure 4: Solar ray distribution at focus plan (1e4 rays has been traced)

As application of the optical analysis, we simulate the energy map at the focus of our system, for a daily mean radiation of $6\ Wh.m^{-2}.d^{-1}$ collected by the parabola defined in table 1.

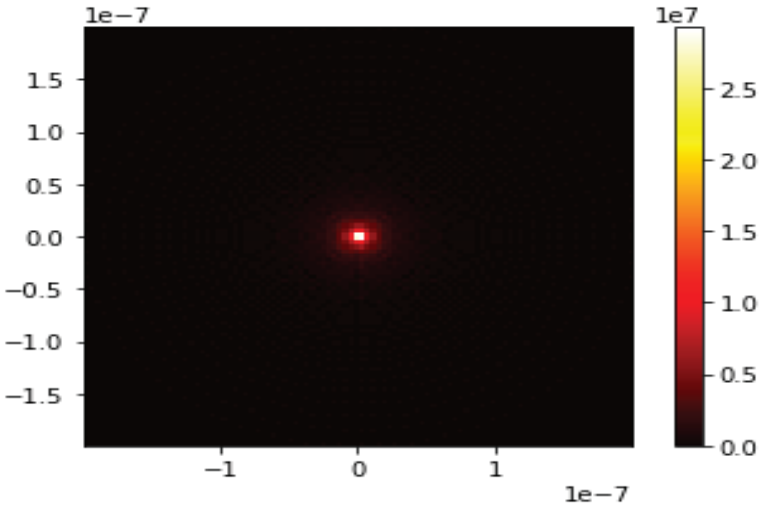

Figure 5: Spatial distribution of energy in the focal plane: the colour map values are in Joules (J).

We can notice that the intensity of the solar ray is concentrated in the centre and is reduced as one moves away from it.

5 Conclusion and perspectives

This paper presents an approach of 3D rays tracing. A theorical model is proposed and an optical simulation is developed in Python environment. The quality of results obtained is satisfactory. The model can make it possible to focus all the rays reflected by a parabolic surface.
This calculation code could be used for many applications.
These results can be improved. We therefore project to:
- Finalize the simulation with the tracking system, based on the theoretically described algorithm;
- Optimize the system by varying the different physical parameters in order to obtain an efficiency matrix;
- Make a thermal heat application of the concentrator;
- Simulate ferromagnetic materials in order to obtain the one with the lowest Curie temperature and which, according to the study conditions, will produce a more intense magnetic field.

6 References

[1] E. Al Ibrahmi, S. E Lachhab, F. Hamdaoui, I. El Amrani, A. Achhar and L. Dlimi, “Modeling of a cylindro-parabolic solar collector and simulation by Matlab software”, *Int. J. of Sc. & Eng. Res.*, vol.8, no.10, pp.1135-1139, Oct. 2017, ISSN 2229-5518.

[2] A. Z. Hafez, A. Soliman, K. A. El-Metwally, I. M. Ismael, “Solar parabolic dish stirling engine system design, simulation and thermal analysis”, *Energy conversion and management*, vol.126, pp.60-75, Jul.2016, doi:101016/j.enconman.2016.07.067.

[3] B. Maaoui, Y. Aoun and S. Benramache, “Réalisation d’un four solaire pour l’élaboration des oxydes métalliques”, *The* 5^{th} *Int. Seminar on New and Ren. En.*, Ghardaia-Ageria, 24-25 October 2018.

[4] A. Chikuwa and J. Lovseth, “Modeling of a novel volumetric absorber, suitable for compact solar concentrator with rock storage”, *Proceeding of ISES Solar World Congress*, Johanesburg, 12-14 October 2009.

[5] J. A. Dufie and W. A. Beckam, “Solar Eng. of Thermal Processes, third edition”, *John Wiley and Sons, Inc.*, Hoboken, New Jersey, 2006.
[6] A. Mobarak and A. A. Rahim, “Determination of local flux distribution of a parabolic dish solar concentrator applying real shape*”,* 12^{th} *Annual Int.Solar En. Conference, ASME*, pp. 79-86.
[7] K. Nyenga, D. Okello and O. J. Nydal, “A ray tracer model for analysis of solar concentrating systems”, *J. of En. In Southern Africa*, vol.30, no.1, pp. 8-20, Feb,2019, doi:10.17159/2413-3051/2019/v30i1a5267.
[8] F. J. Seron, D. Gutierrez, G. Gutierrez, and E. Cerezo, “Implementation of a method of curved ray tracing for inhomogeneous atmospheres”, *Computers & Graphics*, vol.29, no.1, pp. 95-109, Feb. 2005, doi:10.1016/j.cag.2004.11.010.
[9] V. V. Fisanov, “Vector formulations of the laws of reflection and refraction of forward and backward waves”, *Russian Phys. J.*, vol. 58, no 8, pp. 1074-1079, Dec 2015, doi:101007/s11182-015-0614-6.

SII-2b
Comparable numerical study on different working fluids for micro scale power cycle integrated into a pellet fired boiler

Numerical Simulation of the Tesla Turbine Efficiency

Roberto Lisker [1]; Mario Nowitzki[2]; Udo Hellwig[3]; Franz Xaver Wildenauer[4]

Abstract

A cost-effective power cycle shall be developed to supply heat and electricity (co-generation). The aim of this study is to find an appropriate power cycle and working fluid for a friction turbine application. Due to its low production costs, better scalability and low-maintenance requirements, a friction turbine, also known as Tesla turbine, shall be used. In order to find a proper working fluid and estimate the efficiency and power output, a numerical study was performed on five promising working fluids namely Xenon, Argon, Helium, Air and superheated Steam. The simulation model consists of three disks with a diameter of 0,25 m and an outlet diameter of 0,12 mm rotating at constant 10.000 rpm. It is tried to keep the Gap Reynolds number at a constant 73, to ensure a laminar flow regime between the disks. The outcome of the numerical study showed that all working fluids are suitable. The highest efficiency (shaft power / technical power) has been achieved with steam (96%) and a power output of 126 W/gap. The least efficiency with 89% has been realized with air and a Power output of 118 W/gap. The noble gases are in between these fluids.
By comparing the simulation data and taken into account numerical and estimation errors, all five working fluids are at par. Thus, the choice of the working fluid and the power cycle is an economical. While a hot gas air turbine is not as efficient as the steam turbine, the invest and maintenance costs are lower due to less heat exchangers and necessaries like water reconditioning and a phase separator.

1 Introduction

For domestic heating, biomass is seen as an adequate substitution of fossil fuels like oil or natural gas. Combusting biomass (here pellets) is recognized as non-climate hazardous since the amount of Carbon dioxide emitted is equal to the one absorbed (climate-neutral). However, for domestic applications, solid biomass-based co-generation units which produce heat and electricity are not commercially available yet. The main cause is fouling and slagging of the convective and radiative heat exchanging surfaces due to the high amount of ash residues in the flue gas, making it impossible for the direct use in a gas-turbine or gas-engine. To overcome this issue and to establish a power cycle, the combustion process must be separated from the power

[1] Dr. Roberto Lisker, Technical University of Applied Sciences Wildau, Wildau

[2] Dipl.- Ing. Mario Nowitzki, Technical University of Applied Sciences Wildau, Wildau

[3] Prof. Dr.-Ing. Udo Hellwig, ERK Eckrohrkessel GmbH, Berlin

[4] Prof. Dr. rer.nat. Franz Xaver Wildenauer, Technical University of Applied Sciences Wildau, Wildau

cycle. Thus, an external combustion chamber is used to transfer the heat of combustion to a clean working fluid which drives the turbine generator set.
For the cycle design a commercially available pellet fired boiler (Ökofen PES 56) has been selected which shall be equipped with a micro scale power cycle. The pellet fired boiler has a nominal thermal output of 56 kW_{th} and the boiler efficiency is at 93%. The maximum flue gas temperature achieved in the furnace zone is 1400 K and the flue gas volume flow is 0,04 $m^3 s^{-1}$. [1]. The power unit consists of heat exchangers to transport the heat from the furnace to the power cycle and heating system, a turbo-set consisting of a friction turbine, a compressor or pump which circulates and pressurizes the working fluid and the generator which produces a nett power output of 3,5 kW_{el}.
At the moment, the system is in an early stage of development. For the power unit, two processes are conceivable. The first one is a classic Rankine Steam Cycle. Here the working fluid is steam who drives the turbine. The second one is an Ericsson process, a closed gas turbine process, where a gaseous working fluid drives the turbine.
In order to make a final decision about the cycle, the performance of the friction turbine and the turbine efficiency shall be evaluated regarding the working fluid. The working fluids to be evaluated are Steam, Helium, Argon, Xenon and Air. Therefore, parts of the turbine geometry have been modeled and numerous numerical simulations have been done to evaluate the turbine performance.

2 The Power Unit

The power unit shall be integrated in the pellet boiler, a basic scheme is displayed in the following figure. Inside the furnace the heat exchangers are placed. The furnace wall will be used to recuperate the heat coming from the turbine and preheat the working fluid. The second heat exchanger is directly placed inside the furnace and heats the working fluid to the final temperature of 1273K. The rest of the heat is used to generate warm water or heating. The Turbo-Set shall generate a net output of 3,5 kW_{el} under nominal conditions. Furthermore, it shall produce the energy necessary for the compressor and other electrical components of the boiler system (PLC etc.).

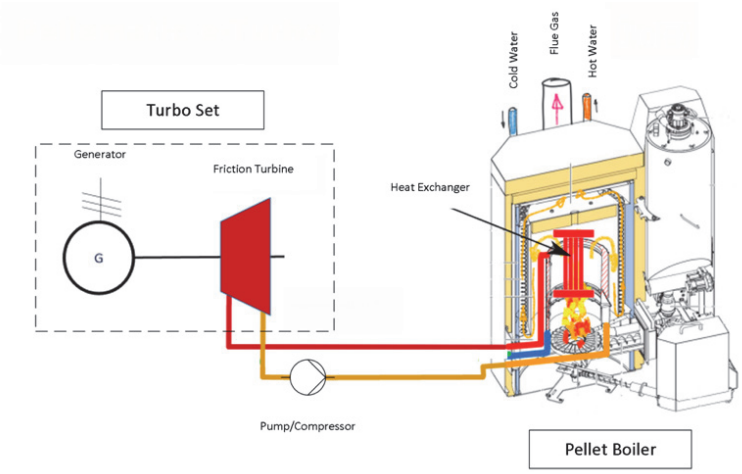

Figure 1 Basic elements of the Power Unit integrated into the pellet fired Boiler. On the left-hand side, the Turbo Set is displayed which is connected to the pellet fired boiler.

2.1 Ericsson Cycle

The Ericsson Process is a reference cycle for gas turbines [2]. At first, the pressurized working fluid is heated to the desired turbine inlet temperature (4-1, Figure 2,left). The pressure is kept constant. Afterwards the Fluid is isothermal expanded (1-2, Figure 2, left) until it reaches the low pressure p', it leaves the turbine and enters the regenerator (2-3, Figure 2, left), who preheats the cold working fluid. Afterwards, the cold working fluid is compressed until the desired high-pressure p (3-4, Figure 2, left). The downside of the cycle is the compression of the gaseous working fluid. Due to the low density of the gaseous fluids the compression takes a lot of energy. In Figure 2 right, the area under the blue curve displays the specific labor needed to compress air at ambient conditions up to 10,5 bars. One can see, that in the range of 1 to 4 bars the majority of the compression energy is needed (Figure 2, red area). To overcome this, the cycle can be operated under pressurized conditions, whereas the lowest pressure p' is higher than the ambient pressure. The higher density accounts for significant energy savings.

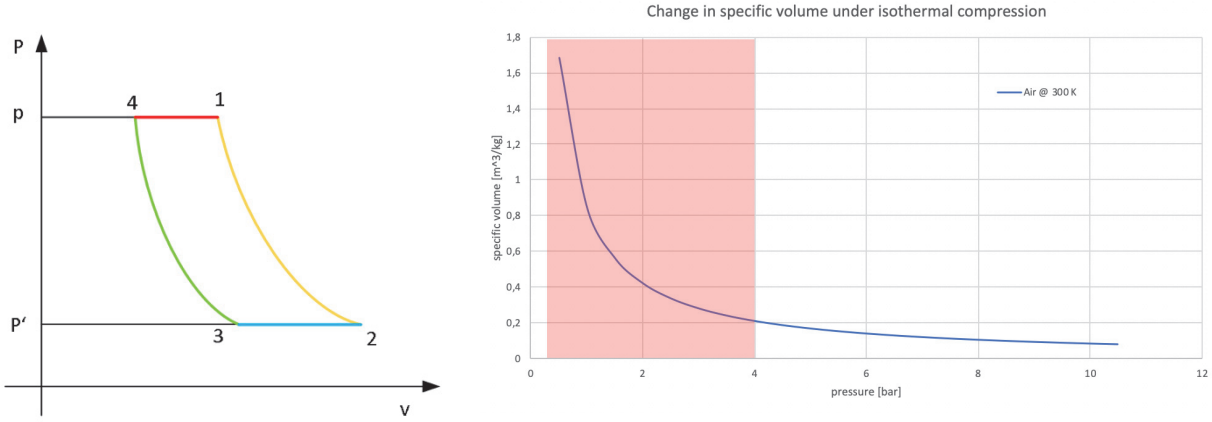

Figure 2 Left: Pressure-Volume Diagram of an Ericsson Process. Right: the change in specific volume of air while compressed.

In order to estimate the turbine size, the cycle has been roughly designed with air. In this case, the lowest pressure will be 4 bars and the highest pressure 9 bars. The turbine inlet temperature is set to 1173 K and the efficiency 0,6. Like the turbine the compressor efficiency is estimated with 0,6 and it has to produce a volume flow of 0,0115 m3 s-1. From these calculations, the gross electrical power production of the turbo-set must be 11 kWel.

2.2 Friction Turbine

The friction turbine also known as Tesla Turbine, was invented by Nikola Tesla in 1909 [3]. It consists of several plane parallel discs arranged on a shaft. The distance between the discs is determined by the viscosity and the boundary layer thickness inside the gap. The working fluid enters the gap at the outer most perimeter and moves on a spiraling path towards the center of the disk, where the outlet is situated. In figure 3 left, a sectional view of a friction turbine model is shown. Due to the reduction in the cross- sectional flow area, the velocities are rising towards the outlet (see figure 3, right). Especially the tangential velocity accounts for energetic losses, which can be minimized by adjusting the gap width and/or rotation rate. In figure 3 the red dashed line represents the ideal tangential velocity. It should be just over the disk velocity, enough to produce the needed drag and minimize the energetic losses.

The advantage of the friction turbine is its simplicity and robustness. Due to the parallel flow of the working fluid to the disk surface, the turbine is impervious against particle laden flows and condensate formation [4].

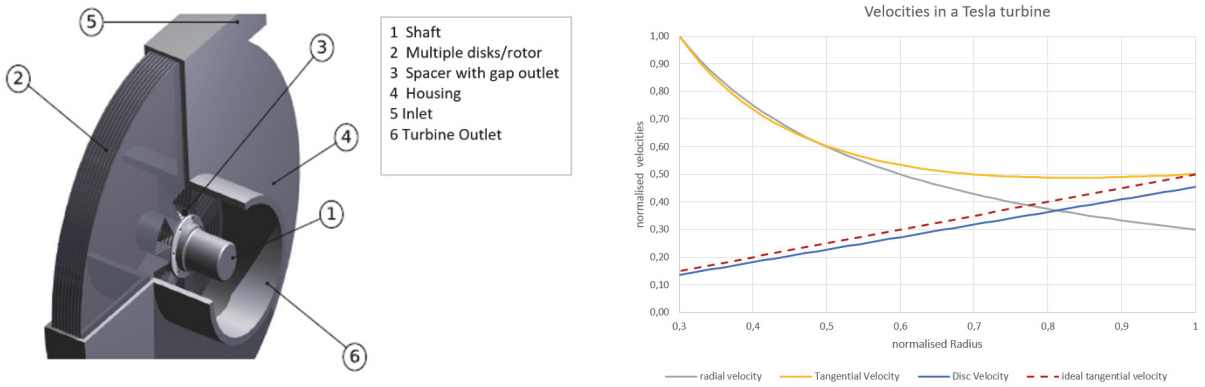

Figure 3 Left: Model of a friction turbine; Right: Normalized velocities inside a friction turbine gap element. The ideal tangential velocity is displayed as a dashed red line. The distance between the yellow and red line is the energetic loss

For the turbine assessment, the efficiency with respect to the working fluid and the gap Reynolds number are essential. The turbine efficiency is calculated according to the following equation

$$\eta = \frac{\Delta h_{tot}}{M\ \omega} \qquad \text{eq.1}$$

whereas Δh_{tot} is the total enthalpy difference between the in- and outlet of the turbine, M the produced momentum and ω is the angular velocity of the flow. In order to make the simulations comparable, the gap Reynolds number (Re_{gap}) will be used. It can be expressed with the inlet mass flow as follows:

$$\mathrm{Re}_{\mathrm{gap}} = \frac{{}^{m}\phi}{2\pi r\eta} \qquad \text{eq.3}$$

whereas r is the outer radius of the disc, ${}^{m}\phi$ is the mass flow of the fluid and η the dynamic viscosity. In order to obtain a high turbine efficiency, the gap Reynolds number should be kept low, which accounts for a laminar flow regime in the gap.

3 The Numerical Model

For the comparative simulation, a simulation model has been developed. It consists of a housing with two tangential inlets, three disks (two gap elements) and a reduced outlet in the center (see Figure 4 left). The original model consists only of one disk, but here the efficiency reducing effect of the gap formed between the housing wall and the rotor could not be modelled. Thus, a three-disk geometry is chosen resulting in 2 full fluid gaps and due to symmetry two half gaps on both sides. In the following table the geometric and operational data are displayed.

Property	Value	Property	Value
Disk outer radius	0,25 m	Rotation rate	10.000 rpm
Disk inner radius	0,12 m	Inlet velocity	140 m s^{-1}
Gap width	0,0003 m	Outlet pressure	1 atm
Gap Reynolds No.	73	Inlet temperature	1273 K

Table 1 Geometric and operational properties of the simulation model

Due to different fluid viscosities, the mass flow must be adjusted in order to maintain a constant gap Reynold number and inlet velocity. To set the mass flow, the inlet channels height is adjusted, in order to achieve a constant inlet velocity at a given channel width. Therefore, the housing inlet height is adjusted. Beforehand, a mesh study has been performed to optimize the calculation time and computational resources. The study has shown, -despite of the laminar flow between two discs-, that within the gap a large amount of mesh cells is needed in transverse flow direction. The reason being, the complex flow phenomena at the most outer and inner perimeter, which cause disturbances, and result into additional pressure and velocity fluctuations. Furthermore, the Mach number can locally exceed one, meaning supersonic flow. Thus, the stability of the numerical solver must be increased to handle local jumps in fluid properties (pressure surge). This can be done by a finer mesh in high Mach number areas. In total about 8 mesh cells are needed in transverse directions, of which 6 are prism layers. This yields to an overall mesh cell amount of about 30 mio. polyhedral cells for one gap element (see Figure 4).

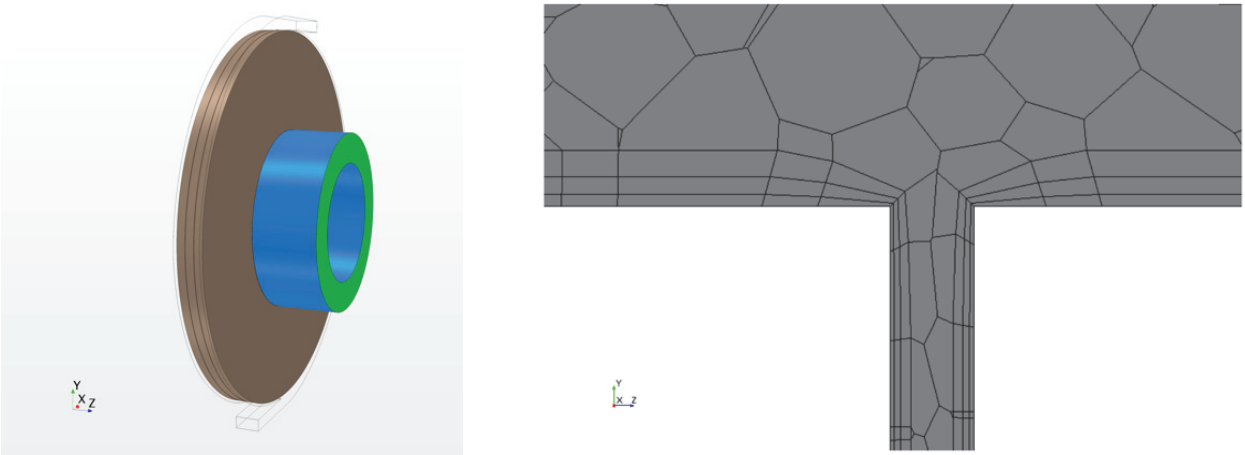

Figure 4 Left: The geometrical model of the turbine used for the simulation. The turbine consists of two inlets (displayed as wireframe) and an outlet in the center of the disks (blue- green). The disks are marked brown. Right: View of the polyhedral mesh at the outer most radius. One can see the prism layers close to the disk wall.

3.1 Mathematical Model

In order to compare different working fluids, the following settings have been done. The simulation is steady state, transient effects can be neglected, and a steady state model is used. An adiabatic expansion is assumed in the friction turbine, even though solving the energy equation is important to include enthalpy changes due to abrupt fluid acceleration/deceleration. One effect of abrupt enthalpy changes is the Joule-Thomson-Effect. Especially in the transition area from the gap to the hollow outflow shaft shall be mentioned. In order to account for this effect, a Real Gas model is needed. Thus, the Van der Waals model is chosen, demanding a laminar flow regime in the gaps. Even though a turbulence model is necessary for the simulation of the inlet housing and hollow outlet shaft. Thus, a transition model is needed which allows to switch between turbulent and laminar flow. Because of the high wall impact the SST Turbulence model is used. For the modeling of the change between turbulent and laminar flow, the Gamma Transition model applied. The models used in the simulation are shown in table 2.

Property	Model
Time	Steady State
Energy	Segregated Enbthalpy
Turbulence	SST Kω
Turbulence transition	Gamma transition
Equation of state	Real Gas Van der Waals

Table 2 Used properties for the solver

3.2 Boundary Conditions

In this study the fluids have a constant inlet velocity of 140 m s^-1 and an inlet temperature of 1273 K. The hollow shaft outlet is a pressure outlet of 1 atm. Onto rotating discs and inner shaft surface a wall tangential velocity of 10,000 rpm is set to simulate rotation.

4 Results

In the table 3, the results of the simulations are displayed. One can see that the efficiency according to equation 1 is high. The highest efficiency has been achieved with Steam (0,95) and the lowest with air (0,89). As mentioned above the gap Reynolds number should be 73 for all simulations. To achieve the constant gap Reynolds number, the inlet housing height was adjusted with subsequently meshing. Due to the insufficient prediction accuracy of the pressure drop (sudden local fluid properties changes), the inlet height has been determined in an iterative process. Hence the gap Reynolds numbers is close to 73 the simulation results can be compared. An exception is air, here the local changes in fluid properties are so dominant, that a gap Reynolds number of 73 could not be reached. 82 was the closest achievable.
In the following table, the results of all simulations with corresponding fluids are displayed.

Fluid	Argon	Air	Xenon	Steam	Helium
Re gap	73,91	82,48	73,76	74,56	73,28
velocity inlet [m s^{-1}]	140	140	140	140	140
inlet temperature [K]	1273	1273	1273	1273	1273
outlet temperature [K]	1269,49	1267,77	1277,67	1270,02	1270,53
technical power [W]	92,71	131,91	117,63	133,6	151,44
shaft power [W]	86,3	118,43	110,297	126,82	138,13
Efficiency [%]	93,09	89,77	93,77	94,92	91,21
Moment [Nm]	0,082	0,113	0,105	0,121	0,132
Pressure drop [bar]	0,253	0,328	0,534	0,413	1,213
Inlet height [mm]	4,03	5,84	1,77	7,9	21,19

Table 3 Summarized results of the numeric simulation

An interesting result is, that despite of different fluids with different properties, the turbine efficiency is close. That implies a dependency of the efficiency on the gap Reynolds number. By taking a look at the shaft power, there are noticeable differences between the fluids. Argon generates the lowest shaft power, although the efficiency is high. Helium has the best shaft power, but the efficiency is the second last. Here a correlation between the shaft power and the

pressure drop matches better. If the pressure drop is high the shaft power is high too, except for Xenon. Xenon is a high-density gas, so the low shaft power and high pressure- drop could be caused by increased inertia forces. In general, a high shaft power is desirable. Helium, which achieved the highest shaft power of 138,1 W, also has the highest pressure drop, more than double than of Xenon which has the second highest pressure drop. In comparison the power output is only 27 W lower. Another fluid worth mentioning is steam. Here the highest efficiency has been achieved and the shaft power with 126,8 W is the second highest. Yet the pressure drop is only a third of Helium.

In the following figure 5 left, the total velocity ($c = \sqrt[2]{c_{tangetial}^2 + c_{radial}^2}$) of the working fluids in the middle of the gap is plotted. By examine the velocities, the high pressure drop of Helium can be explained with Bernoulli's principle. An increase in velocity towards the outlet increases the pressure drop ($\frac{\varrho c^2}{2}$) consequently. Furthermore, for the evaluation, the disk velocity is plotted (red line). In order to obtain an efficient turbine, the tangential fluid velocity should be just over the disk velocity like Xenon or Air. In figure 5 right, the radial velocities are plotted. One can see, that Helium reaches by far the highest velocities at the turbine outlet. The reason is the low density of Helium, which requires a higher volume flow to achieve the same mass flow as the other fluids. This is congruent to the inlet height of the helium simulation. Here the inlet height is more than ten times bigger than Xenon and more than 2 times higher than steam (see table 3). Regarding the velocities, pressure drop, mass flow and shaft power, Steam, Xenon and Air seems to be promising candidates. In terms of efficiency, all fluids are at par.

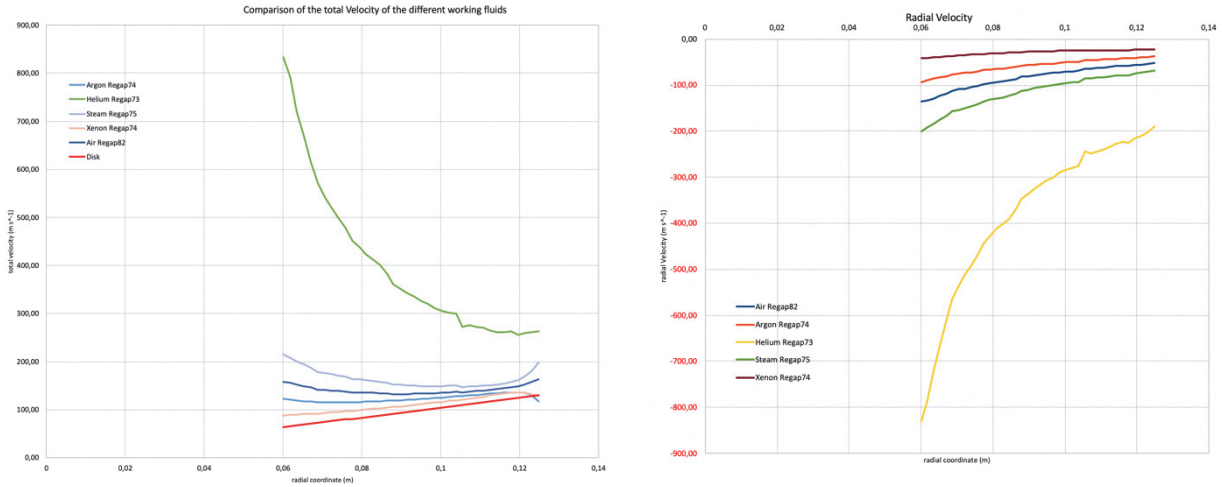

Figure 5 Left: Comparison of the total velocity of the working fluids in the gap the red line represents the disk velocity. For an ideal turbine, the velocities should be as close as possible to the disk. Right: Radial velocities in the turbine gap

5 Conclusion

The goal of this study was to find a proper working fluid for a pellet fired boiler power cycle. In terms of efficiency all working fluids are suitable. They can be regarded as equal. Even though, the efficiency is equal, the shaft power differs. But this can be adjusted by increasing or lowering the number of disks to reach the final necessary power output. Thus, the decision of the working fluid is based on economical reasons. Regarding the turbine, the best balance between shaft

power, efficiency and pressure drop has superheated steam, followed by Xenon, Air and Argon. But the turbine is only one part of the cycle. First of all, the size of the compressor determines the additional power the generator has to deliver. A power cycle based on Helium would have a much higher compressor power consumption, which reduces the cycle efficiency. A Rankine Cycle would have the lowest power consumption due to the high density of water. The Ericsson Cycle with the lowest power consumption should be the Xenon followed by Argon and Air. Regarding the heat transfer, the picture is contrary. Helium has a higher thermal conductivity compared to the other working fluids, meaning the heat exchangers are smaller. Compared to the other working fluids, Xenon needs the biggest heat transfer surface, making it doubtful whether such a heat exchanger could be integrated in a pellet fired boiler. In comparison to Helium the heat exchanger surfaces need to be at least 25 times larger. The heat transfer surface regarding Steam and Air is only 5 times larger than Helium. Larger heat transfer areas account for higher invest costs so the system would be more. For the pellet boiler power unit, the Ericsson cycle is preferred over the Rankine cycle, due to the lower complexity. For domestic power cycles Air has shown the best balance between, pressure drop, shaft power and heat transfer sizes. Nevertheless, despite of the presumably higher power consumption due to the needed higher volume flow rate, Helium might be an interesting alternative because of the smaller necessary heat exchanger surface.

6 Outlook

With the gained results, first insights on the development process ahead are given. It can be concluded that the economical aspect cannot be neglected. The material and operational costs as well as the apparatus complexity of the power unit are dependent on the choice of the working fluid. For the ongoing development process, the power unit will be calculated for Helium and Air to estimate the development, maintenance and operational costs.

7 Literature

[1] Thomaschko L., “Pelet fired turbine and Ökfen”, Presentation kick off Meeting “chilled turbines” consortium, January, 2019; Berlin Moabit .

[2] Bošnjaković, Fran; Knoche, Karl-Friedrich, „Technische Thermodynamik“, 1988, Dresden, Steinkopff, pp. 227-230

[3] Tesla Nikola, “Tesla Turbine”, Pat.No. U.S. 1061206, 1909

[4] Lisker R., “Two Phase flow in friction turbines “, Dissertation, University of Rome Tor Vergata, April 2017, pp. 95-100

SIII-1a
Turnaround in Energy Policy –

Measures to Reduce the Carbon Dioxide Emission from the Private Sector

Lutz B. Giese [1]

Abstract

The greenhouse gases (GHG) carbon dioxide (CO_2), methane (CH_4) and nitrous oxide (N_2O) are considered mainly to be responsible for the additional anthropogenic greenhouse effect, the so-called “global warming”. In the private sector, the “Rational Use of Energy” can be a very effective tool (i) to reduce the greenhouse gas emissions, (ii) to decrease the annual energy costs and furthermore (iii) it prepares the integration of Renewable Energy Sources by saving conventional, mostly fossil energy.
Aim of this paper is (i) to show that by applying energy saving measures, the primary energy demand and thus the individual (direct) carbon dioxide emission can be reduced in a relevant scale. (ii) It is to give laterally information about (ii.i) the energy market structure and (ii.ii) the legal backgrounds in the EU.

1 Introduction

The greenhouse gases (GHG) carbon dioxide (CO_2), methane (CH_4) and nitrous oxide (N_2O) are considered mainly to be responsible for the additional anthropogenic greenhouse effect, the so-called “global warming”. According to the former US Vise-President Al Gore, the scientific community consents that the global warming mainly derived from burning fossil fuels since more than 250 years. Thus, after Kyoto Protocol in 1997 and Paris Agreement in 2015, the policy of the European Community aimed and still aims at reducing the CO_2 emissions drastically. Since 1990, Germany was able to reduce the CO_2 emissions contemporary (Table 1) [1]. Respecting the energy statistics and opinions of experts, in several European member states such as Germany as well as in countries associated to the EU the greenhouse gas emissions could be reduced by means of

1. increasing the energy efficiency (Rational Use of Energy, RUE) by
    a. applying more energy conservation and
    b. expanding the field of cogeneration (Combined Heat and Power, CHP), and finally
2. implementing sustainable energy technologies (Renewable Energy Sources, RES).

For instance, viewing to Germany the total primary energy consumption (PEC, TPES) amounted to 13,262 PJ_{PE} (= 3,684 TWh_{PE}) per year in 2015 [1]. With a population of 81.7 million capita this was same as yearly 45.09 MWh_{PE} per person. Around 40% of this PEC

[1] Lutz B. Giese, University of Applied Sciences [TH] Wildau, Fac. of Engineering and Natural Sciences, Hochschulring 1, D-15745 Wildau, Germany

is allocated to buildings. Furthermore, according to own calculations in Germany more than 1/3 of the primary energy consumption derives from the private building sector including the individual traffic. Totally, each German citizen causes nearly 11 tons of greenhouse gas emission (CO_2 equivalents without amendments) per year. Thus, up to 40% of it is coming from accommodation plus individual transport.

Table 1: Greenhouse gas emissions in Germany between 1990 and 2017 compared to the reference* (base value of the Kyoto Protocol) [1].

	Reference*	1990	1995	2000	2005	2010	2015	2017
Greenhouse gas	**in million tons of CO_2 equivalents**							
CO_2 equivalents	1,223	1,220	1,090	1,007	981	926	893	891
CO_2 equivalents**	1,255	1,251	1,123	1,045	993	943	907	907
CO_2	1,020	1,020	905	861	853	814	780	781
CO_2**	1,053	1,053	940	900	867	832	796	798
CH_4***	121	121	106	89	69	59	57	55
N_2O***	64	64	61	43	43	36	39	38
HFCs	9	6	9	8	10	11	12	11
PFCs	2	3	2	1	1	0	0	0
SF_6	6	4	6	4	3	3	4	4

*: Reference (100%, base value) of the Kyoto Protocol related to 1990 or 1995, respectively (dependent to GHG)
**: Without amendment of land use and forestry
***: Without amendment of land use
Note: CO_2 = carbon dioxide; CH_4 = methane; N_2O = nitrous oxide (laughing gas); HFC = hydrofluorcarbon; PFC = perfluorcarbon; SF_6 = sulphur hexafluoride

2 Legal Background by the EU

To reach the CO_2 reduction goals of the Kyoto Protocol and later of the Paris Agreement, the European Community issued several directives in order to be converted by the member states within a fixed period into national laws and/or ordinances. For instance, in terms of limiting the heat demand of buildings and to improve the energy efficiency, the EC issued

- in 2002 the
  - "Directive 2002/91/EC of the European Parliament and of the Council of 16 December 2002 on the energy performance of buildings (EPBD)" in order to reduce the emissions derived from buildings and to implement the so-called "energy performance certificate (for buildings)" [2],
- in 2010 the
  - "Directive 2010/31/EU EC of the European Parliament and of the Council of 19 May 2010 on the energy performance of buildings" in order to implement the new EPBD (recast) [3],

- in 2012 the
  - "Directive 2012/27/EU of the European Parliament and of the Council of 25 October 2012 on energy efficiency (Energy Efficiency Directive, EED), amending Directives 2009/125/EC and 2010/30/EU and repealing Directives 2004/8/EC and 2006/32/EC Text with EEA relevance" in order to improve energy efficiency actions [4], furthermore
- in 2018 the
  - "Directive (EU) 2018/855 of the European Parliament and of the Council of 30 May 2018 amending Directive 2010/31/EU on the energy performance of buildings and Directive 2012/27/EU on energy efficiency (Text with EEA relevance)" [5],
- and several more.

These legal acts are to turn the political stagnation due to the greenhouse gas emission into action. Thus, in Article 7 of Directive (EU) 2018/855, European Union points out:

> *"The 2015 Paris Agreement on climate change following the 21st Conference of the Parties to the United Nations Framework Convention on Climate Change (COP 21) boosts the Union's efforts to decarbonize its building stock. Taking into account that almost 50% of Union's final energy consumption is used for heating and cooling, of which 80% is used in buildings, the achievement of the Union's energy and climate goals is linked to the Union's efforts to renovate its building stock by giving priority to energy efficiency, making use of the 'energy efficiency first' principle as well as considering deployment of renewables."*

3 Action Plans to Strengthen the CO_2 Emission Savings from Buildings

However, the spirit of all of those issued EC directives is the "holistic approach" which means: whatever we do, whatever we use – the entire sum of all of our individual emissions derives from the sum of all of our activities. Thus, if we do not heat-up our homes but drive our cars, it will affect the climate in the same matter. The climate does not care for the source – as long it is not sustainable – but it cares for the amount of the greenhouse gas emissions.

The EU's energy policy reflects that: for instance, in 2006 and 2010 the European Union issued the "Energy Efficiency Action Plan" (EEAP) as a "broad framework for energy conservation" [6]. The EEAP was followed by a Green Paper entitled "Doing More with Less: Green Paper on Energy Efficiency" [7]. In this document the saving of 20% of the EU energy use had been proposed. However, within the EEAP 75 actions (in 10 priority areas) had been listed, aimed at highly efficient buildings, appliances, processes, cars and energy systems, targeted at developing so called "National Energy Efficiency Action Plans" by each member country such as by Germany the NAPE, based on the requirements of Directive 2012/27/EU laid down in Article 24(2). Generally, the EEAP proposed several measures, such as

- improving the energy performance standards for boilers, copiers, TVs, lighting etc.,
- improving the energy standards for buildings and the promotion of low-energy buildings ("passive houses"),
- growing the efficiency of power generation and distribution,
- limiting the CO_2 emissions from cars down to 120 g/km by 2012 (incl. strengthening the efficiency labeling),
- boosting the energy efficiency especially in new member states,

- establishing awareness and education campaigns,
- improving energy efficiency in urban areas through a "Covenant of Mayors" (exchange best practices), and
- initiating international agreements to establish and improve energy efficiency worldwide.

4 Effects to Improving Energy Conservation in Germany

“Rational Use of Energy” (RUE) can be a very effective tool (i) to reduce the greenhouse gas emissions, (ii) to decrease the annual energy costs and furthermore (iii) it prepares the integration of Renewable Energy Sources. The planner who aims at optimizing the energy demand of buildings should follow the two steps,

1. step 1 is to decrease the building’s demand and increase the efficiency of the heating system → RUE, by
    a. energy saving (= conservation) and/or
    b. (optionally) cogeneration (CHP),

    and (afterwards)
2. step 2 is to apply Renewable Energy Sources → RES.

“Conservation of Energy” – also called as a “Rational Use of Energy” – in private households provides a high potential for saving of energy and emission. In Germany, EU directives in terms of energy conservation in buildings are legally “executed” related to the national laws and ordinances such as the EnEG, EnEV, EEWärmeG and in the near future the GEG (“Gebäude-Energie-Gesetz”). However, unfortunately in Germany still the energy consumption of buildings in average stays too high and furthermore the contribution of RES is too low. According to the data of BMWi, in Germany still space heating shares around 70% of the final energy consumption of the private households [1]. In private buildings, more than 4/5 of the energy consumption is for heat. Legal acts such as “Energieeinsparverordnung” (EnEV) mainly regulate the buildings under construction, but the existing building only marginally [8].

In detail, in Germany in the building sector the modernisation rate amounts only to less than 0.7% yearly while 2% are wanted and needed, as well. According to the data of BMWi, the total primary energy consumption in Germany decreased from 14905 PJ_{PE} in 1990 only down to 13523 PJ_{PE} in 2017, and down to 12832 PJ_{PE} in 2019 [1]. This is a reduction of PED by 9% until 2017 or 14% until 2019, respectively – as heat applications consume up to half of the final energy demand in Germany, changes in the heat demand due to climate variations should be taken into account.

On one hand - regarding this data -, a reduction by 40-50% of the primary energy demand until 2050 (Germany) seems to be very, or maybe too optimistic.

On the other hand - taking for buildings after modernisation a specific annual heat demand of 70 kWh/(m^2*a) for heating plus 12.5 kWh/(m^2*a) for hot water into account (a = year) -, by the measures of „Rational Use of Energy“ the German final energy demand in the private sector could be reduced by 300 TWh yearly (same as yearly up to one hundred Mtons of CO_2).

5 Conclusions

Aim of this paper was (i) to show that by applying energy saving measures, the primary energy demand and thus the individual (direct) carbon dioxide emission can be reduced in a relevant scale. (ii) It is to give laterally information about (ii.i) the energy market structure and (ii.ii) the legal backgrounds in the EU. The today's public opinion is that

"energy is another name for CO_2 emission", and the "*level of emission"* can be expressed (= quantified) by *"correlating with the (fossil) primary energy"* consumption.

Thus, we have to contribute actions in order to reduce both of it.
Buildings (and hereby the private sector) share up to 40% of the carbon dioxide emissions in Germany: increasing the efficiency of buildings and appliances, using Renewable Energy Sources, and applying future transport technologies are effective tools to reduce the emissions. But beside this, further 6 tons of CO_2 emissions remain in the other sectors (transportation, industry, …). Additively, to use cogeneration can save primary energy: own calculations prove that 25-40% of the energy can be saved. But, in Germany decentralized CHP block units seem politically not to be wanted. Cogeneration covers recently less than 20% of the generation of electricity, mostly from large-scale CHP plants. Thus, nearly 300 million tons of CO_2 are emitted from the conventional thermal power plants in Germany. CHP could be a forceful tool - too - to reduce emissions - but today from economic and technical reasons with low funding, CHP is not yet feasible for the private area. The stationary fuel cell technology may change this situation - introduced to market since 2015 -, towards 2030.

In principle, the examples shown here can be applied to other countries. However, due to the climatic and economic differences, all measures must be adapted to the local circumstances. In typical urban areas, the energy consumption can be drastically higher than in the rural areas. But, resuming the data, whereas the Germans are seen as environmentally friendly while they are emitting still more than 10 tons of CO_2 equivalents per capita and year, developing countries finally emit maybe only 1/3 of it - and actually live more sustainable than the Germans.

However, whereas today the discussion about environmental compatibility is focused on ***"the-energy-question-is-bound-(nearly)-only-to-the-global-warming-problem"***, environment is more than only global warming: in earlier times - regarding the 1980s - it had been already realized that there are "EIGHT MAIN AIR POLLUTANTS CAUSING SEVERAL MORE ATMOSPHERIC DISEASES SUCH AS SMOG, ACID RAIN, STRATOSPHERIC OZONE HOLE AND OTHERS" – thus the *greenhouse gases* (CO_2, CH_4, N_2O etc.), the *acidic gases* (SO_2, NO_x, etc.), the *carbon monoxide*, the *NMVOC* (= Non Methane Volatile Organic Compounds), and the *dust* (including fines particles).

6 References

[1] BMWi [German Federal Ministry for Economics and Technology], “Energiedaten - nationale und internationale Entwicklung”, EXCEL file, (internet update 2020/03/31 download: www.bmwi.de), 44 sheets, (2020).

[2] EU [European Union], “Directive 2002/91/EC of the European Parliament and of the Council of 16 December 2002 on the energy performance of buildings [EPBD]”, 2002.

[3] EU [European Union], “Directive 2010/31/EU EC of the European Parliament and of the Council of 19 May 2010 on the energy performance of buildings” in order to implement the new EPBD (recast), 2010.

[4] EU [European Union], “Directive 2012/27/EU of the European Parliament and of the Council of 25 October 2012 on energy efficiency (Energy Efficiency Directive, EED), amending Directives 2009/125/EC and 2010/30/EU and repealing Directives 2004/8/EC and 2006/32/EC Text with EEA relevance” in order to improve energy efficiency actions, 2012.

[5] EU [European Union], “Directive (EU) 2018/855 of the European Parliament and of the Council of 30 May 2018 amending Directive 2010/31/EU on the energy performance of buildings and Directive 2012/27/EU on energy efficiency (Text with EEA relevance)”, 2018.

[6] EU [European Union], “Energy Efficiency Action Plan (EEAP)”, (internet download EU internet platform http://ec.europa.eu/energy/action_plan_energy_efficiency/doc/com_2006_0545_en.pdf), 2006.

[7] EU [European Union], “Green Paper on Energy Efficiency or Doing More with Less” (internet download EU internet platform https://eur-lex.europa.eu/legal-content/EN/TXT/PDF/?uri=CELEX:52005DC0265), 2005.

[8] FRG [Federal Republic of Germany], “Energieeinsparverordnung [2014/16] - Nichtamtliche Lesefassung zur Zweiten Verordnung zur Änderung der Energieeinsparverordnung vom 18. November 2013, (BGBl. I S. 3951), (internet download https://www.bmu.de/fileadmin/Daten_BMU/Download_PDF/Energieeffizient_Bauen/energiesparverordnung_lesefassung_bf.pdf, 2013.

SIII-1b

Design and manufacturing of an unmanned aerial vehicle with air quality control system

Subtitle

H. Smajic[1], T. Duspara[2]

Abstract

Within the scope of this project, a fully functional model of an unmanned aerial vehicle with an air control system was developed and implemented as a prototype. By using the mobile measuring stations, it is feasible to measure the air quality in any part of the city, independent of the measuring altitude.

1 Introduction

The development of unmanned aerial vehicles in the very beginning was secretive, mostly because they were commonly used for military purposes. Today in the 21st century, they are in all segments of life, from military, civilian to recreational [4, 5]. Their landing and take-off is possible from different surfaces, from grassy, sandy to paved surfaces. Unmanned aerial vehicles are aircrafts capable of performing continuous flight without a pilot [1, 2]. The use of drones, especially for civilian purposes, has grown exponentially, in terms of both number, size and weight, as well as the increasing number of applications.

1.2. Classification of unmanned aerial vehicles

In reality, "Drone" refers to a multi-jet aircraft. These vehicles are always unmanned and traditionally consist of three, four, six or eight arms. Each arm features a high performance engine and propeller, allowing the aircraft to lift considerable weight and maneuver around tight spaces. According to the basic division by number of rotors, aircraft are divided into Tricopter (three rotors), Quadcopter (four rotors), Hexacopter (six rotors), Octacopter (eight rotors) etc.

2 Overview of main components of an UAV

To design the unmanned aerial vehicle, it is necessary to specify six main components of every unmanned aerial vehicle.

- Drone Body
- Drive train (Electromotor with propellers)
- Power train (Battery)
- Power distribution system
- Communication system (Radio communication)
- Control system (Flight Computer)

Depending on the purpose of drone, there is one additional subsystem

- Sensor system

[1] Prof. Dr. Ing. Hasan Smajic, TH Koln/Faculty of Vehicle Systems and Production, Institute, Cologne, Germany

[2] BSc Eng. Toni Duspara, TH Koln/Faculty of Vehicle Systems and Production, Institute, Cologne, Germany

For any type of unmanned aerial vehicle, the all major components must be included. They are not related to the number of rotors or the purpose of the drone. The load or device carrying the drone depends on the purpose of the drone. It constitutes the sixth subsystem mentioned in previous chapter. In this case, it is necessary to design a drone capable of carrying a sensor that can interrogate air quality data and parameters. Additional sensor represents the seventh subsystem.

2.1 Selection of components

2.1.1 Body parameters

From the requirements set out, it was clear that a "quadcopter" must be built as an unmanned aircraft with four rotors. The name itself tells us that the aircraft consists of four electric motors which generate the pushing force and lift the aircraft into the air. The material used for the construction of the drone body is PLA plastic with 20% filling. This type of plastic is suitable for the construction of an airplane because it can be produced with rapid prototyping machines (3D printers). To start designing the drone body, it is essential to model and design the frame itself. The diameter of a complete assembly will be about 450 mm. From diameter size, the length of the arms will be derived. The weight of the aircraft should not exceed 1 kg. In this way, the flight time will be extended.

2.1.2 Drive train

To select a suitable drive train assembly consisting of propeller, brushless motor and ESC, suitable propellers and their length must be defined. According to the frame dimensions of 450mm diameter 10" (approx. 250mm) propellers will be eligibile for this prototype. Four propellers have to be purchased, two of as work clockwise and two counterclockwise. A proper electric motor should be selected for the next step. A brushless DC electric motor is most often used for the design and construction of unmanned aircraft. The motor types are declared with KV unit. KV stands for the number of revolutions minute per one volt. Since the aircraft uses a LiPo battery with a nominal voltage of about 11 volts, a suitable motor should be equipped with a unit of about 1000-1800KV. The last component of the drive train system is an ESC speed controller. ESC controllers are quite durable. Using a 30 amp controller for the drivetrain, should be enough to control the speed of electric motors smoothly.

2.1.3 Power source (battery)

The battery has a very importance for airplanes. It drives the power train together with all other components within a drone. A three-cell LiPo battery is most often chosen for aircraft design. The battery types generate a voltage of 11.1 V (3.7 V per cell). The capacity of a battery has a direct effect on flight time. The greater the capacity, the longer the flight time. It is also important that a larger capacity indicates a heavier battery. The capacity of a battery is selected according to the size of the drone body. For a drone body size of 450 mm the suitable battery is a 3-cell LiPo battery with 2500 to 4000 mAh. Accordingly, the most suitable battery is a 3-cell LiPo battery with 2700 mAh and XT60 connection.

2.1.4 Transmitter and receiver

Radio connection assembly consists of two main parts: transmitter and receiver. Every unmanned vehicle system can use the same type of a transmitter and receiver. The transmitter chosen for this project is a FS-i6 six channel regulator. Four of the channels are controlled by

joysticks and the other two are free for programing. The last component that comes with the transmitter is a receiver. Receiver is attached to the drone body. It is connected directly to the flight computer, transmitting the sensor signals via radio connection.

2.1.5 Flight computer

For the data processing in the air a flight controller had to be found first. The controller KK2.1.5 has an LCD display, which makes programming and calibration of the processes much easier. Particular advantages are provided by pre-installed flight types and drone profiles. These features make it easier to set the type of aircraft, check the direction of rotation of all motors, route the current flow through the ESC-s and perform the calibration.

2.1.6 Power distribution

Power distribution to all of components is usually achieved through custom PCB boards. The PCB boards are directing the current flow to all necessary parts using a parallel connection scheme. The board itself has sockets for all four ESC controllers (and can hold up to six units). A big advantage of this board is the integrated connections for other devices that have to operate at a different voltage. A nominal voltage of 5V is required to supply the sensor system, consisting of a microcontroller and detectors. Since the LiPo battery supplies a DC voltage of 11.1V, a direct connection to the sensor system is not possible. By employing the distribution board, a 5V power source is available to supply the entire sensor system.

2.2. Components for drone design

Following the design of the drone concept and the specification and dimensioning of all necessary units, the list of components can be summarized in Table 1.

PARTS FOR DRONE CONSTRUCTION				
Name	**Mark**	**Qt**	**Price/pc (USD)**	**Price (USD)**
ESC	XXD HW30A	4	2,99	11,96
DC Motor	A2212	4	8,99	35,96
Flight computer	KK2.1.5	1	14,90	14,90
LiPo Charger	IMAX B6	1	27,02	27,02
Propellers	1045 10x4.5	1	9,26	9,26
LiPo Battery	3S 2700mAh	1	19,17	19,17
Communication	FS-i6X 10CH	1	54,70	54,70
PDB	FDB XT60	1	2,51	2,51
Battery connector	XT60	1	0,81	0,81
Microcontroler	ESP8226	1	2,79	2,79
Particle sensor	PMS5003	1	30,5	30,5
SHIPPING			$24,02	
ALTOGETHER			209,58	

Table 1: Parts for drone construction

3. Modelling and design of the aircraft

The modelling and construction of a quadcopter consists of the design of the drone body itself. The body consists of a central part and arms that support the rotors. They are the main components of any UAV or drone. To avoid collisions between the propellers and to achieve a compact design, it has already been specified that the diagonal distance between the rotors should be between 400 and 500 mm. The approximate dimensional area of an aircraft is shown in below.

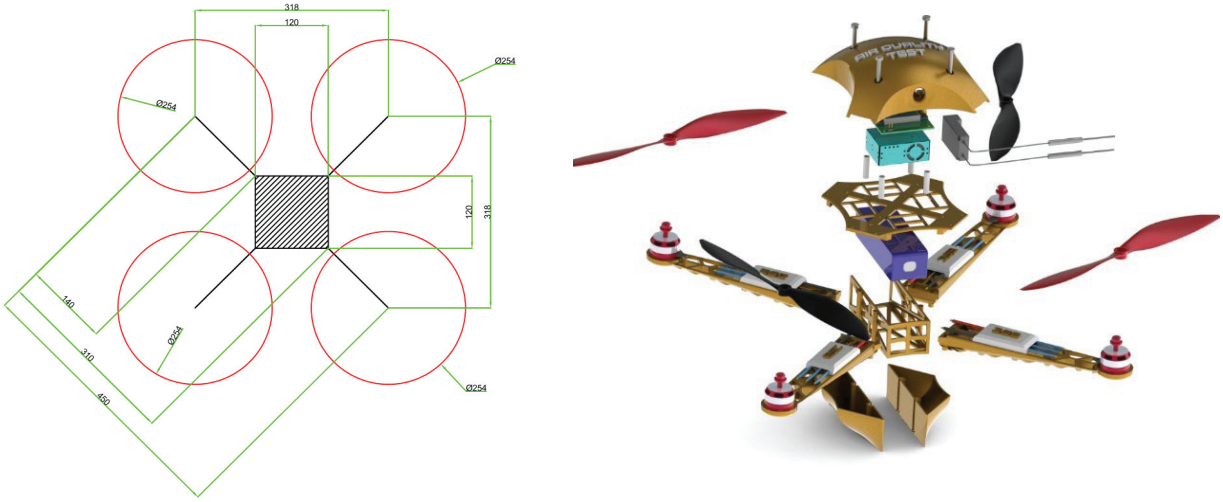

Figure 1: a) Dimensional area b) Exploded drone body with all components

First, it is necessary to determine the dimensions of the central part of an aircraft. The main task of the central part is to carry the electronic components. The part itself should have brackets for battery, flight computer, sensor system, radio receiver etc. The approximate dimensional area for the central part is 120x120mm. According to this it is specified that the arms of an airplane should be between 140 and 200 mm long. During the construction it is crucial to pay attention to the mass of the parts. To reduce the mass of certain parts, it is recommended to model the parts so that they are perforated. By strategically piercing the holes inside the body panels, the mass is reduced in a way that does not compromise the integrity of the structure. Another advantage of reducing mass and piercing holes is that air can flow through the arms. This helps to get more benefit from the propulsion assembly and the propellers themselves. All components are connected by nuts and bolts. The dimensions of the arm model are 190x40x20mm, which fits perfectly within the given dimensional range. The central part of this airplane, which is connected with four arms and to which all other parts are attached, should fit into a dimensional range of about 120x120mm. When attaching the components to the central part, the center of mass should not be forgotten.

For an aircraft to have a stable flight, it is essential that the centre of mass is in the middle of the aircraft. To avoid calculating the center of mass for each individual component and later having to calculate the positions of the components, the easiest way is to simply maintain the symmetry of an airplane [3]. This is achieved by arranging the components in layers. Accordingly, the battery that powers the entire system should be placed under the central part and the flight computer and sensor systems should above the central part. The positioning of the components on the central part is done by model mounts. To arrange the components in layers, we will design spacers. The main task of the spacers is to lift the flight computer above the central part so that the senosr system can be placed in between. The final assembly with all components weighs about 750g. Once the drone body has been designed, it is recommended to create the housing. The main function of the housing is to protect the electronic components. The modelling of the housing contributes to the aesthetic appearance of an aircraft (Figure 1b). The enclosure consists of four parts: upper cap, lower left cap, lower right cap, ESC caps.

4. Air quality measuring system

4.2. Introduction

After the construction of the drone itself, or the drive unit of the project, it is necessary to design and configure the measurement subsystem. Before the plan itself is designed, it is essential to describe what makes up the measurement system and the need behind the construction of this project. The unit is called the Air Quality Index and was developed by the US Environmental Protection Agency. Based on the value of the AQ index, it is possible to extrapolate the level of air quality and the likely health risks to which the population could be exposed after a number of hours or days of exposure to the air itself. The data from the automatic measurement units are obtained hourly from the relevant government institution and published on the official website. Fine, suspended particles, PM2.5, are mainly the product of various combustion processes. Because of their small size, they can penetrate deep into the lungs and reach most, if not all, of the internal organs via the bloodstream, so they pose a far greater health risk than coarse suspended particles.

4.3. Sensor Detection

Since the desired measurement result represents the air quality index, or rather, the concentration of airborne particles, it is necessary to select a sensor with the ability to display the desired measurements. With that in mind, the PMS5003 sensor was selected for this project The PMS5003 is a type of digital and universal sensors which measures airborne particles in the air and displays the readings in digital form. The measurement system of this sensor is based on laser scattering technology. A laser diode within the sensor irradiates particles coming in to the sensor. A receiver across the diode measures the amount of scattered light. The microprocessor inside the sensor allows us to calculate the nominal diameter of the particles and the number of particles using the MIE theory.

The sensor displays values of PM1.0, PM2.5, and PM10 concentrations in $\mu g/m^3$ as output. There are two output options with the sensor: a passive output and an active output. The default output option while powering on the device is active output mode. If the changes in concentration values are very low, the sensor will work in stable mode that will output data every 2,3 seconds. If the sensor detects rapid and increased differences in concentration, it will automatically switch to fast mode with outputs data every 200~800ms. The larger the concentration of the particles, the faster will the sensor respond. Response time also depends on the upload speed to the online server.

4.4. Control system

To fully utilize the PMS5003 sensor, it must be connected to a microcomputer that processes the sensor data and displays it to the user. Since the drone is a mobile unit, the microcomputer must have means for wireless communication. Due to the fact that the drone itself uses a radio link for communication between the transmitter and receiver, and due to the fact that Bluetooth has a short range, it is best to use Wi-Fi communication. One of the important features when selecting the appropriate control system is to secure the power source. Sensors and microcomputers usually work with low voltage (5V). The NODEMCU microcomputer was adopted because it has wireless communication and a direct internal power supply. The microcomputer contains an integrated ESP2668 module for wireless communication over Wi-Fi networks. A mobile device (cell phone) with Wi-Fi is used to connect the microcontroller to the Internet and display the measurement results on either an online server or a local server.

4.5. Sensor system wiring

When approaching the wiring of sensor systems, the first step is to check the pin layout and pin function on each device (microcontroller and PMS5003 sensor). The complete wiring diagram between the sensor system components is shown in Figure 2. All devices in the system are wired to the same power source (LiPo battery). The flight computer is powered by the ESC-s, while other components receive their power from a power distribution unit connected to the battery.

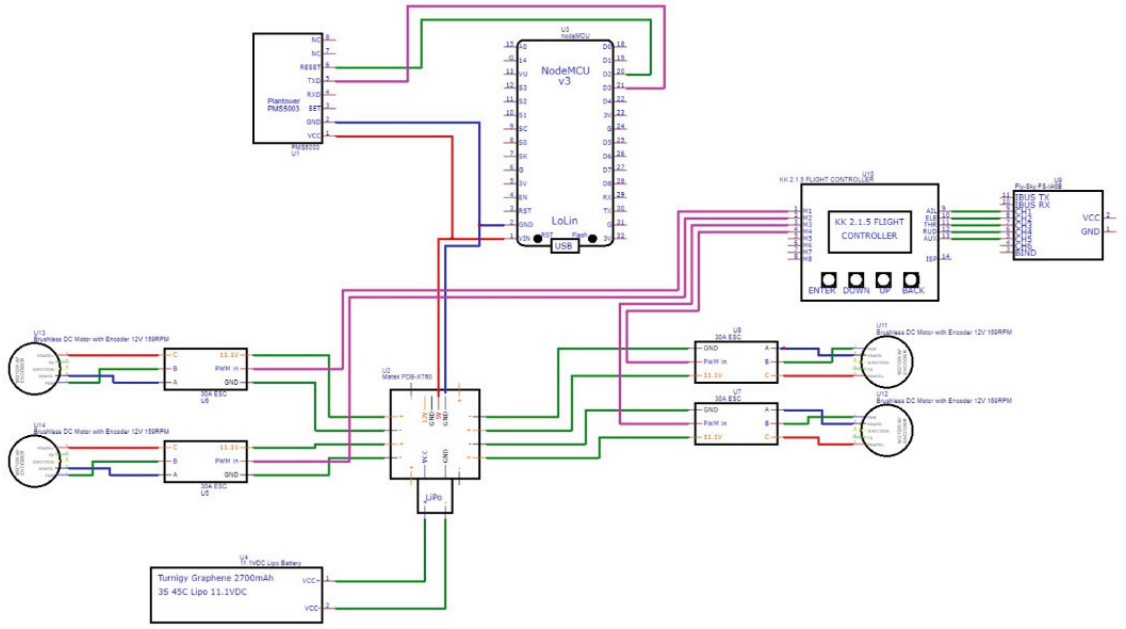

Figure 2 - Drone system wiring

4.6. Measuring system automation

As already mentioned, the development of control system software is done with the integrated development environment Arduino. Additional software still needs to be developed. This software creates a server on a personal computer that stores measurement data. Py-thon programming language was used as the development platform. In order to be able to view the measurement data at any time and any place, the data is automatically uploaded to an online server. Using a Wi-Fi adapter integrated in a microcontroller, the aircraft can be connected to the Internet via a mobile device (personal hotspot). Once the connection between the microcontroller and the mobile device is established and later when the aircraft is connected to the Internet, the data is automatically uploaded to an online server. In this case, the computer connected to the Internet will be the local server where the data is stored.

4.6.1. Server establishment with python

When the main parameters (IP address, connection number, etc.) have been set, the software goes into a cycle. In this loop, the server initially waits for the connection of the client. Upon establishing the connection, the server outputs the IP address of the client and starts receiving data from the microcontroller. During their connection, the server and client constantly send messages to each other to ensure their connection. If the server detects that no data is coming in, the loop stops and the software tries to connect again. When both devices are turned on and connected to the Internet, the connection is automatically activated and data is exchanged.

4.6.2. Software development for sending and receiving measurement data

The second part of automation of measurement systems is the development of software that receives data from the sensor and transmits it to the server. This software has two purposes. The first is to establish the connection between the sensor and the microcontroller to obtain measurement results. The second is sending these results to the server. The controller constantly receives a cluster of data (Figure 5).

```
---------------------------------------
Concentration Units (standard)
PM 1.0: 245            PM 2.5: 396            PM 10: 406
---------------------------------------
Concentration Units (environmental)
PM 1.0: 163            PM 2.5: 263            PM 10: 270
---------------------------------------
Particles > 0.3um / 0.1L air:40317
Particles > 0.5um / 0.1L air:11611
Particles > 1.0um / 0.1L air:2863
Particles > 2.5um / 0.1L air:187
Particles > 5.0um / 0.1L air:11
Particles > 10.0 um / 0.1L air:4
```

Figure 3: Python code output

4.6.3. Results preview and printout

When measurement data has been successfully exchanged between server and client, it is necessary to print them. The code automatically connects the server to Google Cloud and stores the measurement data in an Excel spreadsheet. The measurement data are automatically uploaded online and can be accessed from anywhere.

5. Conclusion

Within the framework of this project, a system for air quality control with unmanned aircraft was successfully designed and implemented. The design and construction with all its components was the first step towards production. The aircraft measures approximately 450x450 mm and is made of PLA plastic using 3D printing technology. For the propulsion system 1400KV brushless DC motors with 10" propellers and 30A ESC-s were applied. The control unit consists of the flight computer KK2.1.5, which is connected to a FS-i6 transmitter and receiver. Power source for the whole system was a three-cell LiPo battery with 2700mAh capacity. The entire aircraft with all its components weighs about 750g and due to its characteristics falls into the "mini" type of a drone. The sensor system includes the microcontroller ESP8226 with built-in Wi-Fi module and the air particle sensor PMS5003. The results are immediately stored on a server after the measurement. The first is a local server (operator's personal computer) and the second is an online Google server. Finally, the data are saved in an Excel table.

References

[1] Cinnamon, I., Kadri, R. and Tepper, F., 2016. DIY Drones For The Evil Genius. New York: McGraw-Hill Education TAB
[2] Yong, Z., 2016. Digital universal particle concentration sensor (PMS5003 Series data manual), 2016 product data manual of PLANTOWER
[3] D. Norris, Build your own quadcopter. New York: McGraw-Hill Education, 20144.
[4] A. Baum, Verkehrsträgerübergreifende Messung von Luftschadstoffen mit Dronen, 1. Tagung des Expertennetzwerks, 14.06.2018, BMVI, Berlin
[5] https://www.drohnen.de/category/drohnen-einsaetze/page/16

SIII-2a

ENERGY RECOVERY FROM SEWAGE SLUDGE AND FERMENTABLE FRACTIONS OF SOLID WASTE FROM THE CITY OF SOKODE BY CO-DIGESTION

Nitale M'Balikine KROU [(1)] ; Gnon BABA [(1,2)] ; Kwamivi N. SEGBEAYA [(1,2),] Ogouvidé Akpaki [(1)]

E-mail : krounitale@gmail.com ; gnonbaba@gmail.com ; kwamininnyo@gmail.com;

Abstract

One of the consequences of the improvement of the living conditions of the populations is the strong demand in thermal energy for the households whereas in the developing countries, the cost of living is a brake with all the social layers to reach supply of butane gas for their energy needs. This study takes place in the context of energy, environmental and sanitation challenges in the city of Sokodé. Indeed, we are witnessing more and more growing needs for butane gas, firewood or charcoal for cooking or lighting in the city of Sokodé as everywhere in other cities of the same size. Thus by the production of energy in situ, the condition of the populations will be able to improve significantly thanks to the recovery of sludge and fermentable fractions of solid waste into biogas. The objective of this work is to produce and recover methane from fermentable waste produced in the city of Sokodé. The methane or biogas recovered will be used as fuel to fuel kitchens in households. The resulting digestate will serve as an organic amendment to agricultural soils in the commune of Sokodé. Laboratory scale tests have been carried out to validate the value of co-digestion of sewage sludge with fermentable solid waste. The results obtained have shown that the methanogenic potential of sewage sludge is low compared to that of fermentable solid waste. The co-digestion of the two products allows a greater production of methane representing an energy gain compared to the methanisation of the sewage sludge alone. This study shows that waste (sludge from public septic tanks, waste from markets, hotels and fermentable households) can be considered an appreciable energy resource. Their Co-treatment would, while reducing the nuisance associated with this waste, produce valuable energy.

Keywords : Renewable energy; Anaerobic Co-digestion; Organic solid waste; drain sludge.

1 Introduction

One of the consequences of the improvement of the living conditions of the populations is the high demand for thermal energy for the households whereas in the developing countries, the cost of living is an obstacle to all the social layers to reach supply of butane gas for their energy needs. Generally in these countries, the most used source of energy in the households is that of charcoal. Excessive use of wood and charcoal leads to deforestation which in turn has a negative effect on the environment. According to the 2010 World Bank report on the energy balance in Togo, biomass remains the main source of energy consumed. It represents on average 70 to 80% of total final consumption and is used to supply the domestic and craft sectors. According to the same report, nationally (Togo), 61% of households use only wood,

[1] Laboratory of Sanitation Water Sciences and Enviroment (LASEE), Faculty of Science and Technology, Department of Chemistry, University of Kara (Togo), BP.404 Kara-Togo, mail: oakpaki@gmail.com

[2] Laboratory of Mangement, Treatment and valuation of Waste (GTVD), Faculty of Science, Department of Chemistry, University of Lomé, P.O. Box 1515, Lomé, Togo

24% charcoal and firewood and 15% only charcoal, 75% of rural households use firewood with a consumption of 347 kg / year / person, while 72% of urban households use charcoal for around 59 kg / year / person [1]. With this vertiginous consumption of wood which is likely to increase in the coming years and that, at the current state of our knowledge, no concrete measure is taken to balance the consumption of wood energy with the production capacity of forests, it can be estimated that Togo is tending towards a chronic inability to meet its wood energy needs and to the disappearance of the forests which constitute the sources of supply. This increased consumption of wood and the strong degradation of forests in Togo is due to the cost of fossil fuels and the difficulty of serving landlocked regions.

At a time when renewable energies are more and more mentioned to supplement or gradually replace fossil fuels, anaerobic digestion is an opportunity to diversify energy resources and to manage the environment sustainably. Anaerobic digestion has significant potential through its double capacity for recovering energy from organic waste and reducing greenhouse gas emissions. It could be seen as an economic, decentralized and ecological solution to these problems through energy autonomy and sustainable agricultural development in rural areas.

This study takes place in the context of energy, environmental and sanitation challenges in the city of Sokodé. Indeed, we are witnessing more and more growing needs for butane gas, firewood or charcoal for cooking or lighting in the city of Sokodé as everywhere in the other cities of the same size. Thus by the production of energy in situ, the condition of the populations will be able to improve significantly thanks to the recovery of sludge and fermentable fractions of solid waste into biogas. The wood and charcoal which constitute the traditional biomass in households in Sokodé generate smoke which is a threat to public health. Co-fermentation of sewage sludge with fermentable waste of domestic or industrial origin can be a good alternative for domestic cooking.

Small-scale biogas fermentation systems offer the possibility of using the waste substrates mentioned above and therefore saving public health, instead of using wood (smoke is also dangerous).

The general objective of this work is to produce and recover methane from fermentable waste produced in the city of Sokodé. The methane or biogas recovered will be used as fuel to fuel kitchens in households. The resulting digestate will serve as an organic amendment to agricultural soils with good fertilizing value in the commune of Sokodé. In fact, all of the nitrogen contained in the methanised material is conserved during anaerobic digestion. However, there is a change from the original organic form to an ammoniacal NH_4^+ form which is more assimilable by plants [2]. The present study aims in particular to evaluate the interest of Co-digestion of sewage sludge with fermentable waste through their maximum production of biogas and methane.

As far as we know, no study has been reported on the Co-digestion of sewage sludge with fermentable municipal waste in Togo. This study could provide a baseline database in Togo using inexpensive and available raw materials that complement each other.

Tests on a laboratory scale have been carried out in order to validate the value of the Co-digestion of the sludge with the fermentable solid waste.

The results obtained will enable the process to be validated and implemented on a large scale at the sewage sludge treatment station in the city of Sokodé.

2. Materials and methods

2.1. Description of the study environment

Organic waste used in this research came from Sokodé, capital of the Central Region and the Prefecture of Tchaoudjo, located between 8 ° 57 'and 9 ° 03' of Latitude North and 1 ° 05 'and 1°11' of Longitude East, 346 km north of Lomé. It has long been the regional capital of the northern zone and especially the second center of settlement of the country. With a population estimated at 111258 inhabitants, Sokodé enjoys a tropical climate of transition between Guinean (wet) and Sudano-Sahelian (dry).

2.2. Raw materials

2.2.1. Origin of substrates and scenarios

The sludge used comes from public toilets. Preliminary modeling studies of biogas production by sludges from dry latrines (DL), public septic tanks (PST) and domestic septic tanks (DST) from the city of Sokodé have shown that DST and DL sludge have a low production of biogas compared to that of PST sludge. Thus, only fresh sludge (from public toilets) is suitable for the production of biogas, with a dryness of at least 3% [3]. Fermentable fractions are obtained after sorting solid waste from hotels, markets and households. The samples used for the experiments were taken in accordance with good sampling and conservation practices.

The test includes four scenarios :

- Scenario 1 : feeding the digester with the drain sludge alone,
- Scenario 2 : feeding the digester with the fermentable fractions of household waste only,
- Scenario 3 : feeding the digester with the fermentable fractions of market and hotel waste alone,
- Scenario 4 : feeding the sludge drain digester mixed with the fermentable fractions of solid waste (households, hotels and markets).

Tests carried out under a mesophilic regime (37°C.) consisted in monitoring the performance of biogas production by these residues.

2.2.2. Ratios

The solid / liquid ratio (S / L) equal to 1/5 has been used [4] because it makes it possible to avoid inhibitions and makes it possible to reach the maximum production of biogas for most substrates [5] and [6]. Thus, to prevent inhibitions, the amount of substrate used is not too large compared to the amount of distilled water. This optimal S / L ratio of 1/5 fixed will also allow bacteria to ensure the fermentation of organic matter, limiting the concentration of nitrogen and / or volatile fatty acids [7].

After mixing the substrates and distilled water, the vials were closed tightly. The vials were then incubated at 37 ° C to perform digestion under mesophilic conditions. The experiments were stopped after 42 days of production when the daily production of biogas was very low.

2.2.3. Grinding

Reducing the particle size of the substrate increases its homogeneity. This reduction in size is necessary because the specific surface that can be attacked by bacteria and enzymes increases with the reduction of particles [8]. In addition, large particles originally can be introduced into small laboratory bottles by grinding. Studies on the effect of grinding food scraps have also been carried out. The results showed that a reduction in particle size to 2 mm allows an increase in methane production of at least 20% [9]. Grinding would release easily degradable particles, which are not always available to bacteria without reducing the particle size [10]

and [11]. In this study, the grinding was done using a laboratory mortar to reduce the particle size. The following pictures show the samples of fresh sludge and fermentable fractions of solid waste

.

Figure 1: Sample of fresh sewage sludge

Figure 2: Sample of FFAW

2.3. Biogas production test: experimental protocol

The protocol is based on preliminary studies in laboratory pilot. This protocol implemented makes it possible to obtain the total biogas production of the effluent representative of its level of anaerobic biodegradability. The experimental device is made up of digesters (1500mL bottles), rubber pipes, graduated cylinders for collecting biogas, a solution of sodium chloride contained in a beaker and supports. In this assembly, the pilot digesters were connected through gas supply pipes, to inverted test tubes (allowing the visual measurement of the volume of biogas produced daily) immersed in a beaker containing a trap solution, consisting of saturated water in NaCl and in acid (hydrochloric acid 5%, NaCl 20% and pH = 2) in order to minimize the dissolution of CO2 from the biogas [12] and [13]. This aqueous solution traps, by the displacement of the liquid, to properly quantify the daily production of biogas (Figure 3).

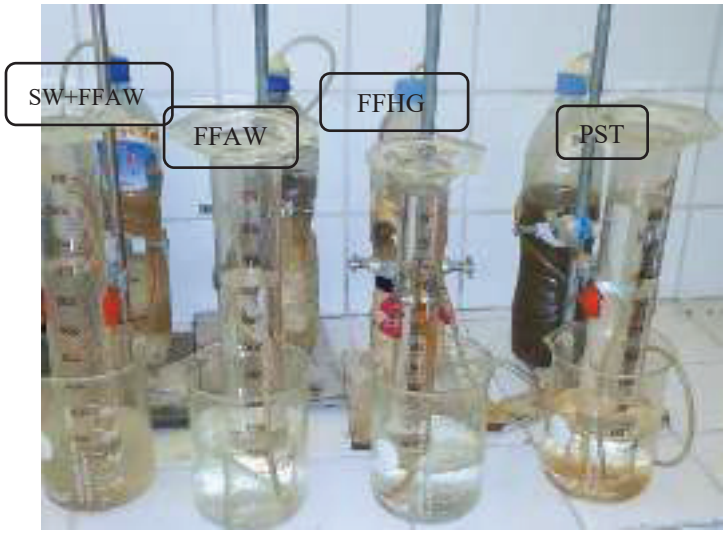

Figure 3: Biogas production system

3. Results and discussion

In order to validate the value of the co-digestion of sewage sludge with the fermentable fractions of municipal solid waste, a comparative study of the production of biogas from these different fermentable substrates was carried out.

3.1 Co-digestion scenario performances

3.1.1. Biogas production by different fermentable substrates

The production measured represents the maximum amount of biogas that can be produced by a given fermentable substrate. This measurement is specific to each fermentable substrate and representative of its level of biodegradability. Figure 4 shows the cumulative biogas production for an anaerobic digestion of 42 days. Depending on the type of substrate, biogas production varies depending on whether it is rich in easily biodegradable organic matter.

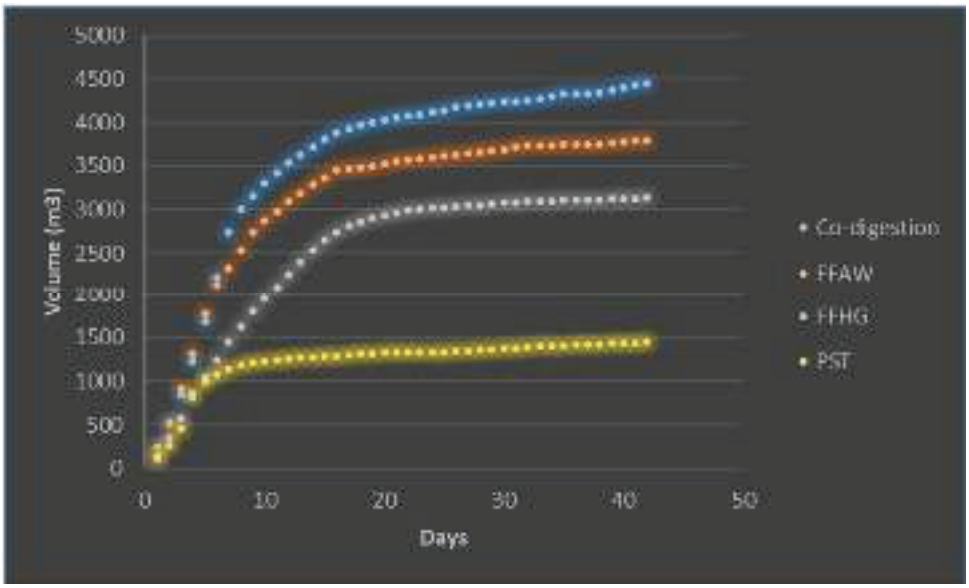

Figure 4 : Cumulative biogas production

- ❖ FFHW : Fermentable Fractions of Household Waste (Corn paste, prepared rice, prepared pasta and mango).
- ❖ FFAW : Fermentable Fractions of Assimilated Waste (Mango, banana, bread, and avocado).
- ❖ PSP : Public Skeptic Tank

This figure shows that, from the same quantity of substrate, the biogas production potential of FFAW is high compared to that of FFHW, which is also higher than that of sewage sludge from public septic tanks. This result is explained by the fact that the biologically degradable part is higher at the fermentable fractions of solid waste than at the level of the sludge; these sludges having already undergone decomposition in the pits thus reducing their digestible matter content. The high biogas production of FFHW (leftover corn dough, prepared rice, prepared pasta) compared to that of sewage sludge is attributed to the presence of residual food starch in these effluents [12]. Waste materials have a low level of biodegradability compared to other substrates. It may be a problem of accessibility of the organic matter or of the composition of the organic matter or else of the limitation of the fermentation by ammonia in more or less significant concentration in these sludges [12]. The best performance of FFAW effluents is attributed to their high organic matter content in the waste because the amount of gas produced by a substrate is positively correlated with the amount of organic matter present [14]. Indeed, most of the fruits used in this scenario are rich either in lipids (example of avocado), or in starch (bread for example), or in carbohydrates (banana). Studies have also shown that the main constituents of mango are water, carbohydrates, proteins, fats (carotene), minerals, pigments, tannins and vitamins [15]. However, lipid products have a high potential for biogas production as well as the methane content [12]. In addition, it has

been shown that fruit residues often have high methanogenic potential and are easily assimilated by bacteria. This assimilation is due to the high contents of pectins at the level of their cell walls and of easily biodegradable organic acids, giving them a relatively rapid kinetics of anaerobic degradation [16]. The organic matter provided by FFAW is much more easily degradable than that from FFHW, which results in their much higher gasification potential.

The results presented indicate that, the association of these fermentable fractions of various origins will allow to improve the individual performances, which allowed us to formulate another hypothesis on the investigation compared to the anaerobic Co-digestion of these sludges with the fermentable fractions of municipal solid waste.

3.1.2. Interest of Co-digestion

The results of co-digestion (Figure 4) show that the production yield of biogas has improved significantly compared to the digestion of these substrates alone. The biogas production potential is increased by almost 35% compared to the phase without the addition of co-substrates (on average 3,580L/gMO compared to 1.233L/gMO) for the sludge. The contribution of co-substrates of lipidic nature allowed an increase in the quantity of biogas produced daily as well as the content of methane [12]. Also, the addition of fermentable fractions of municipal solid waste leads to an increase in the rate of organic matter compared to the phase of sewage sludge alone., As a result, there is a greater production of biogas. The present study shows that a ratio equal to 0.3 gives better biogas production. This result is comparable to that obtained by.Nsavyimana where a sludge VSM/waste VOM ratio = 0.3 was considered optimal for good digestion of waste of a different nature [17].

The biogas produced from the co-digestion of sewage sludge with fermentable market waste contains on average 65.6% CH4 against 34.4% CO2) [18]. On this basis, we estimated volumes of methane and carbon dioxide in the biogas produced. Indeed, from 1L of substrate in 42 days of Co-digestion, an average production of 3.580 L/g MO was estimated, that is to say a volume of 2.348 L of CH4 and 1.232 L of CO2.

Conclusion

The general objective of this study was to produce and recover methane from fermentable waste produced in the city of Sokodé. It is particularly a question of evaluating the interest of Co-digestion of drain sludge with fermentable waste through their maximum production of biogas and methane. The results of the pilot tests on a laboratory scale demonstrate the significant variability that may exist between fermentable residues of different origins. From the same quantity of substrate, the biogas production potential of the fermentable fractions of assimilated waste (from markets, hotels) is high compared to that of the fermentable fractions of household waste, which is also higher than that of emptying from public septic tanks.

Sewage sludge alone has a low production of biogas compared to the fermentable fractions of municipal solid waste. The addition to fermentable sludge under controlled conditions of the fermentable fractions of municipal solid waste with a higher dry matter content has made it possible to increase the production performance of biogas compared to sewage sludge alone. The biogas production potential is increased by almost 35% compared to the phase without the addition of co-substrates (on average 3.580 L / g MO compared to 1.233L/g MO) for the sludge. From 1L of substrate in 42 days of Co-digestion, an average production of 3.580 L / g MO was estimated, ie a volume of 2.348 L of CH4 and 1.232 L of CO2. The results thus

obtained clearly show the interest of the co-digestion of this waste and constitute basic data for the large-scale implementation of this co-digestion on the sewage sludge treatment station of the city of Sokodé. The gas produced will reduce the gas stock problem and supply households with butane gas. The use of this green technology (anaerobic digestion), will avoid the emission of harmful greenhouse gases and will contribute positively to environmental objectives. The methanation of Sokodé's fermentable substrates would produce clean renewable energy available on site without being dependent on imports.5**.**

Acknowledgments

We are grateful for the Head of the Water and Environmental Sanitation Laboratory and Supervisor of this work, Professor Gnon BABA for funding.

References

[1] World Bank, "Environmental Analysis of Togo with Emphasis on the Agriculture, Energy and Mining Sectors," Lomé, 2010.

[2] Almansour, *Energy and environmental assessments of biogas sectors : Approach by standard sector.,* University of Bordeaux 1., 2011, p. 147.

[3] Klingel, Drainage sludge management., First ed., 2002, p. 63.

[4] Deressa, «Production of Biogas from Fruit and Vegetable Wastes Mixed with Different Wastes.,» *Environment and Ecology Research ,* vol. 3, n°13, pp. 65-71, 2015.

[5] Mata-Alvarez, «A critical review on anaerobic co-digestion achievements between 2010 and 2013.,» *Renewable and Sustainable Energy Review,* n°136, pp. 412-427, 2014.

[6] Walker, « Residual biogas potential test for digestates." OFW004-005.,» *Waste and Resources Action Programme,* p. 53, 2010.

[7] Eskicioglu, «"Effect on inoculum/substrate ratio on mesophilic anaerobic digestion of bioethanol plant whole stillage in batch mode.,» *Process Biochemistry,* n°146, pp. 1682-1687, 2011.

[8] Hu, «Influence of particle size and pH on anaerobic degradation of celluloseby ruminal microbes.,» *International Biodeterioration & Biodegradation,* vol. 3, n°155, pp. 233-238., 2005.

[9] Huyard, «Anaerobic co-digestion of wastewater sludges and food waste pulp from aunpacking" process: Enhancement of biogas production and co-metabolism.,» *IWA,* 2012.

[10] Izumi, «"Effects of particle size on anaerobic digestion of food waste.",» *International Biodeterioration & Biodegradation,* vol. 7, n°164, pp. 601-608., 2010.

[11] Bruni, «Anaerobic digestion of maize focusing on variety, harvest time andpretreatment.,» *Applied Energy,* vol. 7, n°187, pp. 2212-2217., 2010.

[12] Pouech, "Interest of co-digestion for the development of slurry and the treatment of fermentable waste at the scale of a territory.," Pig Research Days., N ° 137, pp. 39-44, 2005.

[13] Akpaki, Physico-chemical characterization of the sludge from Attidjin (prefecture of the Gulf-Togo)., Lomé, Water and Environment Chemistry, 2016, p. 167.

[14] Tcha-thom, Search for a sustainable sector for anaerobic digestion of fruit and abattoir waste from Togo: Assessment of the agronomic potential of digestates on the soils of the Kara region., Geochemistry, 2019, p. 205.

[15] Fréhaut, Study of the biochemical composition of mango (Mangifera Indica L.) according to its stage of maturity., Biological Engineering, 2001, p. 65.

[16] Chanakya, «Micro-scale anaerobic digestion ofpoint source components of organic fraction of municipal solid waste.,» *Waste Management,* vol. 4, n°129, p. 1306–1312, 2009.

[17] Nsavyimana, «Anaerobic co-digestion of septic tank drain sludge and fermentable market waste for recovery: Case of Burundi.,» *Life sciences: Environmental sciences & ecology,* 2012.

SIII-2b
Vegetation insulation screen as a passive cooling system in hot humid climate: heat and mass exchanges

Hodo-Abalo Samah[1, 2], Magolmèèna Banna[2], and Belkacem Zeghmati[3]

1 Abstract

Planted roofs are passive cooling techniques that reduce the thermal load of buildings. In this paper, a dynamic mathematical model based on time average Navier-Stokes equations for a planted roof in hot humid climates has been developed for evaluating the cooling potential.Transfer equations are solved using a finite difference scheme and Thomas algorithm. The model was applied for the simulation of the planted roof in togolese climate conditions. Results showed that, evapotranspiration and Solar Heat gain Factor are functions of the Leaf Area Index which is the most important parameter when considering the foliage material. It is clearly proved that the foliage density and hence the vegetable canopy type selection greatly influence the thermal efficiency of the bioclimatic insulation screen. It was found that a larger Leaf Area Index reduces the solar flux penetration and increases evapotranspiration which is an important parameter when considering surrounding microclimate formation.
Keywords - Planted roof; Sensible heat; Latent heat; Evapotranspiration; Solar Heat gains Factor

2 Introduction

Metallic and concrete roofs are very common in buildings in most of the developing countries particularly in tropical regions. The temperatures inside such buildings are far beyond the comfortable conditions in these regions. The direct cooling devices are electrically operated and are not feasible due to unreliable supply of electricity. In such a situation, passive cooling techniques are very appropriate to provide comfort. Passive cooling of buildings can be defined in several ways [1, 2, 3]. One way is to consider any treatment of the building which reduces its cooling load, such as solar control and minimizing internal heat gains. Studies in the literature show that about 30 to 50% of the heat gains inside a building are brought about by roof elements [1]. In hot-humid climates, some methods or techniques are better adapted to improve thermal comfort in buildings. Particularly, the use of thermal insulation screens (ground layer, extruded or moulded polystyrene plates, plaster false ceiling, vegetation canopy) underneath and above the concrete flagstone roof reduces the heat load in a building [4, 5]. The insulation screens are integrated beneath reinforced concrete flagstone as an addi-

[1] Faculté des Sciences et Techniques (FaST), Université de Kara, Kara -TOGO

[2] Laboratoire sur l'Energie solaire LES/GPTE, Université de Lomé, Lomé -TOGO

[3] Laboratoire de Mathématique et Physique des Systèmes, Université de Perpignan via Domitia, Perpignan, France

tional insulation sublayer. The aim of the vegetation surface on roof top design concept is to reduce the heat gain and minimize the cooling load for mechanical air-conditioning. The field study shows that the passive cooling of planted roofs is recognized as one of the effective energy saving means in buildings in warm-humid climates and reduces the indoor air temperature within comfort range. It influences the use of the electrical cooler and air conditioning of the indoor space. Therefore, it can reduce the energy demand of the building which saves a lot of money for the daily electricity bill of urban residents [6]. The green roof plants generate oxygen and provide worth for air pollution control and soil erosion. Green roofs reduce the carbon level that controls global warming. Planted roofs present a very effective and positive impact on urban climate and microclimate as well as on the indoor air temperature of buildings beneath them. In closed spaces with planted roofs, the air temperature beneath the plants during sunny times is lower than that of the air above. For their biological functions such as photosynthesis, respiration, transpiration and evaporation, foliage materials absorb a significant proportion of solar radiation and contribute to reduce heat gains inside a building in the highest solar irradiation regions [7]. With rapid urbanization, there has been high growth in population and building construction in cities. A high concentration of buildings actually raises many environmental issues, such as the Urban Heat Island effect. The Urban Heat Island effect started mainly because of the loss of green areas in the urban environment. Plants when strategically placed around roofs, can be considered a complement of urban greens. These provide visual enhancement, noise control, storm water management, improved water run-off quality, improved urban air quality, extension of roof life, reduction of the urban heat island effect, architectural design and biodiversity. This natural solution also contributes to the thermal benefits in buildings and their surrounding environments. Greenery placed around buildings serves to reduce the surface temperature through direct shading of hard surfaces as well as cool the ambient air through absorbing solar heat for transpiration and photosynthesis. The shaded surfaces also emit less long-wave radiation due to lower surface temperature. All these contribute to lowering energy consumption for cooling and mitigating Urban Heat Island effect in the urban environment. The present study aims mainly to analyse heat and mass exchanges in vegetation screen and its effects on internal heat gains of a building. Important parameters which affect the surrounding environments such as evapotranspiration have been analysed as well as sensible and latent heats fluxes. To analyse heat and mass transfer in vegetation screen insulation system, useful parameters such as Nusselt and Sherwood numbers are the main control variables evaluated.

3 Description of approach and techniques

The green roof system studied is composed of four interacting subsystems: atmospheric environment above the canopy, the vegetation canopy, the substrate or growing medium and the flagstone as a classic roof. The physical model is shown in Figure 1. Parameters defining the outdoor conditions are the solar radiation flux, the ambient air humidity and temperature, the wind speed and direction. The roof is considered large enough and assumed horizontally homogeneous. Heat and mass fluxes are assumed to be mainly vertical so that one-dimensional model is used to describe the thermal behaviour in the roof components. A reference is chosen at the ground level at soil-canopy interface and the abscissas are counted positively in the sense of plant growth (figure 1). The canopy is composed of the leaves and the air within the leaf cover. It is a complex system of sources and sinks of heat and mass such that an exact

description of its physical behaviour is almost impossible. While attempting to figure out a simpler model of a canopy, one is faced with two types of problems. The first is the inherent spatial complexity and dishomogeneity of the foliage. This implies that for an accurate description, the number of simultaneous equations to be solved could be five times higher than the number of leaves in the canopy.

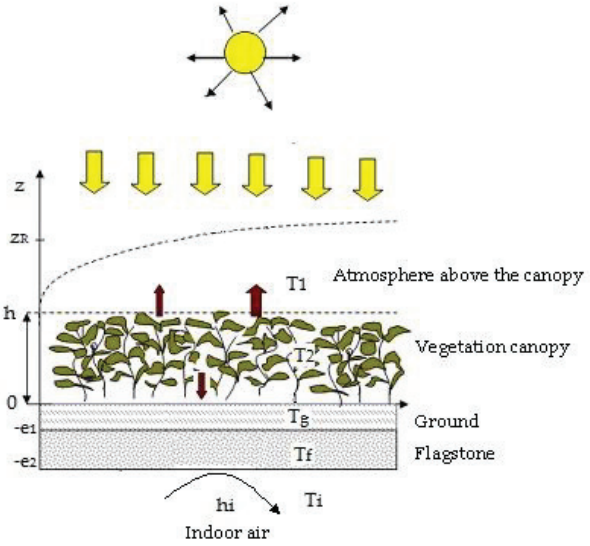

Figure 1: Sketch of a green roof

The second is the turbulent nature of the air stream within a canopy. Its consequence is that the direction and magnitude of the fluxes of energy and mass vary at any moment and cannot be exactly predicted. In spite of this, in much of the literature concerned with the coupling of plants with their environment, heat and mass transfer to and from a canopy are described as vertical fluxes along a concentration gradient across some typical resistances. For a given vegetation canopy, the leaf and the stalk constitute obstacles to airflow and are characterised by the Leaf Area Density LAD(z). This scalar is assumed to be a vertical distribution function. In leaf gas exchange studies, the variable employed to characterise the atmospheric water stress was the leaf-to-air saturation deficit Y(z). This scalar is defined as the difference between dry and wet air bulk temperatures: $Y(z) = T(z) - Tr(z)$.

The transpiration rate depends on the bulk stomatal coefficient $\alpha(z)$ which plays the same role as bulk stomatal resistance r(z) of the plants reported by most authors. The coefficient α is equal to 0 for the dry foliage plants and 1 for the wet foliage. When the vegetation canopy is very dry, evaporation comes under the physiological control of the plant, as it has to pass through the stoma. The bulk stomatal resistance of the canopy is expressed using the Noilhand and Planton correlation [8], the factors considered here are a solar radiation factor f_1, a water stress factor f_2, a factor related to atmosphere pressure deficit f_3 and an air temperature dependence factor f_4. These different factors f_i are detailed in the reference [9].

Transfer equations with appropriate boundary conditions are solved numerically using an implicit finite difference scheme and Thomas algorithm. The diffusion terms are approximated by the central finite difference scheme and the implicit procedure to discretize the temporal derivatives is retained. For a given temperature at substrate-canopy and canopy-atmosphere interfaces and under initial conditions, water vapour, heat and momentum transfer equations are

solved in each zone. The following time and spatial steps Δt =10 s and Δx = 0.005 m are respectively retained. Successive iterations were applied and the solution is considered satisfactory when the following convergence criterion is verified for each time:

$$\left|\left(\phi_{i,j}^{k+1} - \phi_{i,j}^{k}\right)/\phi_{i,j}^{k}\right| \leq 10^{-5}$$

ϕ can be the temperature T or the water vapour density C

4 Results and discussion

The daily ambient temperature and solar radiation are assumed to have a sinusoidal variation during a day. For a given ambient temperature and relative humidity, the dew points are deduced from Mollier's psychometric chart. The saturation deficit scalars of the air as well as the water vapour density at the reference height are calculated. Particular attention is paid to characteristic fluxes such as evapotranspiration, sensible and latent heats fluxes. The local heat gain across the planted roof is evaluated in terms of solar heat gain factor. For a given value of wind speed in greenery, effects of solar radiation and canopy structure (Leaf Area Index LAI) on evapotranspiration, sensible and latent heats fluxes are illustrated in figures and analysed. The determination of water vaporization and its transfer to substomal cavities according to climatic characteristics, canopy structure and stomatal regulation is an essential point in the understanding and interpretation of evapotranspiration. Indeed, hourly evapotranspiration is obtained by summing hourly values of local latent-heat flux from different layers within the canopy and added to the hourly value of evaporation at substrate's level. The evolution of evapotranspiration density as a function of the incident solar flux density is illustrated in Figures 2. The evapotranspiration varies linearly as a function of solar radiation density. The characteristic result of evapotranspiration for different values of Leaf Area Index LAI show how evapotranspiration evolves over a sunny day. An increase in LAI value resulting from vegetation canopy density increases the evapotranspiration value. It's clear that evapotranspiration is more important when the foliage is sufficiently dense.

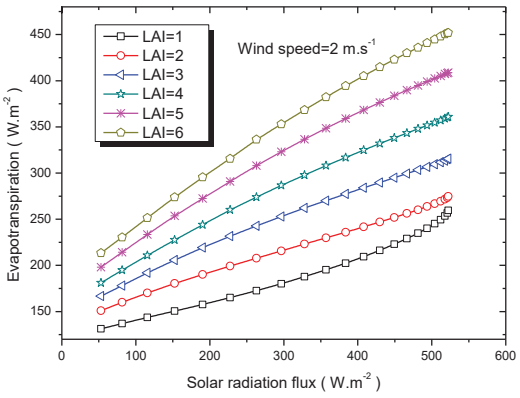

Figure 2: Evapotranspiration as a function of solar radiation density

Net radiation in the canopy is a function of LAI(z); therefore, for a high value of LAI, transpiration heat flux is more important and heat removal involves a decreasing of temperature within the canopy. In fact, according to the intensity of the latent heat flux which depends directly up-

on biological regulation, each part of the plants becomes a local source of heat for weak evaporation or local sink of heat for strong evapotranspiration.

LAI=2

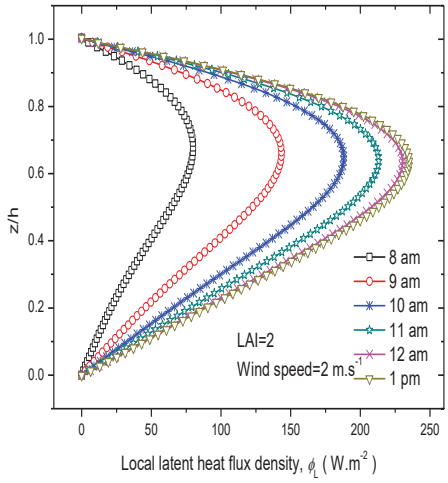

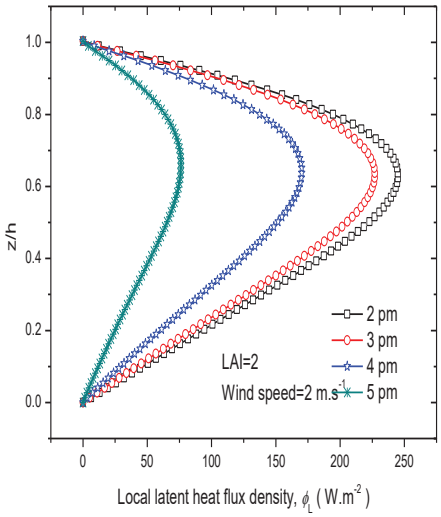

LAI=6

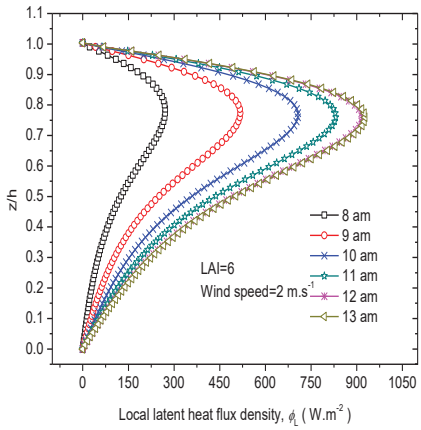

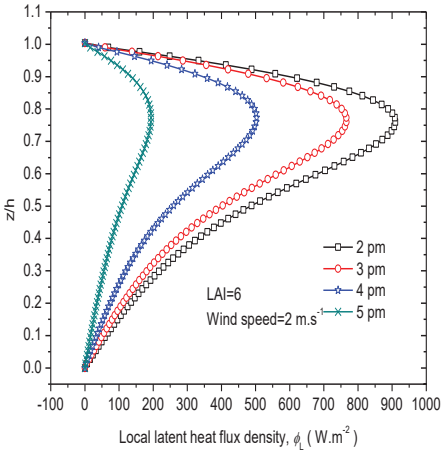

Figure 3: Local latent heat flux density profiles within the canopy

In figures 3 and 4 are illustrated the variation of the sensible and latent heat fluxes at different hours of a day. As expected, according to the leaf density area distribution, maximum transpiration source occurs at the mid-height $h/2$ of the vegetation canopy. A striking decrease in transpiration is observed in the upper and lower parts of the canopy. The distribution of the leaf area density plays a very important role in heat and mass exchange in the canopy. The symmetrical distribution adopted leads to a local latent heat flux density that decreases from mid-canopy height to the soil surface under the canopy as shown in Figure 3. This decrease is more or less modified by the value of stomatal resistance that can reduce, by stomatal closure, water loss, and energy loss by sensible heat flux and the increase in surface temperatures. A strong stomatal regulation in the upper part of the canopy could lead to a maximum flux

density of local latent heat. A specific arrangement of the orientation of the sheets with a minimum captation of radiation in the upper part of the canopy may also lower the maximum flux density of local latent heat. For low foliar coverage, local latent heat flux density is not high enough since the maximum obtained around 2 p.m is about 250 W.m^{-2} while in the case of a dense canopy, this flux density can reach about 900 W.m^{-2}.

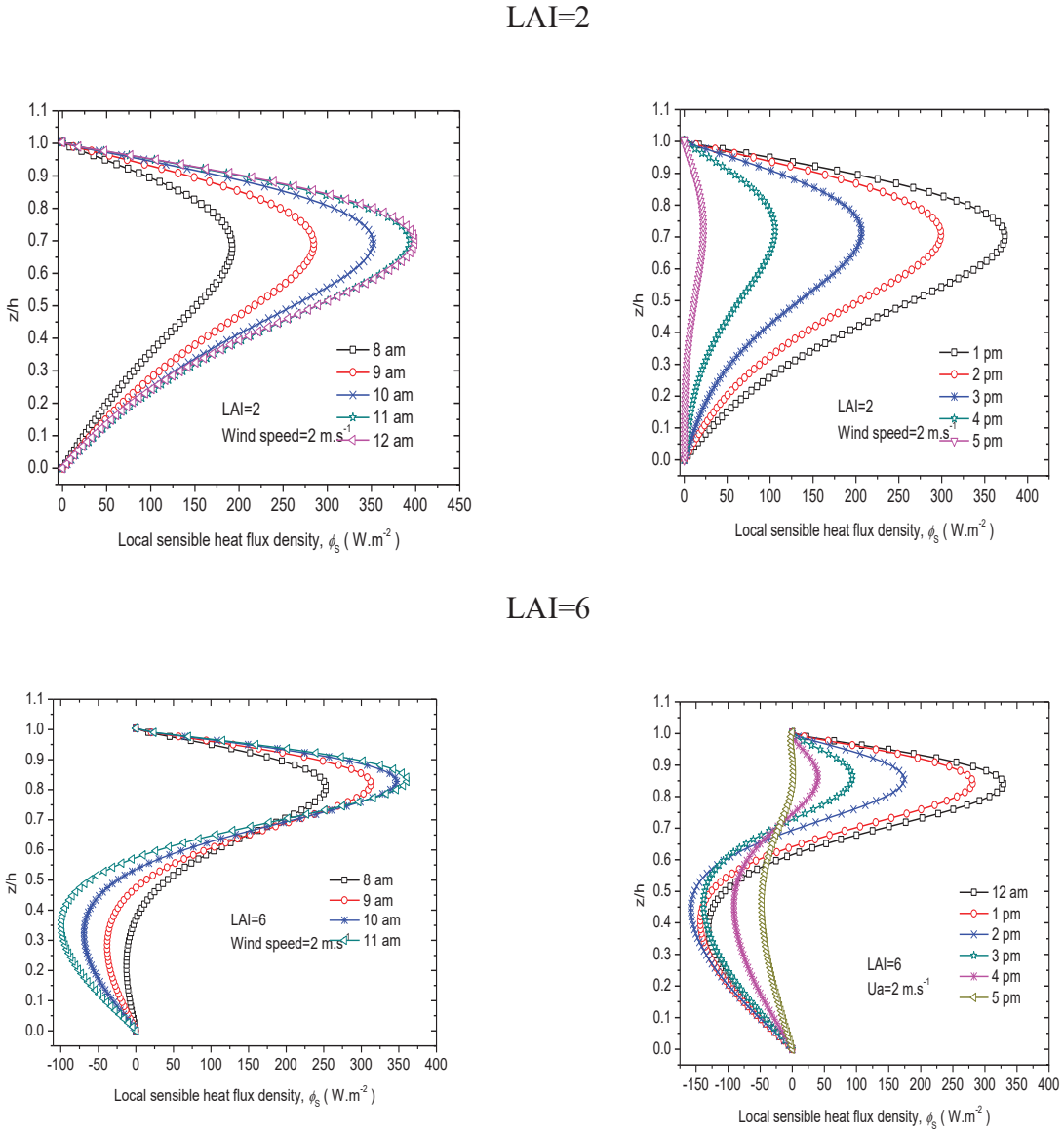

Figure 4: Local sensible heat flux density profiles within the canopy

The local density of sensible heat flux evolves in more complex manner with mostly positive values in the upper parts of the canopy, sometimes turning negative in the lower parts as it's shown in figure 4. Heat flux exchange from the canopy to the atmosphere explained the positive values of sensible heat flux while negative values obtained mostly for large values of LAI are explained by the diffusion of the accumulated heat in canopy towards the colder the substrate. Figure 5 illustrates the temperature profiles of the substrate surface for different LAI values. This figure shows that an increase in LAI causes a decrease in temperatures. A fairly dense vegetation cover considerably reduces the growing medium temperature. This is explained by the fact that the net radiation is strongly mitigated by the leaf material and by the

activity of the stomata which are more numerous. In general, the growing medium surface temperature is sensitive to climatic factors, the type of vegetation cover is highly dependent on the state of drought of this layer.

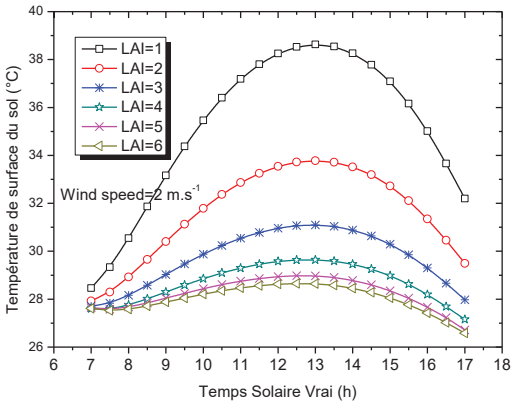

Figure 5: Evolution of surface temperature of the substrate

Phenomena of heat and mass exchanges modelling are described in terms of Nusselt and Sherwood numbers. Figure 6 (a) and (b) presents respectively the variations of the Nusselt and Sherwood numbers as a function of the solar radiation density for differents values of LAI. The both two transfer numbers evolve linearly as a function of solar radiation. For a given LAI, the intensity of heat (Figure 6 (a)) and water vapor (Figure 6 (b)) transfer at the vegetation-atmosphere interface intensify when increasing solar radiation density which in fact controls the stomata regulation. The profiles of transfer nummbers increase with the value of LAI. For high values of LAI, transpiration flux increases significantly and exchanges of heat and water vapor between the vegetation and the atmosphere are very important as shown by the variations of the Nusselt and Sherwood numbers.

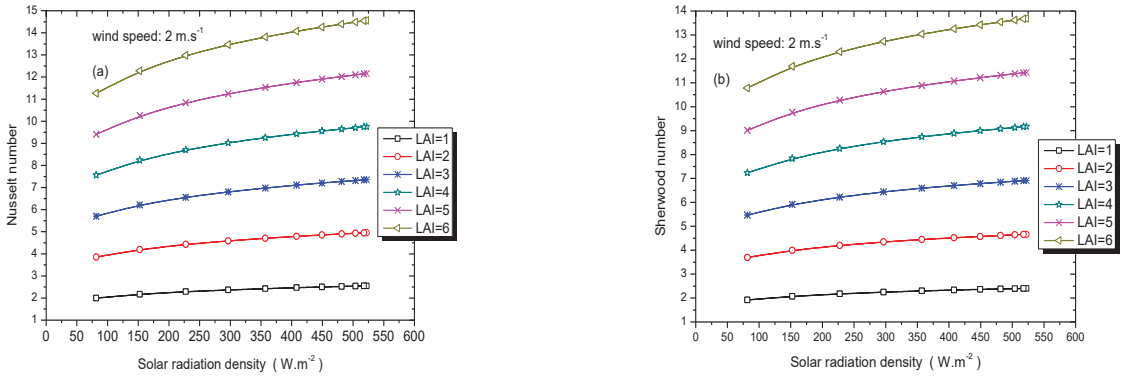

Figure 6: Nusselt (a) and Sherwood (b) numbers as a function of solar radiation density

When considering the degree to which solar gain is transmitted by the fabric of the building, it is helpful to use the concept of solar heat gain factor. This is a useful parameter defined by Koenigsberger [10] as the heat flow rate through the construction due to solar radiation expressed as a fraction of the incident solar radiation. In the present study, the solar heat gains factor of the green roof is defined as the ratio of transmitted solar energy into the interior of the building to incident solar energy. This factor has been calculated for the planted roof and for

the roof without vegetation canopy. Figure 7 clearly indicates that, the vegetation canopy significantly reduces the heat gain in the building. Indeed, for a given wind speed of 1.5 $m.s^{-1}$ and without greenery on the roof top, the solar heat gain factor can reach a maximum value of 45% against 15% for a roof with vegetation canopy (LAI = 3).

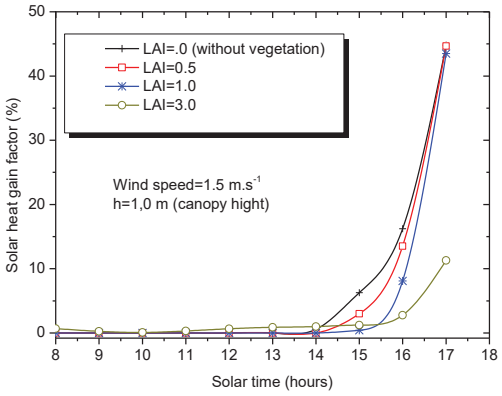

Figure 7: Hourly evolution of solar heat gain factor

5 Conclusions / Perspectives

A dynamic mathematical model based on time average Navier-Stokes equations for a planted roof in hot humid climates has been developed. The effectiveness of vegetation screen as a passive cooling technique is examined theoretically and compared with a classical roof in hot-humid climate conditions. The results showed that solar heat gain factor can be can reduced to 15% for the planted roof against 45% for for bare roof. It is clearer, that cooling load in buildings can be reduced by the application of such bioclimatic screen design. Evapotranspiration and Solar Heat gain Factor are functions of Leaf Area Index which is the most important parameter when considering the foliage density. It is clearly proved that the foliage density and hence the vegetation canopy type selection greatly influence the thermal efficiency of the bioclimatic insulation screen. It was found that a larger Leaf Area Index can reduce the solar flux penetration and increases evapotranspiration which is an important parameter when considering surrounding microclimate formation.

Before, adoption of such a technique in hot humid climate, studies must be conducted not only on plants species selection suitable with minimum maintenance but also on the resistance of species selected to drought and their water consumption for possible application to the arid regions.

6 References

[1] N. M. Nahar, “Studies on solar passive cooling techniques for arid areas”, Energy *conversion and Management*, Vol. 40, pp. 89-95, 1999.

[2] Runsheng Tang & Y. Etzion, “On thermal performance of an improved roof pond for cooling Buildings”, Building *and Environment*, Vol. 39, pp. 201-209, 2004

[3] Dilip Jain, “Modeling of solar passive techniques for roof cooling in arid regions”, *Building and Environment, vol.* 41, pp. 277-287, 2006

[4] H. Abalo Samah & M. Banna, “Performance analysis of Thermal Insulation Screens used for Classic Roofs in hot-humid Tropics”, *International Energy Journal,* Vol. 10, pp. 255-266, 2009.
[5] S Elena Palomo Del Barrio, “Analysis of the green roofs cooling potential in buildings”, *Energy and Buildings,* Vol. 27, pp. 179-193, 1998.
[6] Rumana Rashid, “Financial and Environmental Benefit of Pot Plants’ Green Roof in Residential Building in Bangladesh” *World Journal of Management,* Vol.2, N°2, Pp. 45 – 50, 2010.
[7] Kumar R. & S.C. Kaushik, “Performance evaluation of green roof and shading for thermal protection of buildings”, *Building and Environment,* Vol. 40, pp. 1505-1511, 2005.
[8] Noilham & J.Nad Pl., “A simple parameterization of land surface processes for meteorological model”, *Mon. Weather Rev.*, Vol. 117, pp. 536-549, 1989.
[9] D L. Seen, “An approach to couple vegetation functioning and soil-vegetation-atmosphere-transfer models for semiarid grasslands during the HAPEX-Sahel experiment”, *Agricultural and Forest metrology,* Vol. 83, pp. 49-74, 1997.
[10] Koenigsberger O. H, Ingersoll T G, Mayhew A & Szokolay S V., “Manuel of tropical housing and building design“, *Longman. London*, 1973.

SIV-1a

Construction of PV Systems for Elementary Schools in the Savannah of Togo

Light for Education and Culture

Etienne Dable [1]

1 Background

The savannah region in northern Togo borders on Ghana, Burkina Faso and Benin (Figure 1). It covers 8,596 km2, which is 15% of the total area of Togo. The regional capital Dapaong has about 100,000 inhabitants. The savannah region consists of 5 prefectures, 70 cantons, 1,073 villages and 451 hamlets. The number of inhabitants is growing rapidly. The population figures were 828,224 in 2010 and 890,403 in 2013, a growth rate of 8.2% in only 3 years. With 105 inhabitants per km2 the savannah region is more densely populated than German Mecklenburg-Vorpommern (69 inhabitants per km2).

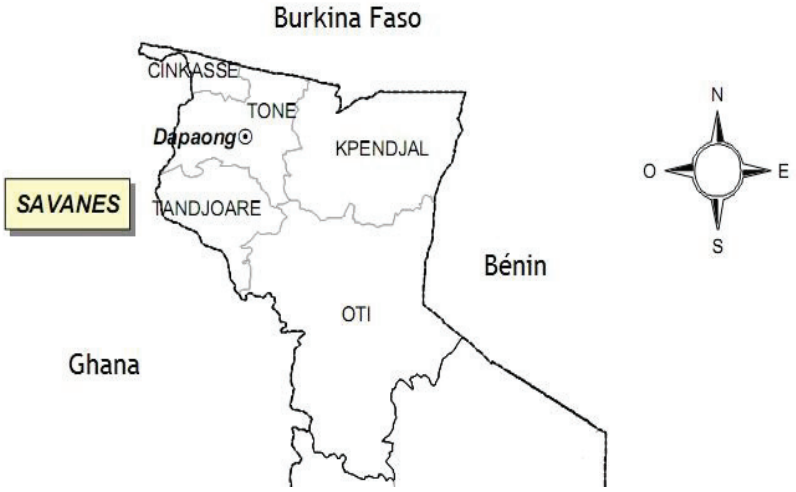

Figure 1: Region of Savannah

The savannah region is the poorest region in the country. In the villages, subsistence farming prevails. Surpluses are sold at village markets or nearby city markets with little profit, since raw products are rarely processed and certainly not processed and the purchasing power in the region is low. The sensitive savannah floors are overused. During the long dry season (October to May) there is a lack of artificial irrigation. The climate change affects the savannah region through shorter and irregular rainy seasons. Deforestation leads to further drying out of the soil. The population is increasing, becoming poorer and poorer and uses almost exclusively wood for cooking in the villages. This leads to further deterioration of the arable land. Harvest yields

[1] Dipl.-Ing. Etienne Dable, IT Village, Dapaong

are falling because improved seeds and fertilisers are also lacking. The infrastructure in the region is at an extremely low level. There are no industrial enterprises in the savannah region. There is an almost complete lack of companies that process and refine agricultural products. There is a lack of storage facilities and cold chains for agricultural products. Only for wood and charcoal there are transport routes from the international highway to regions with better purchasing power. A major obstacle to the establishment of small businesses is the lack of electricity.

2 Bonita-Haus and IT Village

Dapaong is the capital of the savannah region and the northernmost city of Togo. It is the seat of the IT VILLAGE association and since 2013 the first modern private educational centre for vocational and technical training of young people in the savannah, which was built by IT Village with the support of DAZ e.V. – the Bonita-Haus (Figure 2). IT Village now trains 120 young men and women from Togo and Burkina Faso in this educational facility. The training and studies focus on new technologies, agroecology, handicrafts as well as commercial and economic fields of expertise, for which there is a need in the region and which are important for its economic development.

Figure 2: Opening of Bonita-Haus in March 2013

In the past, the Bonita-Haus and the DAZ have created the basis for supporting sustainable development with renewable energy systems. In addition to stationary systems, a development project "Human and Technics - mobile regenerative energy systems in the savannah for life and education" has been carried out in 2016, which can now supply demonstrators for PV systems [1].

Within the framework of active workshops, a mobile PV system was set up with professional school students from various disciplines. The spectrum of professions represented ranged from electrical engineer to welder and car mechanic. The knowledge-hungry and highly motivated vocational students were supervised during the workshop by the three engineers from the Technical University of Applied Sciences Wildau René von Lipinski, Uwe Düsterhaus and Sebastian Schulz (Figure 3). They were actively supported by the local engineer Samuel Yao Wodou, the interpreter Elias Harakawa from Lomé and the electrical engineer Kankpiame Sissob from BONITA Haus.

Figure 3: Brick machine driven with renewable energies

Nowadays, DAZ and IT Village support five primary schools in villages in the savannah. At present about 2,000 students attend these schools. By improving school teaching, the number of pupils attending the 6th grade could be increased from 89 to 298 from school year 2010/11 to school year 2015/16. This has been achieved by:

- Establishment of libraries,
- Equipping 500 pupils from poor families with teaching materials,
- Reduction of school classes by taking over the salary of 26 additional teachers,
- School lunch,
- Construction of 6 school buildings with solar panels.

The solar systems allow the school buildings to be used in the evening hours as well. It is also used to recharge mobile phones and operate refrigerators for school meals. Further school buildings with solar systems are in planning.

3 Concept for decentralized power supply

In 2014 the DAZ in cooperation with IT Village started the electrification of the schools Nagre II, Kourdjoak and Mandime in the savannah by means of solar technology (Figure 4). This system will be used for lighting the classrooms and cooling for the school lunch for the children and will be provided to the residents as a reference for light and electricity. The solar systems have been in operation since 2014 and are stable in operation. What all plants and systems have in common is that they are operated as stationary systems and are not mobile.

In the construction of the BONITA House training centre in Dapaong and the school extension buildings in Nagre II, Kourdjoak and Mandime, architect Francis Kéré from Burkino Faso used adobe construction methods for the first time in the savannah and in Togo. An alternative would have been the concrete construction method. In comparison, the clay construction method offers optimal climatic conditions due to the cool room temperatures, especially in the hot dry season,

and thus enables more concentrated learning and working for students and teachers. Clay bricks are not available on the market and there was and is no alternative machine to the clay brick press in the region. Therefore, the manually operated press was also bought in Belgium in 2010 - it was the only offer DAZ received after extensive research and rebuild with an electrical propulsion system in 2016 (see Figure 3).

Figure 4: Construction area for new school including canteen

In addition with the stationary energy supply at schools (Figure 5), this mobile demonstrator is a good starting point for demonstrating the use of renewable energies. Especially applications of photovoltaics show a great potential for the Sub-Sahara region. Equipping schools with decentralized energy systems gives pupils and teachers the chance for continuous education.

Figure 5: Stationary PV-System

4 Conclusion and Outlook

The BONITA-Haus, IT Village, DAZ and the Technical University of Wildau near Berlin are in deep collaboration since years. This will be extended to the State Universities in Kara and Lomé.

For more than three decades, TH Wildau has been dealing with the use of regenerative energies for application in industrialised and social environments. One topic is the utilization of these energies for regions with non-centralized energy supply. This topic should be the focus of the cooperation between TH Wildau and the Togolese training centres in Dapaong and the Center of Renewable Energy Systems in Kara.

Figure 6: Bonita-Haus's students of Agroecology during the visit of DAZ members in 2016

For all future tasks, a reliable energy supply must be created for the participating companies in Togo and the sub-Saharan region. This requires cooperation in a centre to share knowledge and experience. The use of renewable energies can be created here as an example for the application in regions with non-centralized energy supply. This is a central requirement for the creation of jobs in the rural regions of Africa. Because "Energy poverty is ... synonymous with poverty, because without electricity there is no light for learning, no computer running and no machine to help run small businesses" [4].

5 Acknowledgments

The research was partially supported by the German Federal Ministry for Economic Cooperation and Development (BMZ) (No: bengo6452). We are particularly grateful to our scientific partner TH Wildau for providing support in development as well as during the implementation phases.

6 References

[1] J. O. Löfken, „Afrika entdeckt die Sonne". *tr – Technology Review* vol. 6, pp. 26-32, 2011

[2] D. Kohnert, "Togo". *Africa Yearbook 2005 – Politics, economy and society South of the Sahara*. Melber/Mehler/Walraven (eds.), Brill, Leiden & Boston, in press, 2006

[3] J. Reiff-Stephan, "Solarkraft in der Produktentwicklung – Anwendungen für Westafrika," *EEE-Techn. Design in Forschung, Lehre und Praxis*, TUDPress, Dresden, 2014, pp. 327-340.

[4] F.Woellert and R. Klingholz, "Jobs für Afrika," *BI discussion paper Berliner Institut für Bevölkerung und Entwicklung*, ISBN: 978-3-946332-84-8, vol. 17, 2016

SIV-1b
Implementation approaches for distributed energy management systems in production

Jörg Reiff-Stephan [1]

The energy management of manufacturing facilities must be taken increasing account for an efficient operation within a production process. Future efforts and solutions will focus on improvement of the process stability and on cost reduction to meet the needs of successfully compete in local and global markets especially for SME. The paper describes an approach for manufacturing facilities using an example for thermoprocessing equipment. For this purpose, the TPS-principle Jidōka is used, the mechanism of self-adapting limit setting as well as an implementation is presented prototypically.

1 Introduction

In order to meet the challenges of future value-added networks, manufacturing companies are increasingly dependent on the collection of energy data and its processing in efficient process chains [1,3,5,13]. Industrial energy management systems are therefore becoming increasingly important. The IT networking of production processes is being strongly promoted by the strategies and enablers of Industrie4.0. Process and service orientation, interoperability, horizontally and vertically networked information chains as well as data transmission systems that function in real time with high availability are some of the building blocks for an (energy) efficient production system [2]. Considering the study [14], which was conducted under the auspices of acatech, the three main areas of development are data evaluation and analysis, process management and customer relationship management. Due to this, the following approaches are shown that could enable initial implementation approaches to efficient energy management.

2 Requirement analysis

2.1 Areas of responsibility

For an extension of existing productive structures to include the functionality of an energy management system, it is necessary to obtain a clear picture of the possibilities that the existing production system already offers. The mentioned acatech-competence study makes it clear that process management and process orientation in the German economy obviously still represent inadequately solved challenges, although these have long been vacant, regardless of Industrie4.0 [14].

It will be essential to be clear about the tasks of energy management in the implementation of DIN EN ISO 50.001 and DIN EN 16247-1 (Figure 1). Primary economic parameters such as

[1] Prof. Hon.-Prof. Dr.-Ing. Jörg Reiff-Stephan, TH Wildau, Wildau - Germany

energy prices or key figures on competitiveness are to be considered equally important to the legal and normative requirements resulting from the scarcity of resources and environmental pollution. Last but not least, the certification as an energy-saving company can improve your own image. It is important that this process of analysis and deduction is considered a continuous process of improving the production system. Primary objectives describe the reduction of energy costs as well as the maintenance of a stable, available process.

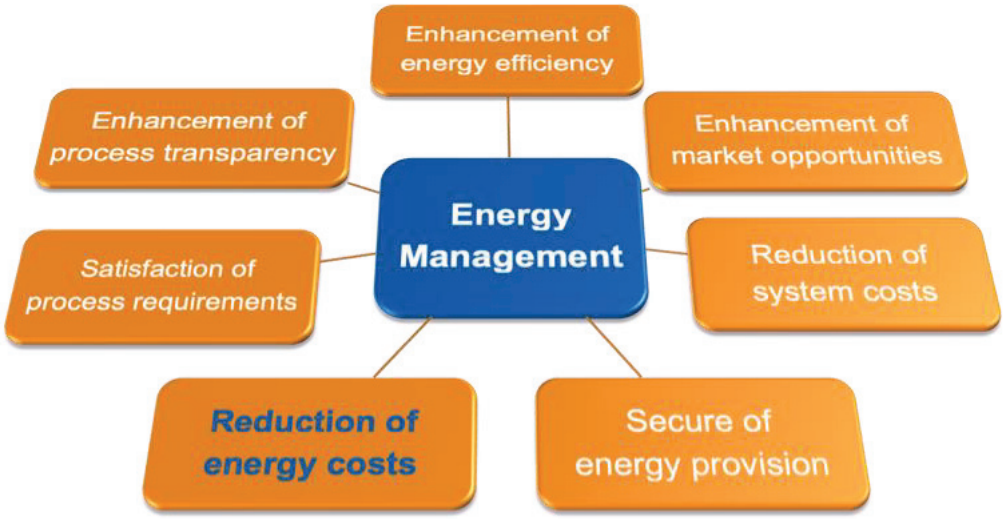

Figure 1: Aims of energy management systems

2.2 Enabler

The capturing, communication and computation of energy-relevant parameters becomes a decisive requirement for the efficient management of energy processes. The rapidly developing digitalization of value-added networks offers excellent starting points for this. The IT integration of things (technical entities), data and services has both vertical and horizontal characteristics [12]. Cyberphysical production systems (CpPS) are being developed, which describe the connection of the information and software components with the mechanical, electronic entities [4].

In detail, vertical integration in this context includes automated decision making across the levels of the automation pyramid, for example to make adjustments of technological information on technical entities (such as motors or oven systems) directly usable for control information at the point of use. In this respect, the horizontal integration is carried out in such a way that operational information from the services (e.g. with the help of energy monitoring systems) together with contextual information (e.g. supply information from the energy exchange) flow directly into the respective production without stopping backwards along the value chain. This integration also intelligently overcomes company boundaries, so that each communication partner can flexibly decide which data granularity is provided. Furthermore, energy suppliers, for example, could obtain forward-looking, real-time information about the requirements of their customers.

Intensive work is being done on methods and tools for querying and providing data in real time. There are several protagonists who, through standardization efforts, try to offer a corresponding general solution. At present, the standard DDS (Data Distribution Service) of the Object Management Group [6] realizes these hard real-time requirements for distributed systems up to application level. The standard has been further developed as open source in many areas, but due to its specific orientation it cannot be applied in all places within the information network. In this respect, the OPC Foundation's OPC-UA (Open Platforms Communication - Unified Architecture) standard is a very broadly based industrial M2M communication protocol [7]. Its service-oriented architecture (SOA) enables the switching of data packets between the various participants based on the OSI layer model. The implementation of your own security services can thus be carried out very efficiently. The lack of time scalability, which currently still prevents a broad application, is being addressed within an ISO working group of the IEEE802.1. The provision of the information with a time-synchronous protocol is to be taken into account in a hard real-time system called "Time Sensitive Networks" (TSN). Which standard will be used in the CpPS application in the future will be decided based on the requirements of the actual applications.

The efficient computing of the communicated information is sometimes regulated in CpPS system by the principles of self-organisation. This is done, for example, with the help of capacity exchanges or service-oriented agent systems. Such systems control the consumption of available resources according to fixed or dynamically generated weightings and react dynamically to changing conditions. Depending on the process, however, the human entity remains the decision maker. In such cases the human being is supported by the self-organized system in the form of simulated variants of different scenarios. The final choice as well as decision is then left to the human being [2].

3 Concept study

Based on the consideration of the distributed control architecture, a concept for energy management is presented, which does justice to the two targeted topics of cost reduction and high process stability.

3.1 Distributed control architecture

Value-added processes in a production system are characterized by the conversion of energy. In the predominant sense, all usable forms of energy are attributed to the provision of electrical energy. Conversion and utilization processes are regulated with control and sensor/actuator entities at the distributed points of use in the value-added process. In the future, these entities can be dynamically adapted to changed process conditions, rearranged or supplemented within the framework of distributed architectures in a heterogeneous production environment.

A hardware PLC could thus become less important in the future, since sensors and actuators can interact with the control software in the cloud using IP-based addressing via standardized communication nodes (Figure 2). The implementation of new field devices requires only minimal effort in terms of wiring. This is then limited to the connections to the power supply and the communication node. In the case of energy-autonomous wireless sensors, the wiring is

completely eliminated. The industrial cloud of production automation is likely to have a private or hybrid structure [9,11]. The control network will thus preferably be limited to the company's borders, but will allow information to be exchanged with other networks as required.

With the IP-based entities the realization of horizontal as well as vertical integration in the production network becomes possible. The system presented in Figure 2 takes an industrial oven as an example and links the essential individual processes for operating it in the digital network. The idea of a virtual PLC has already been taken up here, but is not an indispensable prerequisite for energy management [9]. Regulated access from the cloud systems outside the own company as well as within the own data structures must be guaranteed by protecting the data and services against misuse such as unauthorized access, modification or destruction. In this respect, the objectives of attack security measures are to increase confidentiality, integrity and availability.

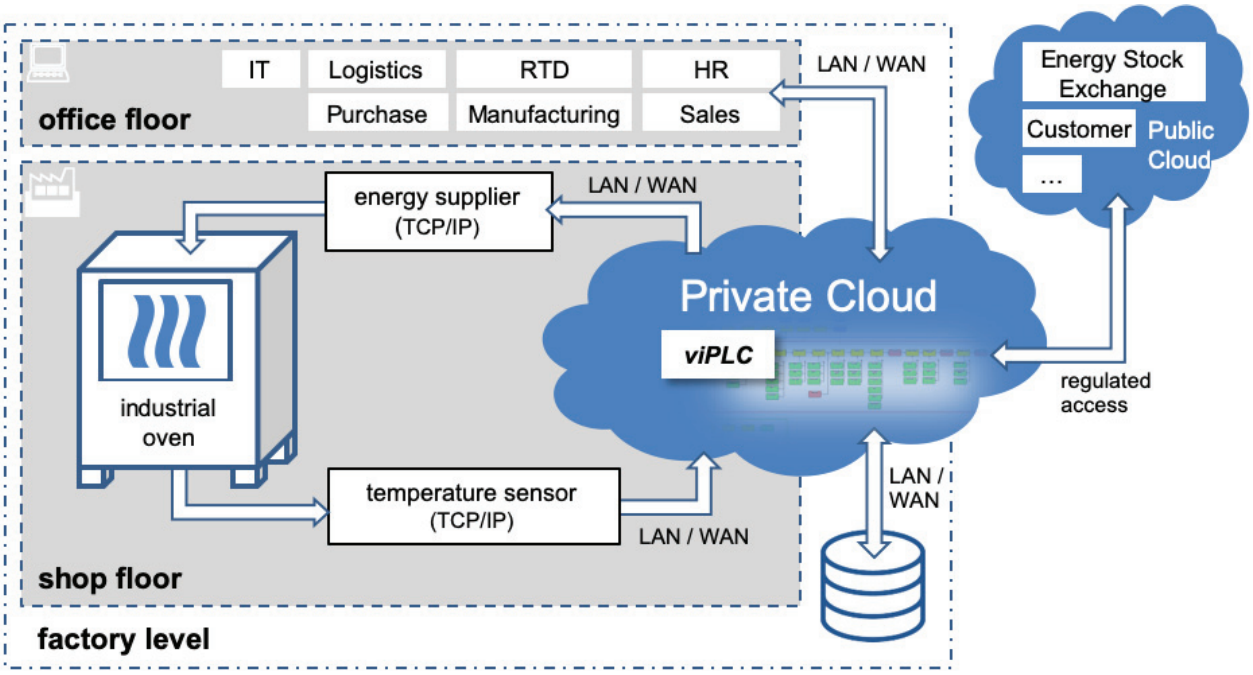

Figure 2: Information flow of a thermoprocessing plant with a cloud-based management system

3.2 Derivation of management tasks

The process sequences are being carried out with increasingly high material and energy efficiency under business management requirements. For example, the energy profile of a process step can be used as a decision factor in production planning processes, thus avoiding load peaks in the factory's internal energy network [13]. Peak loads are sometimes caused by the switch-on processes of machines and systems. Additionally, the average load profile of the actual production process is exceeded many times over. Since the maximum values in the load profile directly influence the energy supply costs, intelligent load management offers high potential for cost reduction [3].

With the knowledge of the cost-optimal provision of electrical energy on the energy exchange, orders can be introduced into the production process. For this purpose, the price development

on the energy stock exchange can be monitored automatically via agents and the waiting process can be released into order processing.

The further aspect of process stability is considered by the exact knowledge of the current energy requirements of production plants, machines and individual assemblies and the possible, comparative temporal consideration, in order to support maintenance and repair processes [8,10]. For this purpose, the detection of abnormal plant conditions based on the trend analysis of energy data is used. A prerequisite for this is the ability of the existing technical entities to collect the relevant data. In this respect, the market offers a wide range of solutions for implementation. A comparison of the solutions shows that the most suitable system can be identified for the respective application [12].

Due to the exact knowledge of the current and future energy requirements of production plants, machines and individual components, the data can be processed, for example, by using the process control concept presented by the TOYOTA Production System (TPS) under the term Jidōka (Autonomation). In the event of a fault, the production process is automatically stopped:
- a production-related reject,
- damage to the production plant as well as
- other wastes such as energy inefficiencies,

avoided. For a stable process, this stop strategy, designed as a self-optimizing system, is supplemented by decision rules to support maintenance and service processes.

4 Applications

4.1 Prototypical test setup

The spectrum for applications for the use of energy data is broad. An application scenario defined with an industrial partner, which combines the above-mentioned aspects, is, for example, the improvement of energy efficiency in a thermal processing plant (see also Figure 2). The service life of thermoprocessing equipment is very long, with an operating life of up to 30 years. With regard to the outdated technologies, there is a high potential for reducing energy consumption through optimization measures. In addition to the optimization of the oven wall structure or the heating technology, intelligent control and regulation technology also leads to improved energy efficiency and process stability. Energy data can be used directly as information for the control and regulation processes of the thermal processing plant or as decision criteria for higher-level functions of production planning and control.

The implementation of the described optimization is illustrated by a laboratory demonstrator. A laboratory oven type VD from MIHM-VOGT&CO was deliberately chosen as the thermoprocessing plant. This older construction type was renewed with regard to the sensor components in order to test the suitability of the optimization measures for applications with brownfield character. A first test setup is shown in Figure 3.

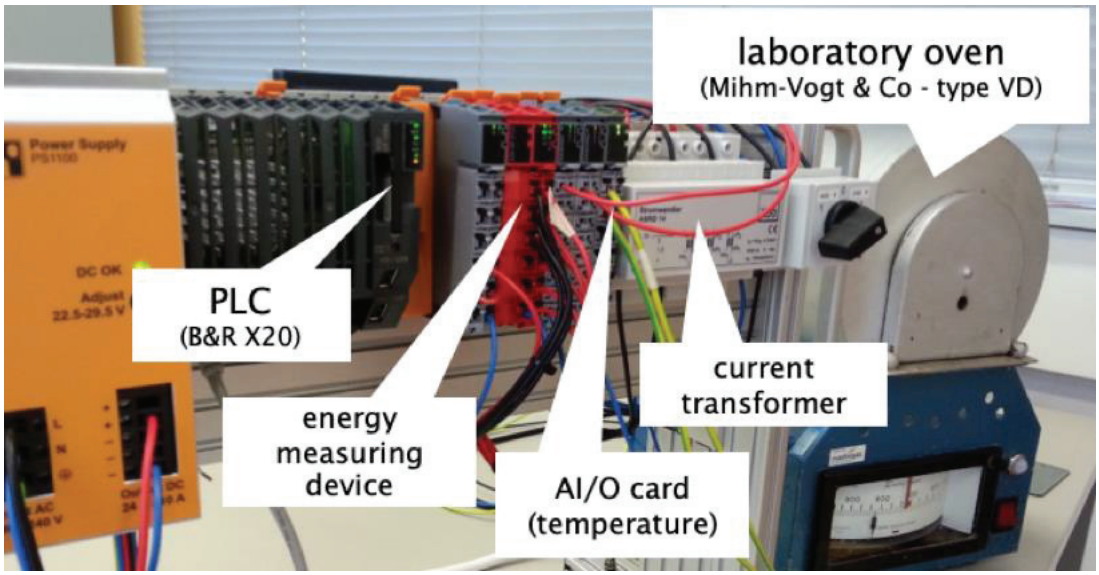

Figure 3: Prototypical test setup

The connection-programmed controller was replaced by a modularized, programmable logic controller of type X20 from B&R AUTOMATION GMBH. The configuration has been expanded with an energy measurement card of the type X20AP3131 and an analog module for integrating the temperature sensor technology. The load currents are coupled in via a current transformer of the type ASRD 14 3X80/5A from MBS AG. The use of the current transformer later simplifies the conversion to the real process plant. Logically, the data is made available from the controller via an OPC-UA interface. A backup of the data is guaranteed via a relational MS®SQL database. From this, the necessary rules for higher-level control tasks as well as the visualization including key figure formation and real-time graphs would be derived.

4.2 Self-adapting control

As mentioned above, the Jidōka principle can be applied to maintain process stability with optimal energy price utilization. For the application under consideration, a reference variable is, for example, the amount of energy required to carry out a thermal manufacturing process. The actual process value is continuously captured and assigned to the energetic fingerprint of the product to be manufactured, as well as being made available to higher-level control processes as a performance indicator. By means of trend analysis, the data can then be used to increase the energy efficiency of the thermal processing plant.

If, for example, for the production of individual workpieces or batches with the same process parameters, and for the thermal production process a continuously higher energy requirement is determined, this can indicate abnormal plant and process conditions. The increased energy requirement is then due, for example, to unfavorable parameterization of upstream processes, undetected thermal bridges or wear of the heating elements or wall structure inside the oven. A trend analysis is used to compare historical data with the current condition monitoring. If the values exceed the warning limit, an inspection order is automatically triggered to take account of the task of maintaining process stability. If intervention limits are exceeded, the process is automatically stopped and the causes of the diverging energy values can be searched for.

A self-adapting control model can be specified as an example for the described technological process. By using the process parameter "active power" (P_W), a control strategy can be described under the target criteria of energy efficiency but also as an adjustment of intervention and automatic shutdown limits. With knowledge of the actual values $P_W(t)$ and a trend analysis for each operating shift, a warning limit (ε_a) and a shutdown/stop limit (ε_h) will be specified as a regulating element and implemented in the process control (Fig. 4). The management system is equally capable of adjusting these limits on the basis of previous process periods. The following functional connection is made for this:

Warning limit: $\lim_{t \to t_1} f(t) = P_W(t) + \varepsilon_a$ (1)

Stopping limit: $\lim_{t \to t_3} f(t) = P_W(t) + \varepsilon_h$ (2)

Apart from energy, the main criterion will be the basic statement on the cause of the increased energy consumption. The discussion according to Figure 4 shows that by operating two shifts (S_1 and S_2), the power consumption (at base load level P_{WGP}) remains approximately stable for continuous operation. Within the third displayed period the function value $f(t) = P_W(t)$ converges against the limit value $f(t_1) = P_W + \varepsilon_a$. Accordingly, at time t_1 and when the limit value is reached, an alarm message is automatically output and a test of the system is initiated. An acknowledgement of the signal without corresponding influence (Q^+) by the operating personnel leads to a self-adaptive limit value adjustment within the controlling system of $\varepsilon_a' = \varepsilon_a + \xi_S \Leftrightarrow \xi_S \in x$ with x = step size. The further operation of the thermoprocessing plant in the subsequent shifts is carried out with adjusted limit values.

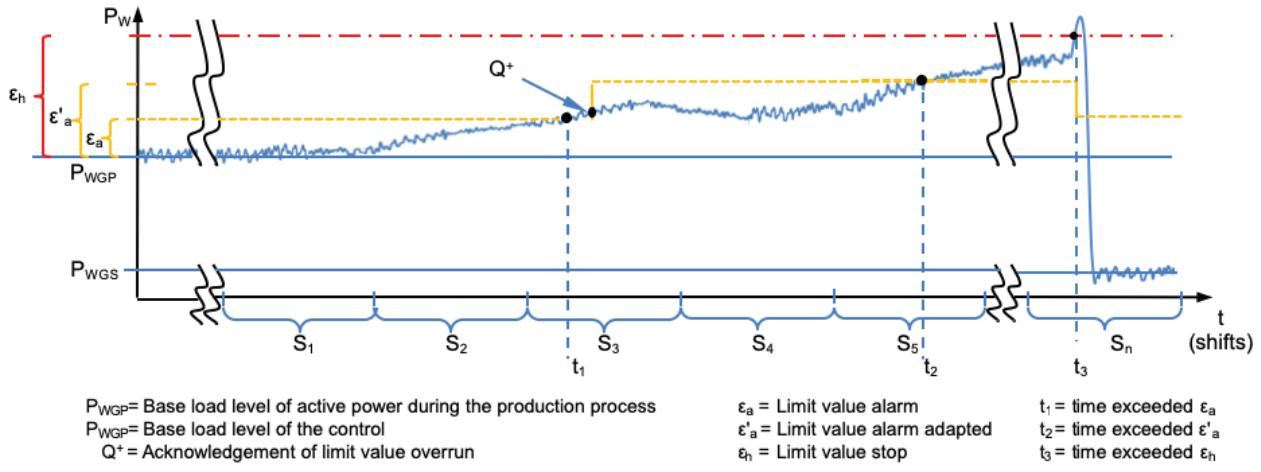

Figure 4: Functional relationship self-adapting limit value setting

The extended case of exceeding the stopping limit according to equation 2 leads to an automatic shutdown of the production system by the control and thus to a reduction of the power consumption to the basic load level of the control system (P_{WGS}). This case occurs if, when the warning limit (ε_a') is exceeded, the plant continues to operate via subsequent histories S_n (with $n \in 6..m$) and the limit ε_h is exceeded due to a sudden rise in the relevant process variable at time t_3. Due to the process, this can occur as a result of delayed reaction times by the

maintenance personnel. After an automatic shutdown of the installation, the limit value for the warning limit (ε_a) is automatically reset to the original value by the guidance system.

5 Conclusion

Energy management is increasingly considered in the design and operation of agile production systems. In particular, the Jidōka principle, in the sense of the TOYOTA production system, is being driven forward by the expanded technological possibilities of physical systems. Due to the accelerated networking of industrial structures, a broad spectrum of data is increasingly available for automated switch-off processes, for example. Thus, the detection of abnormal system states can be done by trend analyses of energy data. A prerequisite for this is the ability of the existing technical entities to collect and evaluate the corresponding data. The presented PLC-oriented overall concept enables, in addition to the measurement of energy-relevant process parameters, the provision via a flexible MS®SQL database and OPC-UA connection to the control platform. In the future, the design and integration of a virtual process computer in a private cloud of the plant operator is also planned. The aim will be to increase the flexibility of future production plants with high process, data and service availability.

6 References

[1] M. Blesl and K. Kessler: “Energieeffizienz in der Industrie.” *Berlin: Springer Vieweg*, 2013

[2] BMBF: “Industrie 4.0. MetamoFAB (Metamorphose zur intelligenten, vernetzten Fabrik).” Retrieved on: 14.06.2020, url: http://www.metamofab.de , 2020

[3] E. Tönsing: “Energiekostenreduzierung durch betriebliches Energiemanagement”. *Fachartikel im Rahmen der Initiative „Energie effizient nutzen–Schwerpunkt Strom “*, Wirtschaftsministerium Baden-Württemberg, 1996

[4] M. Shafie-Khah and P. Siano. "A stochastic home energy management system considering satisfaction cost and response fatigue." *IEEE Transactions on Industrial Informatics 14.2* (2018): 629–638. doi: 10.1109/TII.2017.2728803

[5] W. Kahlenborn, S. Kabisch, J. Klein, I. Richter and S. Schürmann: “Energiemanagementsysteme in der Praxis: ISO 50.001: Leitfaden für Unternehmen und Organisationen.” Berlin: *Bundesministerium für Umwelt, Naturschutz und Reaktorsicherheit*, 2012

[6] OMG: Whitebook DDS. Version 1.4 April 2015. Retrieved on: 14.06.2020, url: http://www.omg.org/spec/DDS/, 2020

[7] OPC Foundation. Whitebook OPC-UA. Version 1.04 November 2017. Retrieved on: 14.06.2020, url: https://opcfoundation.org/developer-tools/specifications-unified-architecture/part-1-overview-and-concepts, 2020

[8] R. Langlois: “Modularity in technology and organization.” *Journal of Economic Behavior & Organization*, vol. 49. pp. 19–37, 2002

[9] R. Langmann, and M. Stiller: Industrial Cloud – Status und Ausblick. *HMD Praxis der Wirtschaftsinformatik*, vol. 52, pp. 647-664, Wiesbaden: Springer Fachmedien, 2015

[10] O. Niggemann, J. Jasperneite, and A. Vodencarevic: “Konzepte und Anwendungsfälle für die intelligente Fabrik”. *Industrie 4.0 in Produktion, Automatisierung und Logistik.* Wiesbaden: Springer Fachmedien, 2014

[11] Institut für Steuerungstechnik der Werkzeugmaschinen und Fertigungseinrichtungen: Industrielle Cloudbasierte Steuerungsplattform für eine Produktion mit cyberphysischen Systemen. *Retrieved on: 07.06.2020, url: http://www.projekt-picasso.de*, 2020

[12] J. Reiff-Stephan, M. Richter, and R. von Lipinski: “Intelligent sensor systems for self-optimising production chains”. *Proceedings of 1st International Conference and Exhibition on Future RFID Technologies*. Eger: Eszterhazy Karoly University of Applied Sciences, 2014

[13] G. Vladova, A. Ullrich and J. Reiff-Stephan: „Der Mensch im Umfeld von Industrie 4.0.“ *Berlin: Springer Vieweg, 2017*, S. 23-30

[14] ANSI/ISA–18.2–2009 – “Management of Energy Systems for the Process Industries”

[15] J. Reiff-Stephan, and René von Lipinski: „Energiedaten als Führungsgröße“. pp. 32-41, atp edition 58 (2016) 9